Title
Abrupt monsoon weakening and links to extratropical North Atlantic cooling

Author
Liu, Yuwei

Publication Date
2014

Peer reviewed|Thesis/dissertation

Abrupt monsoon weakening and links to extratropical North Atlantic cooling

by

Yuwei Liu

A dissertation submitted in partial satisfaction of the
requirements for the degree of

Doctor of Philosophy
in

Geography

in the

Graduate Division

of the

University of California, Berkeley

Committee in charge:

Professor John C. H. Chiang
Professor Inez Y. Fung
Professor Kurt M. Cuffey

Spring 2014

Abrupt monsoon weakening and links to extratropical North Atlantic cooling

Abstract

Abrupt monsoon weakening and links to extratropical North Atlantic cooling

by

Yuwei Liu

Doctor of Philosophy in Geography

University of California, Berkeley

Professor John C.H. Chiang, Chair

The monsoon is the most important mode of seasonal climate variation in the tropics, responsible for bringing life-giving rainfall to the heavily-populated regions of East Asia, South Asia, and West Africa. Previous paleoproxy and modeling studies have shown that the North Atlantic can exert considerable influence on the strength of the East Asian, South Asian and West African monsoons: colder temperatures over the extratropical North Atlantic lead to their weakening. This dissertation focuses on understanding the mechanisms of the teleconnection from extratropical North Atlantic sea surface temperature (SST) to the East Asian, South Asian and West African monsoons, and the spatiotemporal characteristics of the teleconnection in present and future climate.

We investigate the atmospheric teleconnection mechanism between extratropical North Atlantic cooling and the West African monsoon weakening in an atmospheric general circulation model (GCM), focusing on the role of atmospheric temperatures as the mediator. We find that the simulated atmospheric cooling readily reaches North Africa and the Sahel, and that the cooling in turn weakens the West African monsoon. We explicitly show the latter connection by imposing atmospheric cooling anomalies on the northern boundary of a regional climate model of the Sahel; it responds with a rainfall reduction over the Sahel that is similar to the GCM. In the GCM simulation, extratropical North Atlantic cooling is augmented by a positive low cloud feedback and advected downstream, cooling Europe and North Africa, where the cooling is further amplified by a reduced greenhouse effect from decreased atmospheric specific humidity. The results suggest a thermodynamic pathway for the extratropics-tropics teleconnection found in paleoclimate studies of the last glacial period.

We then investigate whether this teleconnection is relevant in monsoonal changes in present-day and future climates. We focus on the Sahel drought that started during the late 1960's and persisted until the late 1990's. By analyzing 20th century observations and reanalysis, we find a late 1960's climate shift over Eurasia and Africa, characterized by a reduction in summer monsoon rainfall, and surface cooling and pressure increases over the Eurasian and North African continental

interiors. The spatial patterns resemble the simulated impact of extratropical North Atlantic cooling in paleoclimate simulations. This late 1960's climate shift is reproduced in GCM simulations with imposed 20th century observed SST and climate forcing. Our analysis of these simulations suggests that the shift originates from an abrupt cooling of extratropical North Atlantic SST over the late 1960's. Idealized GCM simulations with prescribed extratropical North Atlantic cooling also simulate the climate shift. The result herein shows that the observed climate signature of the 1960's abrupt shift in Eurasian and North African climate is consistent with the influence of the abrupt extratropical North Atlantic cooling that occurred in the late 1960's.

Lastly, we investigate if the extratropical North Atlantic is relevant for the future monsoon climate evolution, through analyzing climate projections of the 21st century from the Coupled Model Intercomparison project phase 5 (CMIP5). The dominant pattern of climate change in future projections is global warming; there is also an important pattern that is related to the change of extratropical North Atlantic temperature relative to the global mean. This pattern features coherent changes in extratropical North Atlantic temperature, and Eurasian and North African temperature and precipitation, similar to the pattern found for the late 1960's shift or paleoclimate. We show this in two ways: first, by applying a principle component analysis (PCA) to the spatial patterns of temperature and rainfall changes at the end of the 21st century across CMIP5 models; and second, by applying the PCA to the correlation pattern of extratropical North Atlantic temperature with temperature and precipitation for each ensemble member. The results suggest that the extratropical North Atlantic teleconnection to the Eurasian and North African monsoons is also relevant in future climate projections. As such, it suggests for better understanding of the processes controlling extratropical North Atlantic climate in order to constrain estimates of future monsoon activity.

Contents

List of Figures

Acknowledgements

I thank my advisor, John. He has been patient, open and agreeable, gradually shaping my understanding of and attitude toward science and research, and way of thinking. His means of mentoring is as effective as subtle, like described in a Chinese poem: Good rain knows its time right/It will fall when comes spring/With wind it steals in night/Mute, it moistens each thing. This is because the mentoring was carried out through not only carefully-designed training, but himself being an industrious and conscientious scientist. I also thank John for (the willingness of) the interaction beyond research, some key words including the World Cup, Marathon and biking.

I thank Inez, Kurt and Rob. Particular thanks to Inez. She is a living encyclopedia, always willing to share her broad knowledge and deep insight of every aspect of science. Until now I still feel nervous before meeting with her, as much as I feel motivated after. And they are due to the some reason: her criticalness and passion toward science. I appreciate those feelings and the transition in between, which make me grow. Her attitude also influences me indirectly, through her group. I thank members of the Fung group for our scientific discussion.

Thanks to all the members of the Chiang group. Thanks in particular to Andrew, Shih-Yu, Ching-Yee and Ivana. Andrew and I witnessed the growth of each other for the past 6 years. If the wording of this page looks different from the rest of the thesis, that is because this is the only part of writing Andrew has not proofread for me. Shih-Yu showed me how one could enjoy both academia and life.

I would like to thank my collaborator, Christina and Chia. Thanks also to those whose discussion has greatly improved my work. An incomplete list includes: Alexandra Giannini, David Battisti, Chris Folland, Michela Biasutti, Alexandra Jonko, and William Collins.

Thank Jian Jin. 因为懂得，所以慈悲。

Thank my parents. They must have foreseen this day when they gave my name 28 years ago: education, great.

Thank my friends, in particular, Mamade, who came from the region of drought I study and has been supporting and leading the community; Sakura, the discussion with whom on China-Japan relation makes up most of my exposure to non-physical geography.

Back in 2008, I was a senior student at Peking University looking for US graduate schools to apply for. Then things happened randomly, as they usually do

-- someone who was looking to sharing the cost of FedEx suggested me to apply for Berkeley with him. I did, got accepted, moved here and lived for 6 years, and now am considering coming to Berkeley as one of the most sensible decisions I have made. I would like to thank randomness. It takes the credit (blame) of so many good (bad) things in research, career and every aspect of life, that vpwtuie gjtbnjjsoz igwjgfvw bhutowg (I don't know what to say here and decide to let randomness speak for itself).

Chapter 1 Introduction

Climate changes in extratropical North Atlantic can alter tropical convection; it is one of the most prominent teleconnections in global climate, but also one of the least understood. Variations in climate records in the extratropical North Atlantic and the remote tropics from the last glacial period (~100,000 to 15,000 B.P.) show striking resemblance: when extratropical North Atlantic was warmer, the marine intertropical convergence zone (ITCZ) stays more northward and the Asian and West African monsoons become stronger; and vice versa. This dissertation is to understand the influence of extratropical North Atlantic climate changes on the tropical convection. We focus on detecting such influence in modern climate observation and future climate projections, and unraveling the atmospheric teleconnection mechanisms in idealized climate model simulations.

1.1 Millennial climate changes in the last glacial periods

Alternate cold and warm states occurred over the extratropical North Atlantic throughout the last glacial period, each lasting from hundreds of years to several millennia (Chiang and Friedman 2012; Cronin 2013). These cold and warm states, referred to as stadials and interstadials respectively, were identified in oxygen isotopes in Greenland ice cores. The isotope records also show sharp spikes suggesting abrupt transition to the relative warm interstadials. These warm interstadials usually last for hundreds of years, before the climate returns to stadials. Such a sequence of temperature changes are referred to as Dansgaard-Oeschger (DO) events, named after their discoverers, Willi Dansgaard and Hans Oeschger (Dansgaard et al. 1993).

Immediately preceding several large DO events are Heinrich events, identified by Heinrich (1988). The Heinrich events denote stadials of detrital sediment deposition by iceberg-rafting, usually accompanied by strong cooling in extratropical North Atlantic.

1.1.1 Response in tropical precipitation

The marine ITCZ is an equatorial band of heavy precipitation around global oceans, characterized by the convergence of the trade winds. Peterson et al. (2000) examined a 90,000-year ocean sediment core taken from the Cariaco Basin and showed that the northward (southward) shifts in the Atlantic ITCZ were concurrent with interstadial (stadial) conditions. By reviewing marine ITCZ changes over the Pacific and Atlantic during the last 30,000 years, Koutavas and

Lynch-Stieglitz (2004) concluded that the ITCZs in both ocean basins respond coherently to northern high latitudes climate changes, by moving north (south) in response to warming (cooling).

The monsoon, derived from the Arabic word for season, originally denotes the seasonal reversal in the direction of prevailing wind between summer and winter (Gadgil 2003). The summer monsoon brings warm and moist air from tropical oceans inland, forming the summer monsoon precipitation, an important component in the monsoon systems; whereas dry and cold wind from mid- and high-latitude continent characterizes the winter monsoon. The summer monsoon precipitation is of greater direct societal significance than the marine ITCZ, especially to agricultural societies. Weakened monsoon leads to less rainfall and usually lower crop yields.

Monsoon weakening over West Africa, adjacent to the Atlantic, periodically occurred throughout the late glacial period and the Holocene (Mulitza et al. 2008; Shanahan et al. 2009; Niedermeyer et al. 2009; Stager et al. 2011). A direct consequence of the West Africa monsoon weakening is drought over the Sahel, a semiarid region across Africa between the dry Sahara in the north and wet Guinea Coast in the south. Mulitza et al. (2008) found that both the Ai/Si and Fe/K ratios in the terrigenous sediment off the Senegal River mouth decrease during the Heinrich events, when the extratropical North Atlantic experienced strong cooling. The Ai/Si and Fe/K ratios are higher in the Senegal River sediment than the Sahel dust; and lower ratios off the Senegal River mouth suggest an increase in dust mobilization over the Sahel and a decrease in Senegal River discharge, implying drought conditions over West Africa. The relationship between extratropical North Atlantic sea surface temperature (SST) and the West African monsoon strength sustains through the Holocene (Shanahan et al. 2009).

1.1.2 Mechanisms of extratropical North Atlantic influence on tropical precipitation

Previous studies on the extratropical influence on tropical convection focused on the shift of the marine ITCZ. By imposing ice cover in high-latitude northern hemisphere (NH) of an atmospheric general circulation model (AGCM) coupled to a slab ocean, Chiang and Bitz (2005) found cooling across all longitudes in NH and a southward displacement of marine ITCZ, regardless of whether the ice was imposed over the North Atlantic or other ocean basins. They proposed a thermodynamic pathway over the ocean where SST, water vapor and surface wind synergize to propagate the extratropical North Atlantic cooling signal equatorward and shift the ITCZ. They also noted, from an energy flux perspective, that the cooling requires an increase in the poleward energy transport to the northern extratropics, which is accomplished by the southward shift in the location of the ITCZ. The energy perspective was later demonstrated by Kang et al. (2008), using an aquaplanet GCM for interpreting the response of tropical precipitation to extratropical forcing, in a context of zonally symmetric climate. Both frameworks focus on the response of marine ITCZ to extratropical SST cooling, and show a central role of tropical SST feedback.

1.2 Coordinated monsoon weakening

In addition to the West African monsoon change, both the South Asian and East Asian monsoons weakened during extratropical North Atlantic stadials (Wang et al. 2001; Gupta et al. 2003; Stager et al. 2011). Stager et al. (2011) showed that the height of Heinrich stadial 1 (16,000-17,000 years ago) coincided with a pronounced megadrought in the Afro-Asian monsoon region. Speleothem records from Hulu cave in China (Wang et al. 2001) show impressive one-to-one correspondence between stadial events in Greenland to monsoon weakening in Asia, throughout the last glacial. The link between North Atlantic cooling and Asian monsoon weakening also occurred during the Holocene, albeit at a weaker level (Gupta et al. 2003).

In the modern climate, a severe Sahel drought occurred in the late twentieth century, starting as an abrupt reduction in summer rainfall in the 1960's, and lasting for over two decades with limited recovery to date (e.g. Nicholson 1979; Folland et al. 1986). The severity of the drought is depicted in Nicholson et al. (1998): "Reportedly, a million people starved, 40% to 50% of the population of domestic stock perished, and millions of people took refuge in camps and urban areas and became dependent on external food aid".

A few studies have noted coincident summertime rainfall reductions in Asia. Ren et al. (2004) found that the Northern China portion of the East Asian monsoon region experienced a long-lasting drought since the 1960's, with similar local circulation changes as in the Sahel. Zhang and Delworth (2006) argued that rainfall variability in phase with that over the Sahel also occurred in the South Asian monsoon.

We compare the observed changes to summer rainfall over the Sahel, North China and India in Figure 1.1. All three regions exhibit similar inter-decadal variability of rainfall, the most striking of which was the monotonic dip in the 1960's.

1.3 Future monsoon rainfall change

CMIP5 models simulate an increase in mean precipitation of the East Asian summer monsoon (EASM) and the South Asian summer monsoon (SASM), but there is large uncertainty in simulated summer precipitation over the Sahel, India and North China (Christensen et al. 2013). The projection of the West African monsoon, for example, exhibits large model spread (Christensen et al. 2013). In addition, the failure in reproducing some monsoon components call to question the models' credibility in projecting future monsoon rainfall. A key to constraining the uncertainty and improving the predictability of future monsoon precipitation change is to understand how models simulate the spatial distribution of temperature changes, and how it is related to that of the precipitation change. In particular, the connection of extratropical North Atlantic to tropical convection in

paleoclimate studies suggest a significant role of the North Atlantic in future monsoon rainfall changes.

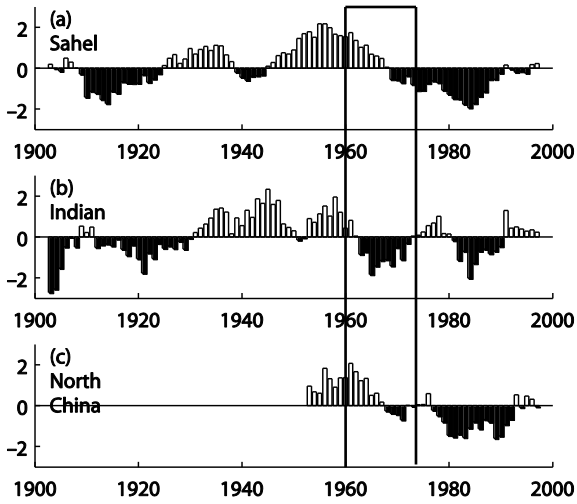

Figure 1.1 June -August variation of (a) Sahel rainfall, (b) All India rainfall and (c) North China rainfall. Data has been normalized and low-pass filtered with a 7-year running mean. Source of the indices: Sahel rainfall - Todd Mitchell at the University of Washington, using station data from NOAA Global Historical Climatology Network; North China rainfall - averaged over stations in the region of 35°N-45°N and 110°E-125°E, station data from Wang et al. (2000); All India rainfall from Parthasarathy et al. (1994).

1.4 Questions, hypothesis and structures of the dissertation

We address in this dissertation three questions related to the extratropical North Atlantic influence on tropical convection, as revealed in paleoclimate studies. Chapter 2 focuses on the mechanisms of communication from the extratropics to the tropics. Previous studies center on ITCZ shift in response to extratropical thermal forcing. Instead, we focus on the Sahel rainfall reduction in response to extratropical North Atlantic cooling that happened during the Heinrich events. We hypothesize that the atmosphere, as opposed to the tropical ocean for the ITCZ shift, plays a central role in mediating extratropical climate change signals to the West African monsoon. We show the viability of this hypothesis by analyzing the results from a general circulation model (GCM) and a regional climate model (RCM). The results in Chapter 2 have been published as Liu et al. (2014).

In Chapter 3, we investigate the late 1960s' rainfall changes over the Sahel, East Asia and South Asia. The question addressed is whether these changes are connected; and if so, what the common cause is. The hypothesis is that they signature a coherent monsoon weakening, and the monsoon weakening in turn is associated to a large-scale climate shift over Eurasia and Africa. We detect the joint variability of observed rainfall and other climate fields that are relevant to monsoons, and examine the monsoon change one by one. Our results support the hypothesis. We also utilize 20th century climate simulations and undertake idealized

GCM simulations to suggest the monsoon weakening and climate shift have their origin in the extratropical North Atlantic, as happened in the last glacial period. The results in Chapter 3 have been published as Liu and Chiang (2012).

We turn to future climate in Chapter 4. We examine if the climate change patterns associated with extratropical North Atlantic in paleoclimate studies and 20th century observations exist in 21st century climate simulations. We compare those patterns in Coupled Model Intercomparison Project Phase 5 (CMIP5) 20th century and 21st century climate simulations. We investigate whether these models exhibit a consistent relationship between those changes, despite having large spread in simulating future changes in extratropical North Atlantic temperature and tropical rainfall.

1.5 Future work

The impact of extratropical North Atlantic climate change has been felt in the past, current and future climate, and involves complex physical processes and multiple climate realms. A complete understanding of the extratropical North Atlantic climate change impact requires studies across all the periods, processes and realms, well beyond the scope of this dissertation. Below, we outline the outstanding questions to address in order to advance knowledge of this teleconnection.

The transient climate response to North Atlantic cooling in climate models should be investigated in order to further understand the teleconnection mechanisms. This follows our research that identifies atmospheric temperature as the bridge connecting those changes to tropical monsoons, and that demonstrates how the equilibrated atmospheric temperature change is maintained in response to those changes. Focus should be given to the transient response of both the atmospheric circulations and related energy transport, and radiative feedbacks. The result will elucidate how the atmospheric temperature change is built up, a key step of the extratropics-tropics connection.

Results in Chapter 2 show that clouds augment the North Atlantic signal. This is supported in previous studies. Kang et al. (2008) showed that cloud feedbacks are important for the sensitivity of tropical rainfall response to extratropical forcings. Martin et al. (2013) showed that a realistic climatology of stratocumulus cloud is a prerequisite to correctly capture the Atlantic-African teleconnection. The 1960's climate change studied in Chapter 3 provides a valuable example to test if models' simulation of North Atlantic influence is related to their efficacy of simulated clouds. One can use long-term land-based observation, like that from the International Comprehensive Ocean-Atmosphere Data Set (ICOADS, Woodruff et al. 2011) to compare how well models simulate cloud changes related to the late 1960s' shift. The results will be compared with simulated impacts of extratropical North Atlantic climate change, to study the cloud influence. One can also perturb the cloud parameters in a climate model and investigate the sensitivity of the simulated impact of North Atlantic climate change, to constrain the uncertainty of regional climate sensitivity.

In Chapter 2 we also find evidence suggesting a ' ventilation' mechanism, originally proposed by Chou and Neelin (2004), acts as the mechanism for West African monsoon weakening to North Atlantic cooling. This mechanism should be investigated through analysis of the change in moist static energy, and how it suppresses convection.

So far the focus has been given to the teleconnection from the extratropical North Atlantic to Africa. The South and East Asian monsoons are another region of interest. The zonal propagation of the North Atlantic influence on the Asian monsoons differs from the teleconnection to West Africa, as this pathway is mainly along midlatitude jets, and the East Asian monsoon is particularly sensitive to midlatitude dynamics. A few studies feature a wavetrain that connects the North Atlantic to the monsoons (e.g. Luo et al. 2011; Lee and Hsu 2013), but changes in Eurasia surface and air temperature, altering land-sea contrast, have also shown to be important in teleconnecting the changes in the North Atlantic SST to the Asian monsoons (e.g. Goswami et al. 2006; Wang et al. 2009). Both the dynamics and thermodynamics should be analyzed to develop a mechanistic view of the influence of the extratropical North Atlantic on the Asian monsoons. Successful development of the mechanism will help improve both understanding and predictability of the Asian monsoons.

Chapter 2 Atmospheric teleconnection mechanisms of extratropical North Atlantic SST influence on Sahel rainfall

2.1 Abstract

We investigate the atmospheric teleconnection mechanism connecting North Atlantic cooling to the West African monsoon weakening in an atmospheric general circulation model. We find that the simulated atmospheric cooling, originating from the extratropical North Atlantic forcing region, readily reaches North Africa and the Sahel. Atmospheric cooling anomalies imposed on northern boundary of a RCM of the Sahel responds with a rainfall reduction over the Sahel that is similar in the GCM; this indicates the central role for the atmospheric cooling in the teleconnection. In the GCM simulation, extratropical North Atlantic cooling is augmented by a positive low cloud feedback and advected downstream, cooling Europe and North Africa, where the cooling is further amplified by a reduced greenhouse effect from decreased atmospheric specific humidity. The results suggest a thermodynamic pathway for the extratropics-tropics teleconnection found in paleoclimate studies of the last glacial period. The teleconnection may also be applicable to understanding the North Atlantic influence on Sahel rainfall over the 20th century. This work was published in Liu et al. (2014).

2.2 Introduction

Drought conditions periodically occurred over the Sahel throughout the late glacial period and the Holocene, and have been tied to abrupt cold events, the Heinrich events, over the North Atlantic (Mulitza et al. 2008; Shanahan et al. 2009; Niedermeyer et al. 2009; Stager et al. 2011). More recently, a severe Sahel drought occurred in the late twentieth century, starting as an abrupt reduction in summer rainfall in the 1960' s, and lasting for over two decades with limited recovery to date (e.g. Nicholson 1979; Folland et al. 1986)

Variation in the Atlantic meridional overturning circulation (AMOC) is thought to be the leading cause of the North Atlantic abrupt climate changes. A slowdown of the AMOC reduces the ocean heat transport into the North Atlantic, cooling the extratropical North Atlantic in particular where the mean ocean heat transport convergence occurs. This hypothesis was first proposed by Broecker et al. (1985), and subsequently supported by many other studies (see Alley 2007 for a review). Moreover, simulations of the AMOC slowdown in various coupled climate models (e.g. Vellinga and Wood 2002; Zhang and Delworth 2005; Cheng et al. 2007; Chiang and Friedman 2012) all show global climate impacts including a drying of the Sahel, similar to what is inferred from paleodata (an example can be seen in Figure 5 of Chiang and Friedman 2012). Thus, there is strong model evidence for a causal link between the North Atlantic cooling and Sahel drought.

Previous studies have led to a hypothesis that atmospheric teleconnections of extratropical North Atlantic cooling cause the impacts in the Sahel seen in AMOC slowdown experiments (see Chiang and Friedman 2012 for a review). Motivation for this hypothesis comes from the fact that an atmospheric general circulation model (AGCM) coupled to a slab ocean, with cooling prescribed in the extratropical North Atlantic (50N-70N) is able to produce very similar global climate changes as in AMOC slowdown experiments. An example simulation using the Community Atmosphere Model 3-slab ocean is shown in Figure 2.1. (The simulation is described in detail in Chiang and Friedman 2012.) The simulation shows intense cooling over the extratropical North Atlantic that extends over the whole Northern Hemisphere (NH), in particular to North Africa (Figure 2.1a), and a strong rainfall reduction over the Sahel. A significant weakening of the monsoon winds occurs over North Africa as indicated by the anomalous northeasterly wind (Figure 2.1b), co-incident with a meridional pressure gradient anomaly between the anomalous high pressure to the north, and low pressure to the south. The model results thus show a continental climate change primarily in temperature and sea level pressure (SLP), which may act to bridge the extratropical North Atlantic cooling to the rainfall reduction over the Sahel.

The mechanism for this atmospheric teleconnection is however still not known; this is the focus of our study. Our approach is centered on the temperature and SLP changes over the Sahara, north of the Sahel, that are apparent in the above simulations. Previous studies support the idea that temperature and (consequently) SLP over North Africa alters Sahel rainfall. Haarsma et al. 2005) found in observations that Sahel rainfall was related to mean SLP over the Sahara, the latter in turn was related to surface temperatures over North Africa. Biasutti et al. 2009) argued, based on lead– lag correlation, that variation in the Sahara SLP caused variation in the Sahel rainfall. A cursory examination of climate changes associated with Sahara temperature supports this association: the left column of Figure 2.2 shows the difference of precipitation, surface temperature and SLP over the North Atlantic and North Africa for July to September between the eight coldest and eight warmest periods in the Sahara since 1979. It shows that a colder Sahara is accompanied by higher Sahara SLP and reduced Sahel rainfall (and increased rainfall along the Guinea Coast). The cooling over the Sahara may weaken the land-sea contrast and thus the monsoon flow. In addition, advection of air with low moist static energy (MSE) limits the northward extent of the land convection zone by displacing high MSE air that favors deep convection, a process known as the “ ventilation” mechanism (Chou et al. 2001). The intrusion of low

MSE resulting from cooling in the north may thus reduce rainfall over the Sahel. Taken together, these results suggest that cooling in North Africa driven by extratropical North Atlantic cooling can reduce the rainfall over the Sahel, possibly by weakening the land-sea thermal contrast and reducing the MSE.

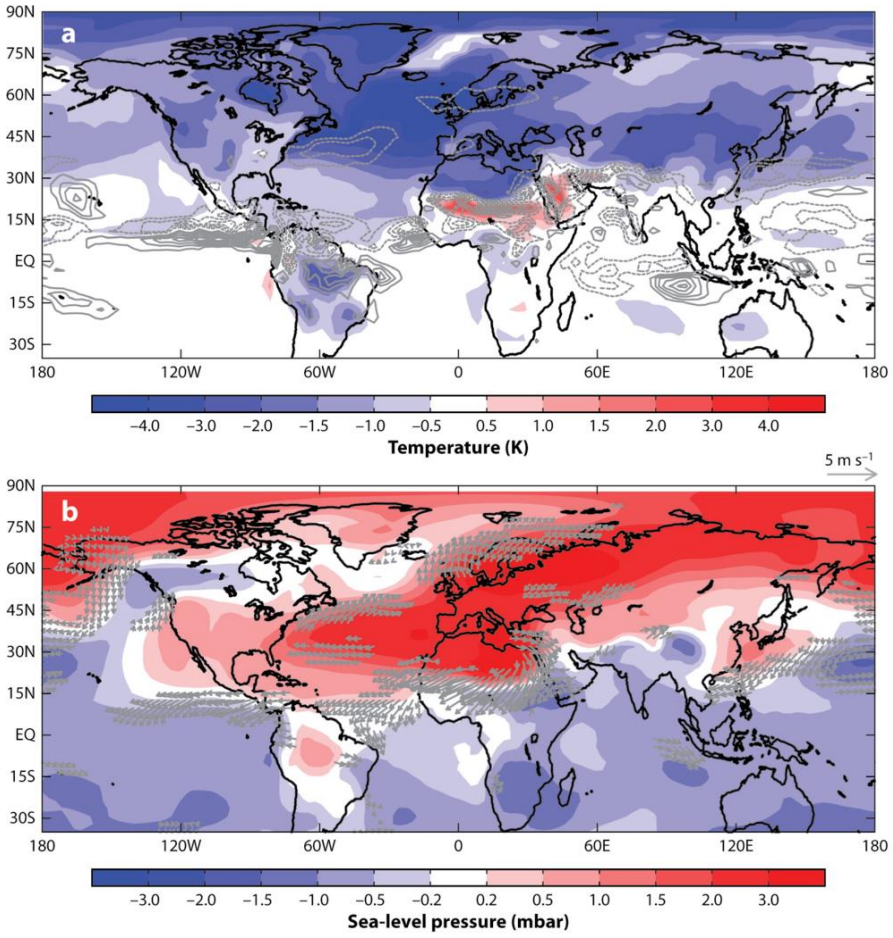

Figure 2.1. July through September anomalies from a Community Atmosphere Model 3-slab ocean simulation, where a 30 W m^{-2} cooling is applied to the slab ocean in the midlatitude North Atlantic. Both control and cooling simulations were 30 years long, and the anomalies are derived from the last 20 years. (a) Temperature (shaded; K) and precipitation (gray contour; interval is 0.5 mm per day, and dashed lines are negative). (b) Sea-level pressure (shaded; millibars) and lowest-level wind anomalies (reference vector is 5 m s^{-1}; only anomalies exceeding 1 m s^{-1} in magnitude shown). The images show the hemispheric impact of North Atlantic cooling and resulting modification of the tropical circulation. Adopted from Chiang and Friedman (2012)

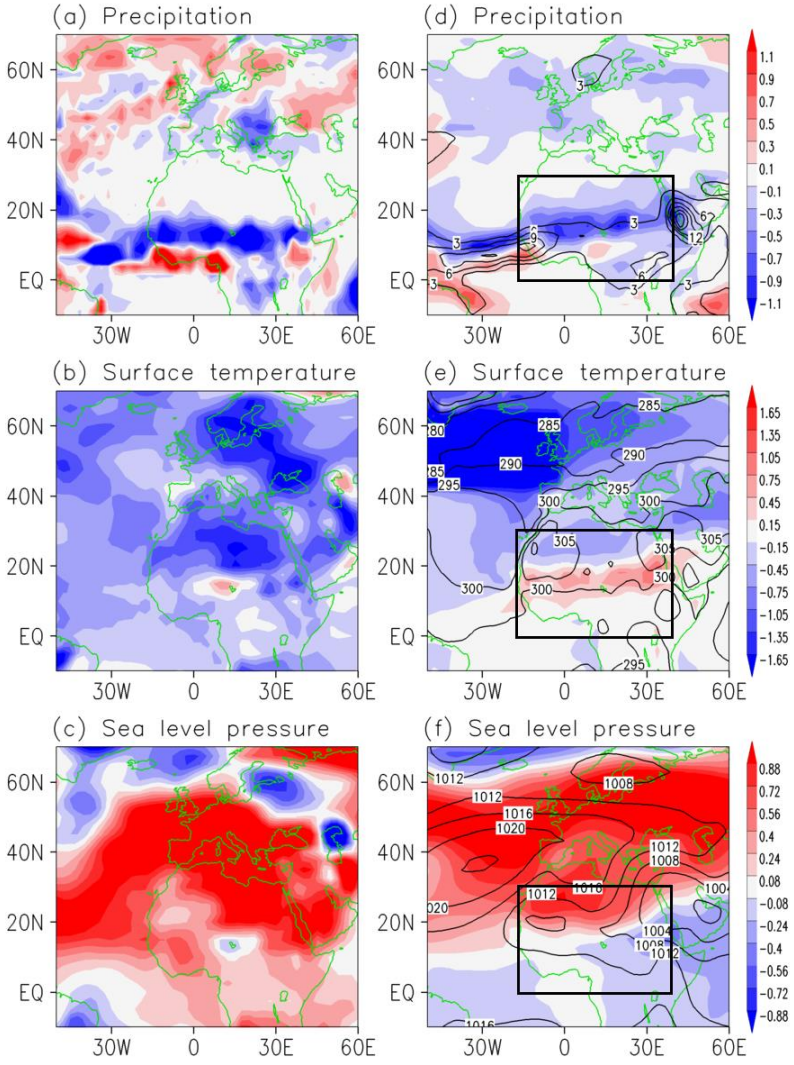

Figure 2.2 July through September averaged precipitation (upper panels; mm/day), surface temperature (middle panels; K) and sea level pressure (lower panels; hPa). Left column: difference of observed precipitation and reanalysis surface temperature and SLP between Sahara cold years (1979, 1981, 1984, 1985, 1992, 1993, 1996-1997) and Sahara warm years (1998-1999, 2001-2003, 2005-2006, 2008). Right column: control run (contour) and anomalies in the cooling minus control run (shading), in the AGCM simulation using CAM3.5 coupled with a slab ocean model with 2K cooling prescribed in between 45-60 over North Atlantic. Both observation and model simulation show Sahel rainfall reduction, and broad cooling and a SLP increase over Sahara. The color bar for each row is relevant to both panels of the row. The black box denotes the plotted domain of WRF simulation in Fig. 5a-5c. Observations and reanalysis data source: precipitation, GPCP combined precipitation data, developed and computed by the NASA/Goddard Space Flight Center's Laboratory for Atmospheres as a contribution to the GEWEX Global Precipitation

Climatology Project (Adler et al. 2003); Surface temperature and SLP: NCEP/NCAR Reanalysis 1 (Kalnay et al. 1996).

Our study analyzes the AGCM-slab ocean simulation which produces a reduction in Sahel rainfall in response to prescribed extratropical North Atlantic cooling, with the goal of developing a mechanistic view of this teleconnection. We hypothesize that the North Atlantic influence is communicated to the Sahel through cooling air temperatures over North Africa. We show the plausibility of our temperature hypothesis by showing that the Sahel rainfall in a regional climate model (RCM) simulation is reduced when we impose tropospheric cooling (and related geopotential height and humidity changes) in the lateral boundary conditions of the model over the North African region. We then apply various diagnostic analyses on the AGCM model simulation, including a moisture budget analysis over West Africa. We also analyze radiative feedback and atmospheric energy transport to determine how extratropical North Atlantic cooling is communicated to lower latitudes. Ultimately, our goal is to understand how and why North Atlantic stadials are linked to rainfall change over the Sahel during past climates, and also to see if such mechanisms are applicable to today' s climate.

2.3 Experiments and methods

2.3.1 Experiments

We use the National Center for Atmospheric Research (NCAR) Community Atmosphere Model version 3.5 (CAM3.5) coupled to a fixed-depth slab ocean model, which interacts thermodynamically with the atmosphere, but has no representation of ocean dynamics (Collins et al. 2006; Chen et al. 2010). The atmospheric model is configured with 26 vertical levels, and 64x128 horizontal grids. A monthly-varying ' Q-flux' is derived from surface fluxes extracted from a fixed-SST simulation forced with global SST climatology, and applied to the model slab. All greenhouse gas and aerosol forcings are constant as present day values.

The slab ocean model is required, as the thermodynamic ocean-atmosphere interaction is essential to communicating the extratropical influence to the tropics (Chiang and Bitz 2005). We use the base configuration described above to undertake two sets of simulations. In the first set, we replace the slab ocean in the North Atlantic over the 45N-60Nlatitude band with climatological monthly-varying SSTs, and run this configuration to equilibrium. In the second set, we also apply fixed SSTs over the same North Atlantic region, but uniformly cool the applied SST by 2K. The applied cooling is less than half of the typical estimates of extratropical North Atlantic SST changes from interstadials to stadials (~4-6K, van Kreveld et al. 2000), but is sufficient to force a significant reduction in Sahel rainfall (see Section 2.4). Both simulations are run for 60 years, and the climatology of the last 20 years is used for analysis. The difference between the climatologies is used as the response to the extratropical cooling. The GCM

anomalies are shown as the July-August-September (JAS) average in the following sections.

To explicitly show that the cooling over Sahara (and related low MSE) can drive a Sahel rainfall decrease, we apply the cooling to the lateral boundary condition in a regional model simulation of the Sahel. The regional model allows us to isolate the impact of atmospheric cooling anomalies from the Sahara on the Sahel, enabling us to directly test the hypothesis that extratropical North Atlantic cooling leads to Sahel rainfall reduction through cooling the Sahara. We use the NCAR Weather Research and Forecasting Model (WRF; Skamarock et al. 2008) version 3.3. It is a non-hydrostatic model with 28 vertical levels, with the top of the atmosphere set to 50 hPa. The domain chosen for the simulation is from 16.9W to 39.9E and from 30.7S to 29.3N, incorporating the whole of Africa and in particular the Sahara.

The choice of horizontal resolution and physics options basically follows that of the WRF simulation of North Africa by Patricola and Cook (2010). The horizontal resolution used is 90 km, and the physics schemes are the Mellor-Yamada-Janjic planetary boundary-layer scheme (Janjic 1994), the Monin-Obukhov Janjic surface-layer scheme (Monin and Obukhov 1954; Janjic 1994; Janjic 1996; Janjic 2002), the Purdue Lin microphysics scheme (Lin et al. 1983), and the RUC land-surface model (Smirnova et al. 1997). Patricola and Cook (2010) showed that WRF with these options is able to simulate a sufficiently accurate climatology over the Sahel. We use the Zhang-McFarlane cumulus scheme (Zhang and Mcfarlane 1995), which differs from Patricola and Cook (2010) but is the same convection scheme used in our CAM3.5 AGCM simulations. We also use newer radiation schemes that are available in WRF version 3, the RRTMG longwave and shortwave scheme (Mlawer et al. 1997). The simulation time step is 180 seconds.

The National Centers for Environmental Prediction (NCEP) – Department of Energy (DOE) Atmospheric Model Intercomparison Project (AMIP-II) reanalysis (R-2) 6-hourly data (Kanamitsu et al. 2002) are used to specify the lateral boundary conditions for the control simulation. Monthly temperature, geopotential height, and relative humidity anomalies from the GCM runs are then added to the 6-hour reanalysis data for the cooling simulation. The anomalies are added only at the northern boundary (and the relaxation zone) of the domain, since the purpose of the WRF simulation is to test our hypothesis that it is through modifying atmospheric temperature/energy over the Sahara that extratropical North Atlantic influences Sahel rainfall. Climatological skin temperature in the reanalysis data is used for SST. SST changes are not the focus of our study; and since the land makes up most of the domain, SST has little influence in our simulations. For both the control and cooling simulations, we conduct an ensemble of 10 runs, starting from June 2 of each year from 2000 to 2009 and ending on September 2 of the following year. We run each simulation for fifteen months in order for the soil moisture to spin up, as soil moisture spin-up is important in the semi-arid Sahel region. The daily data from July and August of the following year are averaged as the summer climate. We averaged the ten summer climates separately for the control and cooling runs, and examined their differences.

2.3.2 Diagnosis

Two sets of diagnostic analyses are applied to the GCM simulation. In order to understand the communication of the cooling from the extratropical North Atlantic to other regions, we diagnose the atmospheric energy budget by examining both the top of atmosphere (TOA) energy flux and the atmospheric energy transport. We utilize a radiative kernel technique to separate changes of the TOA energy budget due to individual component changes (Soden et al. 2008):

$$\delta R \approx \sum_i \frac{\partial R}{\partial X_i} \delta X_i, \tag{2.1}$$

where δR is the change in TOA energy flux, and terms inside the summation designate the change of R due to individual component X_i, including surface temperature T_s, atmospheric temperature T, water vapor q, surface albedo α and clouds C. The differential $\partial R/\partial X_i$, which represents the change in TOA energy flux due to a unit change in each component, is the radiative kernel. Kernels for q and C are further split into shortwave (SW) and longwave (LW). We use radiative kernels calculated in CAM3 (Shell et al. 2008; Soden et al. 2008) for all components but clouds. TOA energy flux change due to clouds is calculated as the adjusted cloud radiative forcing (CRF), defined as the difference between the TOA all-sky and clear-sky fluxes, with changes of CRF caused solely by non-cloud components removed (Shell et al. 2008). We also calculate the horizontal advection of MSE to examine how circulations adjust to balance the prescribed cooling and TOA radiative flux changes.

In order to understand the Sahel rainfall response to extratropical cooling, we diagnose the vertically integrated moisture budget equation as in Chou and Neelin (2004) and Chou et al. (2009) with some modification:

$$\delta P \approx -\langle \omega \frac{\partial \delta q}{\partial p} \rangle - \langle \mathbf{v} \cdot \nabla \delta q \rangle - \langle \delta \omega \frac{\partial q}{\partial p} \rangle + \langle \delta \mathbf{v} \cdot \nabla q \rangle + \delta E, \tag{2.2}$$

where $\langle . \rangle$ denotes vertical mass integration through the troposphere, and P, ω, q, p, E and v denote precipitation, pressure velocity, specific humidity, pressure, evaporation, and horizontal velocity, respectively. The total rainfall change, δP, thus can be approximated by the summation of 1) anomalous vertical moisture transport associated with anomalous moisture δq , 2) anomalous horizontal moisture transport associated with anomalous moisture δq, 3) anomalous vertical moisture transport associated with anomalous vertical flow $\delta \omega$, 4) anomalous horizontal moisture transport associated with anomalous horizontal flow $\delta \mathbf{v}$ and 5) anomalous evaporation, as shown from left to right respectively in the right hand side (RHS) of the equation above.

2.4 Climate response to extratropical North Atlantic cooling

2.4.1 Climate response over the Atlantic and North Africa

Surface temperature and SLP are closely related to the Sahel rainfall in both observations and model simulations (Haarsma et al. 2005; Biasutti et al. 2009; Liu and Chiang 2012); therefore we begin presenting the GCM-simulated JAS averaged climate response to extratropical North Atlantic cooling by showing those three fields (right column of Figure 2.2). In the control run, the oceanic ITCZ is located north of the equator over the Atlantic, extending into northeast Brazil and the west coast of the Sahel. Prescribed extratropical North Atlantic cooling in turn leads to a cooling of the North Tropical Atlantic SST and a southward displacement of the Atlantic ITCZ; these responses are well-known (e.g. Chiang and Bitz 2005). Precipitation in the Sahel is reduced by over 25% in response to the cooling, with a maximum anomaly of over 1 mm/day (Figure 2.2d). Temperatures to the north and west of the Sahel are colder, with a ~1K surface cooling across the midlatitude Atlantic and Europe (Figure 2.2e). The cooling south of 40N, though smaller, extends all the way to near the equator over the ocean, and to the boundary between the Sahara and the Sahel over North Africa. The maximum cooling over the Sahara is more than 0.5 K, and located near the simulated heat low around 20N. Over the Sahel, temperatures are warmer in association with reduced rainfall, which supports a reduced evaporative cooling and increased solar radiation at the surface.

SLP over the Sahara is also increased in association with the North Atlantic cooling (Figure 2.2f); this response is likely causally linked to the cooling (discussed later). The pressure increase over North Africa peaks near the climatological Sahara Low with a magnitude of ~1 hPa, leading to decreased meridional SLP contrast between the Sahara and the Gulf of Guinea. Overall, a broad cooling and coincident SLP increase appear over the Atlantic and North Africa, and rainfall is reduced over the Sahel with a slight increase over the Guinean Coast, consistent with results from previous studies on extratropical North Atlantic cooling (e.g. Mulitza et al. 2008; Liu and Chiang 2012). The simulated response in North African climate to extratropical North Atlantic cooling resembles the observed difference of climate in cold and warm Sahara periods (left column of Figure 2.2), lending confidence to our hypothesis that temperature over the Sahara broadcasts the extratropical signal to the Sahel.

Extratropical North Atlantic SST cooling induces changes in atmospheric temperature, specific humidity, and clouds, which exert feedbacks to the initial temperature change by altering the TOA energy budget. We present these changes of in Figure 2.3. Mean tropospheric temperature, defined as the mass-weighted vertical average of atmospheric temperature from the surface to 100mb, broadly decreases in the domain (Figure 2.3a). Mean tropospheric specific humidity, calculated similarly to mean tropospheric temperature, decreases in response to the cooling (Figure 2.3b), following the Clausius-Clapeyron relation in regions where relative humidity varies little, especially north of the Sahel. The drop in humidity appears to peak over convective regions, in particular in the Sahel where mean tropospheric humidity is reduced by about 0.3 g/kg; this is consistent with the

reduction in convection there. Changes in both mean tropospheric temperature and humidity (and also geopotential height which is small, not shown) result in a substantial decrease in MSE (Figure 2.3c), with two maxima corresponding to the maximum change of temperature in the extratropics, and of humidity in the Sahel.

In the extratropics, cooler SST over the North Atlantic favors boundary layer inversions, leading to an increase in low clouds (surface to 700 mb, Figure 2.3d). In the tropics, low clouds decrease over the Sahel in association with the reduction in convection. High clouds (400mb to the model top) decrease over both the northern ocean and the Sahel and increase over the southern edge of climatological ITCZ and northeast Brazil, in accordance with the rainfall change (Figure 2.3e). The change in middle clouds (700 mb to 400 mb) generally follows that of low clouds except for a slight decrease over the extratropical North Atlantic (not shown).

2.4.2 Vertical profile of climate anomalies over North Africa

The GCM-simulated Sahelian rainfall reduction in response to extratropical North Atlantic cooling largely results from anomalous convection and monsoonal flow. We present vertical profiles of the circulation, temperature and humidity anomalies from the cooling minus control GCM simulations to illustrate this point (Figure 2.4). All fields are averaged between 10W and 30E. Substantial cooling reaches 20N, with a maximum of more than 0.7K in the middle troposphere (Figure 2.4a). The strong cooling over the Sahara results in a meridional temperature gradient anomaly. Over the Sahel between 10N and 20N, a vertical dipole is seen with warming near the surface and cooling in the middle and upper troposphere. The dipole is likely a consequence of the increase in the Bowen ratio at the surface and the suppression of deep convection; combined, they lead to less water vapor being evaporated into the atmosphere from the surface and brought to the middle troposphere for condensation, while more heat warms the lower troposphere in the form of sensible heat. The specific humidity is reduced considerably over North Africa and the reduction is largely confined to the lower troposphere, consistent with the reduction of convection there (Figure 2.4b). The magnitude of change generally reaches 0.3 g/kg, and can exceed 0.5 g/kg in the lower troposphere over the Sahel.

The vertical wind anomaly shows a 20% increase in subsidence north of the Sahel and a decrease in ascent over the Sahel (Figure 2.4c). The substantial sinking anomaly near the climatological subsidence zone over the Sahara acts to balance the cooling through adiabatic compression. Over the Sahel, there is a dipole with enhanced (weakened) uplift below (above) 800mb, indicating decreased deep convection and a slight enhancement of shallow thermal convection.

The upper level tropical easterly jet (TEJ) at 200mb, with a climatological core around 10N, induces upper level divergence and thus lower level convergence and convection (Nicholson 2009). In the experiment, the TEJ is weakened in response to the negative temperature gradient (Figure 2.4d), similar to the observed circulation change in Sahel dry years as found by Nicholson (2009).

The mid-level African easterly jet (AEJ) is only vaguely simulated at 600mb around 17N in the control run. A strong easterly anomaly, however, appears at 12N between 500mb and 800mb in the experiment, suggesting a southward shift

and strengthening of the AEJ. The easterly anomaly is likely caused by the positive temperature gradient as a result of the low-level warming between 10N and 20N (Figure 2.4a). Grist and Nicholson (2001) found in observations that the AEJ induces cyclonic (anticyclonic) shear to its south (north) and that a southward AEJ shift likely displaces the rainbelt southward, thus reducing the rainfall over the Sahel. Cook (1999) and Patricola and Cook (2008) found that changes in the AEJ, which depend on the meridional temperature/soil moisture gradients, can also reduce rainfall by transporting moisture away from the Sahel. Therefore, a positive feedback exists in our simulation: as a rainfall decrease reduces soil moisture and thus leads to surface warming, a consequent positive temperature gradient in the low level strengthens the AEJ and displaces it southward, which in turn further reduces rainfall over the Sahel.

The southwesterly monsoon flow, which extends to 800mb climatologically, is weakened by up to 30% in the lower troposphere (Figure 2.4d and e), probably due to the diminished meridional temperature/pressure gradient. Climatological northerlies from the Sahara converge with the monsoon flow over the Sahel. The strengthened northerlies in the cooling simulation bring anomalously dry and cool air to the Sahel, weakening the low-level convergence and shifting it southward.

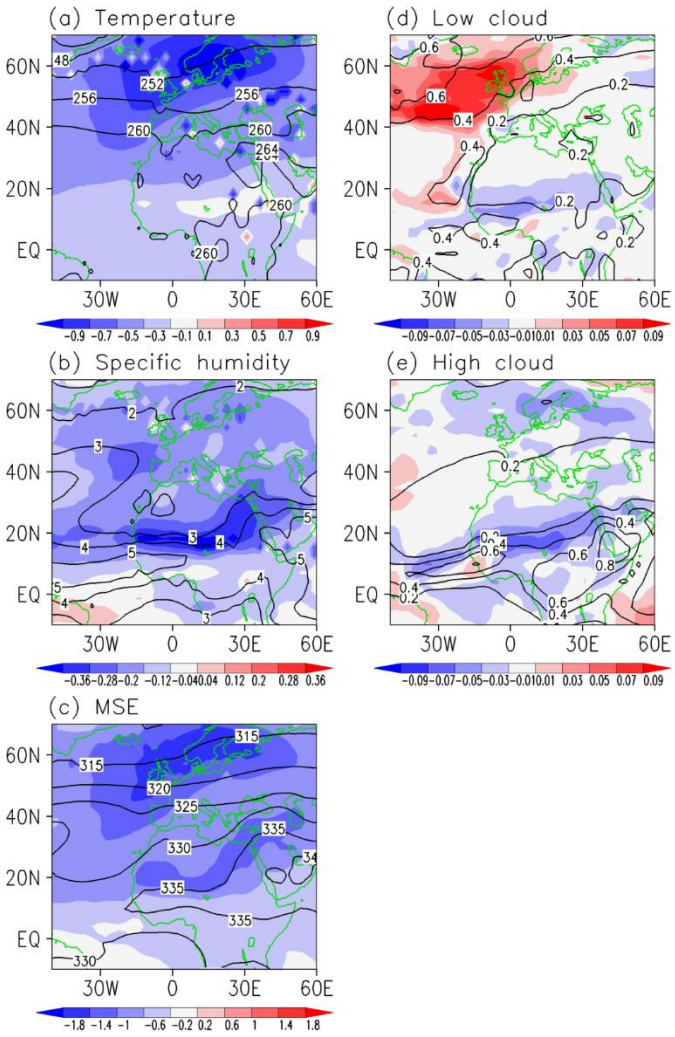

Figure 2.3 July through September averaged (a) mean tropospheric temperature (K), (b) mean tropospheric specific humidity (g/kg), (c) mean tropospheric moist static energy (kJ), (d) low cloud coverage (fraction) and (e) high cloud coverage (fraction) in the CAM3.5 simulation for both the control run (contour) and anomalies in the cooling minus control run (shading)

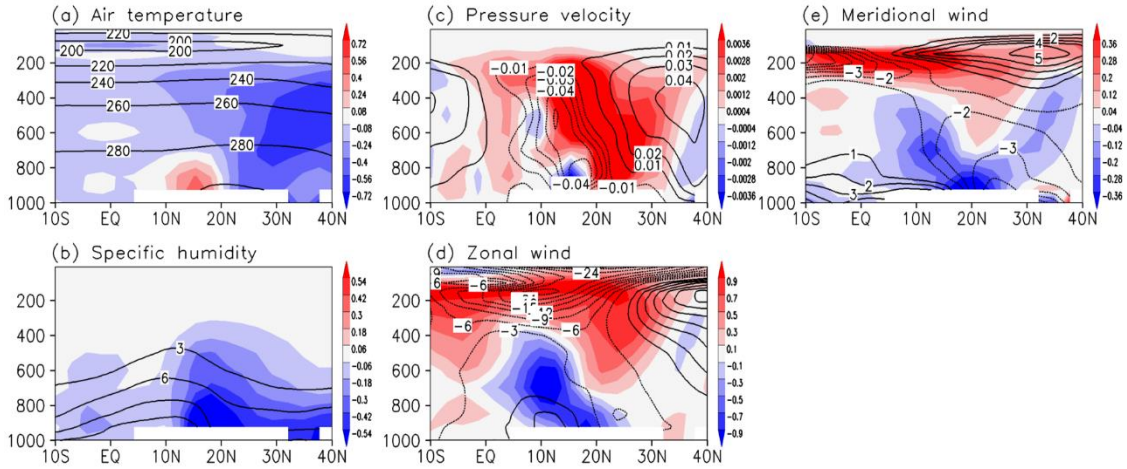

Figure 2.4 Same as Figure 2.3 but for pressure-level vertical profile of (a) air temperature (K), (b) specific humidity (g/kg), (c) pressure velocity (Pa/s), (d) zonal wind (m/s) and (e) meridional wind (m/s). All fields are averaged between 10W and 30E. Regions of no data (topography) are left blank.

2.5 Testing the temperature hypothesis using a WRF simulation of the Sahel

While the GCM-modeled Sahel climate response is consistent with the influence of atmospheric and surface cooling over the Sahara, it does not demonstrate causality. We explicitly show that the cooling can drive a rainfall decrease over the Sahel, by applying temperature, humidity, and geopotential height anomalies as exterior boundary condition in a WRF simulation of the Sahel. With those GCM anomalies applied only to the northern boundary of the RCM domain, the WRF simulation produces a response in Sahel climate to Sahara tropospheric cooling comparable to the response in Sahel climate to extratropical North Atlantic cooling in the GCM. The simulated precipitation anomaly (Figure 2.5a) exhibits finer structures due to the higher resolution of the WRF model, but the overall change resembles that in the GCM. Drying with a maximum of over 1 mm/day appears between 10N and 20N over North Africa; both the location and magnitude of this drying are comparable to the GCM response (Figure 2.2d). Scattered drying and wetting are shown south of the Sahel in WRF, leading to a neutral or slightly positive overall precipitation change as in the GCM. The overall precipitation change, in particular the substantial decrease in the Sahel, suggests a retreat of the monsoon convection, consistent with the ventilation mechanism where low MSE from the north limits the extent of land convection. Precipitation north of 10N along the west coast, which is influenced by the oceanic ITCZ (Figure 2.2d), exhibits little change, as change in SST is not taken into account in the WRF simulation.

The regional model also reproduces the surface temperature and pressure response to atmospheric cooling (Figure 2.5b and c) with magnitudes comparable to those in the GCM experiment. Cooling spreads from the northern boundary of the domain to the vicinity of Sahel, where the surface warms as a result of the rainfall reduction. As WRF does not output SLP, we take surface pressure instead for comparison. The surface pressure in WRF (Figure 2.5c), similar to the SLP in the GCM (Figure 2.2f), increases over the Sahara, reducing the strength of the Sahara Low and thus the pressure gradient between North Africa and the tropical Atlantic.

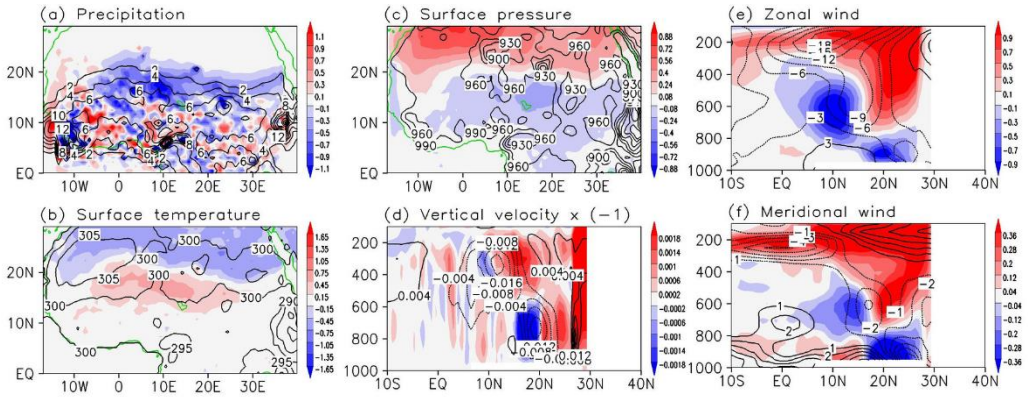

Figure 2.5 July-August averaged climate over Africa for the control run (contour) and anomalies in the experiment (shading) of the WRF simulation with temperature, geopotential height and relative humidity anomalies from the AGCM cooling runs forced at the northern boundary of the domain. (a)-(c), surface fields: (a) precipitation (mm/day), (b) surface temperature (K) and (c) surface pressure (hPa). Only portion of the domain north of the equator is shown for clarity. (d)-(f), pressure-level vertical profile of wind component: (d) vertical velocity (multiplied by -1 in accordance with the sign of pressure vertical velocity; m/s), (e) zonal wind (m/s) and (f) meridional wind (m/s). All vertical profiles are averaged from 10W to 30E and the plots are extended to 40N to have the same scale as in Figure 2.4. Regions of no data (topography and north of 30N in the plots for vertical profiles) are blank. The WRF cooling simulation generally simulates the Sahel rainfall reduction, and associated temperature, pressure, and circulation changes as in the GCM.

Vertical profiles of the WRF-simulated wind anomalies, averaged from 10W to 30E are also shown in Figure 2.5 (compare to the GCM fields in Figure 2.4). The WRF responses to prescribed anomalies relevant to cooling on the northern lateral boundary condition are largely comparable to those of the GCM simulation, except that since the mean Sahel uplift region is located somewhat north (˜20N) of the GCM uplift region (˜17N), the WRF anomalies are similarly shifted. The sinking anomaly north of 20N and the vertical dipole over the Sahel are apparent in WRF simulation (Figure 2.5d), although the near-surface uplift anomaly south of 20N looks deeper in WRF than in the GCM. The response of the zonal wind (Figure 2.5e) in the upper troposphere, which basically follows the thermal wind, is

identical with that in CAM (Figure 2.4d). However, unlike the anomalous low-level northerlies south of 30N in the GCM, WRF exhibits anomalous low-level northerlies from 15N-30N, and anomalous low-level southerlies to the south of 15N (compare Figure 2.5f and Figure 2.4e). As a consequence, there is a slight southward shift of the low-level convergence center toward the Guinea Coast, bringing about the anomalous low-level convergence around 18N and compensating divergence around the 600mb level. The shifted convergence is weaker and the convection is shallower in the cooling simulation compared with the climatology, consistent with the reduction in rainfall.

Differences in details aside, anomalies relevant to cooling from CAM3.5 forced only at the northern lateral boundary of the WRF domain generally simulate the Sahel rainfall reduction and associated temperature, pressure, and circulation changes as in the GCM experiment which is forced with extratropical North Atlantic SST cooling. Our WRF simulation thus provides strong evidence that the Sahel rainfall changes in the GCM experiment result from large-scale cooling in tropospheric temperatures north of the Sahel.

2.6 How is the cooling communicated and maintained?

Cooling over the Sahara is key to our proposed teleconnection. It then begs the question of how the temperature changes are communicated from the high-latitude North Atlantic. We have shown that the prescribed 2K SST cooling in the extratropical North Atlantic causes significant cooling in the Atlantic sector, with a magnitude generally larger than 1K in the midlatitude Atlantic and Europe, and as much as 0.5K near the Sahel. How is such a strong cooling response maintained both near and far from the source?

We first explore this question by evaluating the radiative feedbacks that help amplify and maintain the cooling far from its source region. TOA radiative flux anomalies in response to the North Atlantic cooling in the GCM simulations are shown in Figure 2.6, separated into contributions by cloud, moisture, and temperature changes (downward is positive, so negative values mean energy loss and thus more cooling of the atmosphere, acting as a positive feedback). As shown in Figure 2.3, a sizable increase of low clouds, presumably stratus, appears over the ocean in association with prescribed cooling; this is likely due to the surface-cooling induced boundary layer inversion. The stratus cloud cover exerts a strong positive feedback by reflecting more SW than it absorbs LW (Figure 2.6a and c). This cooling effect dominates in the extratropics. On the other hand, cloud cover decreases over North Africa, in particular over the Sahel, consistent with the reduced convection there. Reduced cloud cover allows for more incoming SW to the atmosphere but also leads to more outgoing longwave radiation (OLR) (Figure 2.6a and c). The two competing effects largely cancel, leaving a slight SW gain over the Sahel, which partially contributes to the surface warming. Overall, cloud feedbacks are positive and dominant in extratropics, but relatively weak in tropics (Figure 2.6e).

A negative LW flux anomaly due to reduced tropospheric humidity appears across the North Atlantic and into Europe and North Africa (Figure 2.6b), leading to a considerable increase in clear-sky OLR, a major positive radiative feedback in

tropics. Water vapor is also a SW absorber and thus contributes to a small positive feedback to cooling from reducing shortwave absorption (not shown). Maximum cooling from the LW moisture feedback is collocated over the Sahel with the maximum of water vapor reduction. Another positive feedback involves the surface albedo change (not shown), as the brighter surface reflects SW as more ice forms in high latitudes. Decreased incoming SW due to albedo is also found over the Sahel, with a smaller magnitude than that in high latitudes.

Taken together, total clouds, moisture, and surface albedo yield an overall positive feedback in the Atlantic sector, as well as over North Africa (Figure 2.6f). In particular, the positive SW cloud feedback dominates in the extratropics whereas the positive LW moisture feedback prevails in the tropics. All the positive feedbacks lead to further energy loss in addition to the prescribed cooling, and such energy loss requires a decrease in surface and tropospheric temperature and change in lapse rate to compensate by reducing OLR (Figure 2.6d).

To better quantify the significance of the cloud and water vapor feedback on enhancing atmospheric cooling, we estimate the atmospheric temperature anomalies associated with those feedbacks. We start with the vertically integrated energy budget, which, in equilibrium, is

$$0 = \delta F_A + \delta F_s + \delta R\ , \qquad (2.3)$$

where δF_A is anomalous horizontal heat convergence, δF_s is anomalous surface flux into the atmosphere (which is nonzero over the extratropical North Atlantic in our simulation), and δR is the change in TOA energy flux. Expanding δR as in equation $\delta R \approx \sum_i \frac{\partial R}{\partial X_i}\delta X_i$, (2.1), and rearranging the above equation give

$$\delta T = -\frac{1}{\frac{\partial R}{\partial T}}(\delta R_c + \delta R_{wlw} + \delta R_{rest} + \delta F_A + \delta F_s). \qquad (2.4)$$

The first three terms in the parentheses on the RHS are the TOA energy flux anomalies related to total cloud feedback, δR_c, LW water vapor feedback, δR_{wlw}, and all other feedbacks, δR_{rest}, respectively. Each energy flux anomaly in the parentheses is divided by the vertical integral of the air temperature kernel, $\partial R/\partial T$, to yield the partial temperature change of a " slab" atmosphere due to the anomaly. We present the first two terms on the RHS of equation $\delta T = -\frac{1}{\frac{\partial R}{\partial T}}(\delta R_c + \delta R_{wlw} + \delta R_{rest} + \delta F_A + \delta F_s)$. (2.4), partial temperature changes due to clouds and water vapor, in Figure 2.6g and h. As the spatial variance of the temperature kernel is small (not shown), the spatial pattern of the feedback-derived air temperature change generally follows the TOA flux anomalies, but the magnitude is three times as large as the simulated mean tropospheric temperature anomaly (Figure 2.3a). The temperature decrease due to cloud feedbacks is over 2K in most of the extratropical North Atlantic, with a maximum of over 4K; whereas the maximum modeled mean tropospheric temperature cooling is ˜1K; the water

vapor feedback dominates in the tropics, in particular over North Africa, and the consequent partial temperature change is slightly larger than that in the simulation.

We now examine how the energy transport by the atmopheric circulation adjusts to balance the TOA radiative flux changes. We calculate the change in the horizontal advection of MSE (Figure 2.7a), decomposed into contributions by anomalous MSE advection by the climatological flow (Figure 2.7b), and advection of climatological MSE by the anomalous flow (Figure 2.7c). The residual, mainly consisting of the non-linear term, is small and thus neglected. Overall, horizontal MSE advection propagates cooling from the extratropical North Atlantic downstream - to Europe, the subtropical North Atlantic, and North Africa (Figure 2.7a). The magnitude much larger than that of the radiative feedbacks. The low MSE advection is completed mainly by the climatological westerlies in the extratropics (Figure 2.7b), and by anomalous northely flow over North Africa (Figure 2.7c). The advection further decomposed into contributions from each component of MSE, reveals that over the Sahara the cooling is induced by cold air invasion, while in the Sahel it is caused by decreased latent heat energy input from weakened monsoon flow (not shown).

Intrusion of air with low moist static energy (MSE) to the subtropics limits the poleward extent of the continental convergence zone by displacing high MSE air that favors deep convection, a mechanism known as ventilation (Chou et al. 2001). If the advection of low MSE air into North Africa is indeed the mechanism for the Sahel rainfall reduction, can the Tropical North Atlantic – which also cools in response to imposed extratropical North Atlantic cooling – act to augment drying over the Sahel? In order to test this, we perform two idealized simulations: in the first, we apply extratropical North Atlantic cooling but keep the Tropical North Atlantic SST fixed to the climatology (by replacing the slab ocean there with prescribed SST); in the second, we prescribe SST cooling only over the Tropical North Atlantic at the same level as in the 'usual' slab-ocean simulation with extratropical North Atlantic cooling. Thus, the first simulation tests the teleconnection without the Tropical North Atlantic SST feedback, and the second is the feedback contribution. The results (figures not shown) show that the Tropical North Atlantic SST feedback does indeed augment the Sahel drying, but the majority (over two thirds) of the drying is achieved without this feedback. This result is consistent with the ventilation argument, as the westerlies are stronger in the midlatitudes whereas in the tropics the climatological flow is easterly.

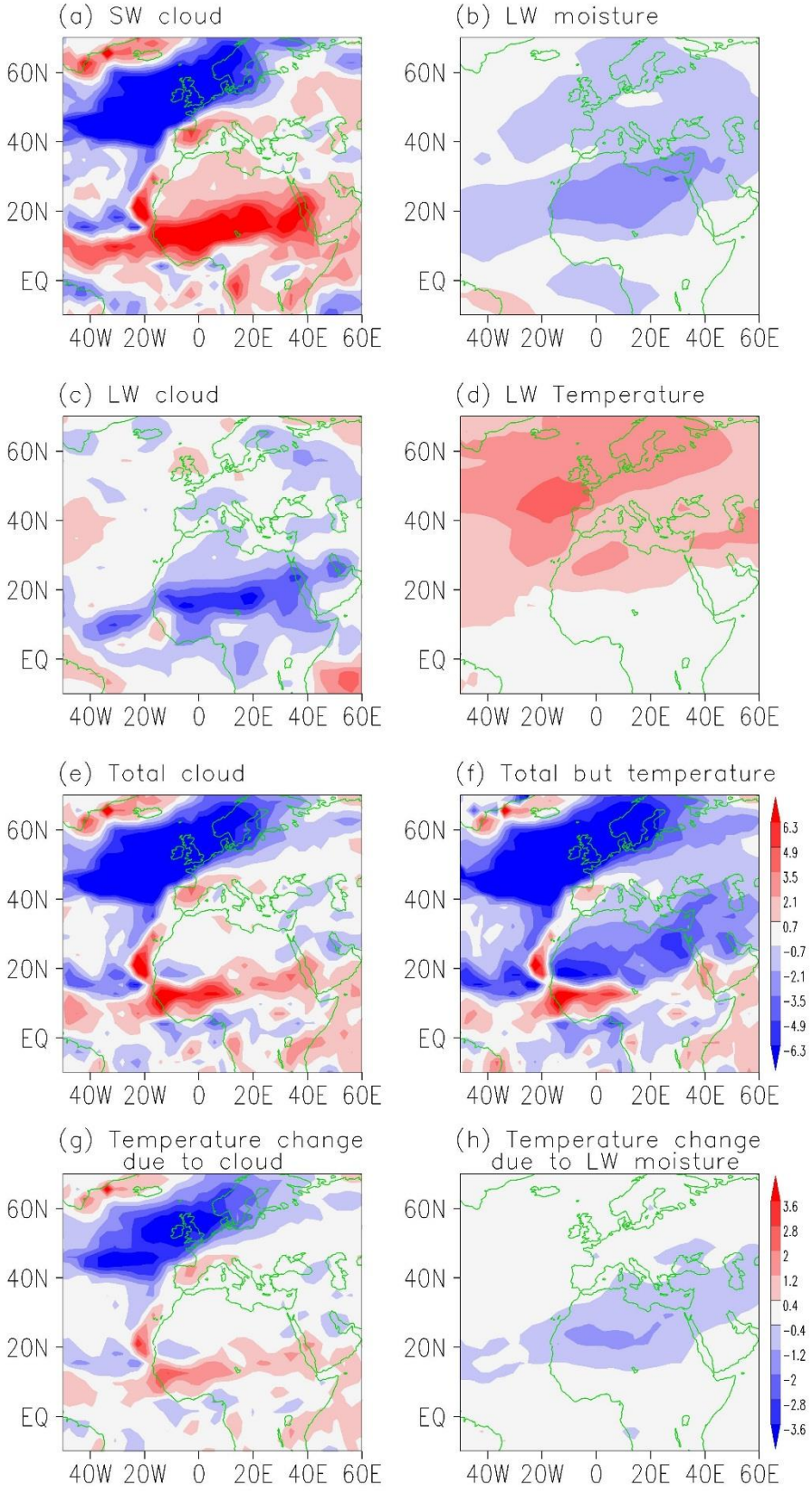
(a) SW cloud
(b) LW moisture
(c) LW cloud
(d) LW Temperature
(e) Total cloud
(f) Total but temperature
(g) Temperature change due to cloud
(h) Temperature change due to LW moisture
60N
40N
20N
EQ
40W 20W 0 20E 40E 60E
6.3
4.9
3.5
2.1
0.7
-0.7
-2.1
-3.5
-4.9
-6.3
3.6
2.8
2
1.2
0.4
-0.4
-1.2
-2
-2.8
-3.6

Figure 2.6 July through September average of TOA Energy flux anomalies due to the feedback of (a) cloud shortwave, (b) moisture longwave, (c) cloud longwave, (d) surface and air temperature longwave, (e) total cloud and (f) total with the exception of temperature, and of partial temperature anomalies due to (g) total cloud feedback and (h) longwave moisture feedback, in the CAM3.5 simulation. The color bar for (a) - (f) is to the right of panel (f), and for (g) - (h) is to the right of panel (h). The units for (a) - (f) are W m^{-2} and for (g) - (h) are K. The figures show that positive cloud (moisture) feedbacks strongly augment the cooling in extratropics (tropics)

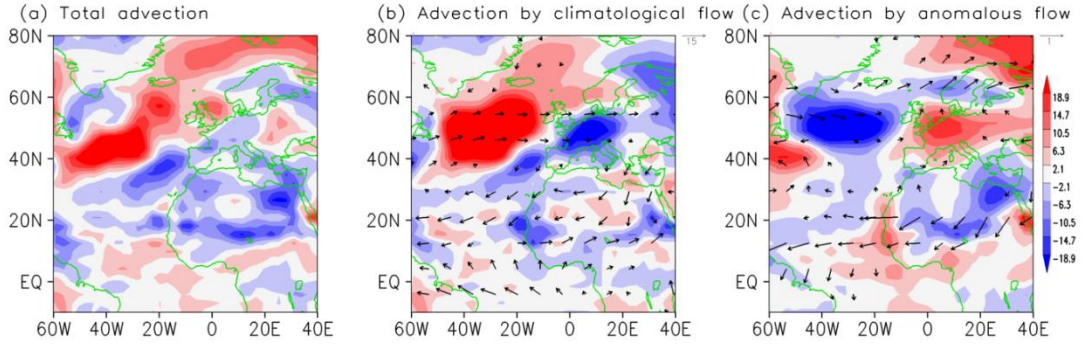

Figure 2.7 July through September average of vertically integrated horizontal MSE advection anomalies in the CAM3.5 simulation (unit: W m^{-2}). (a) total anomaly, (b) the anomaly related to the climatological flow from the control run, (c) the anomaly related to anomalous flow. Arrows are 925mb mean flow (b) and anomalous flow (c) (unit: m/s). The figure shows that the advection of low MSE air cools North Africa.

In summary, radiative feedbacks, tropical SST feedbacks, and atmospheric transport cooperate to communicate extratropical cooling to the Sahel. Extratropical North Atlantic cooling - augmented by a positive low cloud feedback - is advected downstream by the climatological midlatitude westerlies, cooling Europe and North Africa. Circulation changes over North Africa further reduce the MSE, by importing cold air and countering the advection of latent heat energy from the monsoon flow. Cooling over North Africa is further amplified by a reduced greenhouse effect from decreased atmsopheric specific humidity. Finally, a cooler Tropical North Atlantic also acts to augment drying over the Sahel.

2.7 Moisture budget analysis of the Sahel rainfall response

Our results thus far point strongly to cooling north of the Sahel as the cause of the Sahel rainfall change. In this section we diagnose the moisture budget over the Sahel in the GCM simulation, to infer how the rainfall changes are linked to the cooling.

2.7.1 Moisture budget analysis

Figure 2.8 shows each term of the vertically-integrated moisture budget from the RHS of equation $\delta P \approx -\langle \omega \frac{\partial \delta q}{\partial p} \rangle - \langle \mathbf{v} \cdot \nabla \delta q \rangle - \langle \delta \omega \frac{\partial q}{\partial p} \rangle + \langle \delta \mathbf{v} \cdot \nabla q \rangle + \delta E$, (2.2) (note these terms, factoring in the latent heat of vaporization, are plotted in energy units, W m^{-2}). Changes in specific humidity contribute considerably to the reduction of rainfall over the Sahel (Fig. 8a and 8b), and its effect is mainly through vertical transport anomalies. Humidity decreases primarily in the lower troposphere, resulting in a negative vertical moisture gradient anomaly (Figure 2.4b). Therefore over the Sahel (a region of mean ascending motion) this term leads to drying (Figure 2.8a). The reverse effect - that a weakened vertical humidity gradient makes the downward transport less arid - holds for subsidence regions of the Sahara. The humidity exhibits a positive meridional gradient anomaly over North Africa, as the Sahel dries out more than the Sahara (Figure 2.3b). With the climatological wind being northerly at the boundary between the Sahara and Sahel, the humidity anomaly wets the transition zone (Figure 2.8b).

The term of the largest magnitude on the RHS of equation (2.2) is the anomalous vertical moisture transport caused by the sinking anomaly (Figure 2.8c). The dipole at the very western edge of the Sahel with a negative anomaly in the north and positive anomaly in the south marks the southward shift of the Atlantic marine ITCZ. Further inland, such a dipole-like signature is only seen in Central and East Africa, with the rest of the area being dominated by near-uniform drying.

Reduced horizontal moisture transport by changes in the horizontal winds contributes significantly to the local rainfall reduction over central Sahel (Figure 2.8d). This is mainly due to a reduction of the southerly flow, as demonstrated in a further split of this term into contributions from zonal and meridional wind (not shown). Evaporation decreases between 15N and 20N (Figure 2.8e), primarily in association with the reduced soil moisture; warmer temperatures here would tend to increase evaporation, but evaporation over the Sahel semi-arid region is moisture- rather than temperature-limited. This is in contrast to West Africa along 10N, where surface warming actually increases evaporation.

2.7.2 Processes of the Sahel rainfall reduction

Three major processes of the Sahel rainfall reduction are suggested from the above analysis. The first is the " direct moisture effect" , the change in vertical moisture transport due to anomalous specific humidity. This effect has been proposed previously by Chou and Neelin (2004) to explain the tropical precipitation response to global warming; they demonstrated that an increase in gross moisture stratification due to low-level moisture increases with global warming leads to increased rainfall in climatological convergence regions, as part of the rich-get-richer mechanism. In our cooling simulation, the direct moisture effect acts in the opposite way by decreasing rainfall in convective regions, or rich-get-poor (Figure 2.8a). The decrease in specific humidity comes about partly due to the tropospheric cooling in vicinity of the Sahel that makes the atmosphere hold less moisture, and partly as a result of circulation changes.

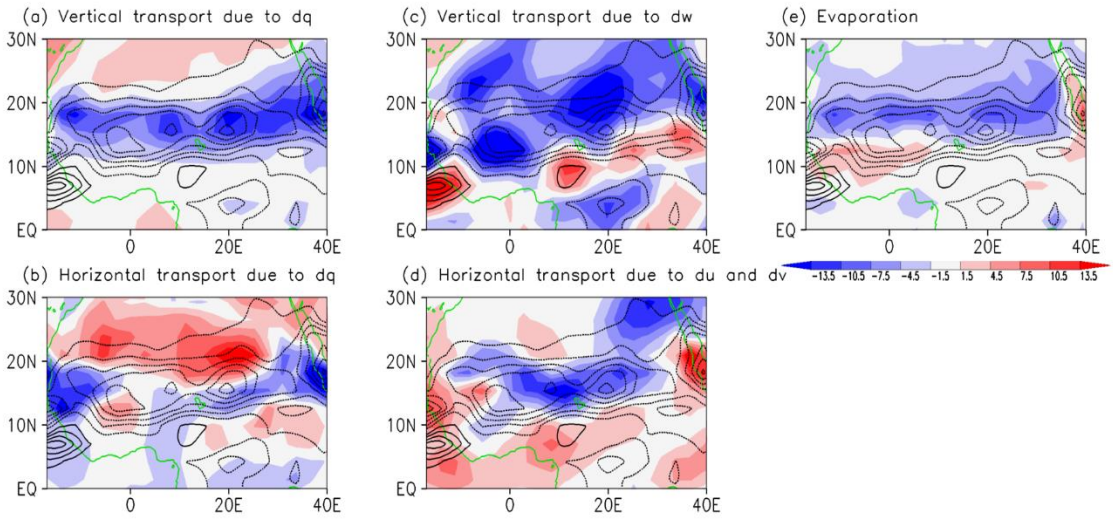

Figure 2.8 July through September average of vertically-integrated moisture budget anomalies in the CAM3.5 simulation. Contour: total precipitation anomaly. Shading: (a) vertical moisture transport anomaly due to anomalous moisture, (b) horizontal moisture transport anomaly due to anomalous moisture, (c) vertical moisture transport anomaly due to anomalous vertical wind, (d) horizontal moisture transport anomaly due to anomalous horizontal wind and (e) evaporation anomaly. The unit is W m^{-2}. Contour interval: 5 W m^{-2}. The color bar for all panels is at the bottom of panel (e)

The second process, the change in the vertical moisture transport due to anomalous vertical wind, also contributes significantly to Sahel rainfall reduction. This term is a dynamic feedback associated with a reduction of low-level moisture content (Chou and Neeling 2004). An analysis of the local MSE budget (not shown) following Chou and Neelin (2004) reveals both an increase of moist stability due to drying and an increase of dry instability due to low-level warming. The former overtakes the latter, resulting to a more stable atmosphere, consistent with the weakened convection.

The third process is related to the monsoon flow. Cooling over the Sahara reduces the land-sea contrast in the West African monsoon regime, leading to a positive pressure anomaly in the Sahara and a weakening of the meridional pressure gradient (Figure 2.2f). The southwesterly monsoon flow carrying moisture inland from the Gulf of Guinea is reduced accordingly, while dry air advection from the Sahara to the Sahel increases (Figure 2.4e); these lead to the moisture transport changes due to anomalous horizontal wind seen in Figure 2.8d.

In addition to the three main processes, reduced evaporation over the Sahel plays a significant role in reducing rainfall. This presumably arises from a soil-moisture feedback – a positive feedback loop is set up once decreased precipitation reduces soil moisture, which in turn weakens evaporation and thus lower-tropospheric moisture available for precipitation. The evaporation effect is more restricted to the northern part of the rainfall reduction, presumably because soil moisture is a greater limiting factor for precipitation close to the Sahel-Sahara

transition. On the other hand, toward the Guinea Coast the increased evaporation tends to enhance rainfall.

Taken together, the Sahel rainfall reduction is associated with reduced specific humidity, reduced vertical flow and weaker monsoon flow, and reduced local evaporation. Those changes are consistent with the decreased land-sea contrast created by the cooling and consequent circulation change, and dynamic/thermodynamic feedbacks of the two. However, given that the moisture budget is a diagnostic analysis, no causal relationship should be drawn from the results before further mechanistic study is done.

2.8 Concluding notes

2.8.1 Conclusion

We investigate teleconnection mechanisms of how extratropical North Atlantic cooling reduces summertime rainfall over the Sahel, using simulations of atmospheric general circulation model (the NCAR Community Atmosphere Model version 3.5, CAM3.5) coupled with a slab ocean. The hypothesis we propose is that the extratropical North Atlantic influence is communicated to the Sahel through air temperatures over North Africa, and that the Sahel rainfall is a direct response to the temperatures. Forced by 2K cooling in extratropical North Atlantic SST, the AGCM simulates surface cooling which spreads throughout the North Atlantic and surrounding continents, and penetrates into the Sahara; rainfall decreased by more than 25% in the semi-arid Sahel area between 10N and 20N across Africa (Figure 2.2). Other climate signatures are linked to the cooling, including a low cloud cover increase in the extratropics, SLP increase and humidity and MSE decrease north of the Sahel (Figure 2.2 and Figure 2.3), enhanced subsidence over the Sahara, and weakened upper level easterly jet and low level monsoon flow over the Sahel (Figure 2.4).

We then use a regional model – the Weather Research and Forecasting (WRF) model – to explicitly show that cold air anomalies over the Sahara can drive rainfall decreases over the Sahel. We apply cooling and related decreased geopotential height and humidity forcings derived from the GCM simulation as the northern lateral boundary condition in the WRF model, whose domain is set over Africa; the resulting changes to the Sahel rainfall and North African climate were broadly similar to the GCM response (Figure 2.5). Our WRF simulation thus strongly bolsters our hypothesis that the Sahel rainfall changes in the GCM forced with extratropical North Atlantic cooling result from large-scale cooling to the tropospheric temperatures north of the Sahel.

Our analysis suggests that the teleconnection is mediated by the advection of anomalously cold, dry air from the extratropical North Atlantic to North Africa (Figure 2.7). Climatological midlatitude westerlies bring low MSE air from the extratropics to North Africa, where the MSE is further reduced by increased (decreased) import of cold (wet) air by anomalous northerlies. This ventilation effect removes heat from land and thus hinders convection, as shown in Chou et al. (2001). We also find that the Tropical North Atlantic, which also cools in response

to the extratropical North Atlantic cooling, augments the Sahel drying; but this feedback response is relatively small.

We find that radiative feedbacks also augment the teleconnection. A radiative kernel (Shell et al. 2008; Soden et al. 2008) analysis on our simulation show that the positive cloud shortwave feedback considerably enhances the cooling in the extratropics, in particular over the North Atlantic, while positive moisture longwave feedbacks dominates in the tropics (Figure 2.6). It suggests that these feedbacks are able to leverage the effects of extratropical North Atlantic cooling: specifically, increased low clouds form over the extratropical North Atlantic in response to the imposed surface cooling could have led to over a 2K uniform drop in atmospheric temperature, if no negative feedback or horizontal heat convergence were present (Figure 2.6g); Decreases in tropospheric specific humidity reduce the associated greenhouse effect – this cooling is specifically effective in acting remotely from the North Atlantic (Figure 2.6h).

Finally, we analyze the vertically-integrated moisture budget over the Sahel, following Chou and Neelin (2004) and Chou et al. (2009), to explore the link between the contiguous cooling and the Sahel rainfall response. The decreased Sahel rainfall was primarily balanced by the direct moisture effect, stability increase, and monsoon weakening, processes that were tied to the ambient cooling and resulting circulation changes (Figure 2.8). Positive feedbacks between soil moisture and precipitation also contributed to the rainfall reduction. These analyses explicitly link the rainfall reduction to the cooling, but do not assign causality.

Our analysis demonstrates the plausibility of the atmosphere-mediated mechanism for the propagation of cooling, and the key factors in maintaining the teleconnection once it is set up. However, more work is required to develop and test the teleconnection mechanism. An examination of the evolution of transient radiative feedbacks, atmospheric circulation and related energy transport, and the interaction of the two after the onset of the extratropical North Atlantic cooling, would be useful in this regard.

2.8.2 Relevance to the 20th century Sahel Drought

The proposed teleconnection mechanism may be relevant to the recent Sahel drought that occurred in the late 1960's (e.g. Nicholson 1979; Folland et al. 1986). Various sources including greenhouse gases, anthropogenic aerosols, SSTs, and local land changes are linked to the Sahel drought (Folland et al. 1986; Folland et al. 1991; Xue and Jagadish 1993; Rowell et al. 1995; Fontaine et al. 1998; Rotstayn and Lohmann 2002; Bader and Latif 2003; Giannini et al. 2003; Held et al. 2006; Biasutti and Giannini 2006; Hoerling et al. 2006; Zhou et al. 2008; Kawase et al. 2010; Liu and Chiang 2012), among which SSTs, in particular over the Atlantic, have been shown to play a key role. Folland et al. (1986) showed that the onset of the Sahel drought was tied to an interhemispheric SST gradient with cooling in the Northern Hemisphere and warming in the Southern Hemisphere, particularly in the Atlantic. Apart from the gradient, a striking feature related to the drought is intense cooling in high-latitude North Atlantic. The effect of this SST pattern in drying the Sahel has been confirmed in subsequent studies (Folland et al. 1991;

Rowell et al. 1995; Fontaine et al. 1998). Liu and Chiang (2012) specifically showed that the Sahel drought is tied to cooling over Eurasia and North Africa, and both the drought and cooling are a consistent climate signature with the observed extratropical North Atlantic SST drop in the late 1960's. This linkage suggests that the paleo-scenario that extratropical North Atlantic cooling leads to a Sahel rainfall reduction also applies to the twentieth century. The current study may shed light on the mechanism of teleconnection from the North Atlantic to the Sahel in modern climate.

Chapter 3 Co-ordinated abrupt weakening of the Eurasian and North African Monsoons in the 1960s and links to extratropical North Atlantic cooling

3.1 Abstract

Previous modeling and paleoclimate studies have suggested that cooling originating from extratropical North Atlantic can abruptly weaken the Eurasian and North African monsoons. The climatic signature includes a widespread cooling over the Eurasian and North African continents, and associated increase to surface pressure. Motivated by these studies, we explore whether such co-ordinated changes are similarly exhibited in the observed 20th century climate, in particular with the well-documented shift of Sahel rainfall during the 1960's.

Surface temperature, sea level pressure and precipitation changes are analyzed using combined principal component analysis (CPCA). The leading mode exhibits a monotonic shift in the 1960's, and the transition is associated with a relative cooling and pressure increase over the interior Eurasia and North Africa, and rainfall reduction over the Sahel, South Asia and East Asia. The local circulation changes suggest that the rainfall shift results from the regional response of the summer monsoons to these continental-wide changes. A similar CPCA analysis of atmospheric general circulation model (AGCM) simulations forced by 20th century observed forcings shows similar results, suggesting that origins of the climate shift reside in the sea surface temperature changes, in particular over extratropical North Atlantic. Finally, an AGCM forced with extratropical North Atlantic cooling appears to simulate these climate impacts, at least qualitatively.

Our result shows that observed climate signature of the 1960's abrupt shift in Eurasian and North African climate is consistent with the influence of the abrupt high-latitude North Atlantic cooling that occurred in the late 1960's. It remains to be shown that a definitive causal relationship exists, and mechanisms elucidated.

3.2 Introduction

One of the most prominent 20th century regional climate shifts was the abrupt shift to drought conditions in the Sahel region of West Africa (Nicholson 1979; Folland et al. 1986; Giannini et al. 2003; Bader and Latif 2003; Held et al. 2005; Hoerling et al. 2006; Rotstayn and Lohmann 2002; Biasutti and Giannini 2006). The Sahel Drought started as an abrupt reduction in summer rainfall in the 1960's, and lasted for over two decades with limited recovery towards the present day. Recent work has suggested that, rather than being an isolated local climate shift, the Sahel Drought was in fact part of a global climate phenomenon. Baines and Folland (2007) documented worldwide abrupt shifts in summertime regional climates during the 1960's, particularly in the tropics and over the oceans. They concluded that the Sahel Drought was a regional manifestation of a larger near-global climate shift, and of which more examples were to be found.

Previous studies, though few, have noted coincident summertime rainfall reductions in other Northern Hemisphere monsoons. Ren et al. (2004) found that the Northern China portion of the East Asian monsoon region experienced a long-lasting drought since the 1960's, with similar local circulation changes as in the Sahel. Zhang and Delworth (2006) argued that rainfall variability in phase with that over the Sahel also occurred in the South Asian monsoon. As shown in Figure 1.1, rainfall over the Sahel, North China and India exhibits similar inter-decadal variability, the most striking of which was the monotonic dip in the 1960's. Whether the coincident changes to these monsoon regions resulted from a common origin, however, remains to be determined.

Monsoon variability in the three regions has been extensively studied, with focus directed towards the influence of tropical sea surface temperature (SST) variability (Bader and Latif 2003; Giannini et al. 2003; Zhou et al. 2008; Kucharski et al. 2009). Giannini et al. (2003) showed that an atmospheric general circulation model forced by global observed SST was able to reproduce the pattern of the Sahel rainfall low-frequency variability, and furthermore attributed the changes to warming in tropical South Atlantic and the Indian Ocean. Bader and Latif (2003) separated the effect of the two ocean basins and argued that the Indian Ocean warming played a more crucial role. Kucharski et al (2009) similarly showed that decadal drying of South Asian Monsoon was forced by warming in the Indian Ocean and the Pacific. Zhou et al. (2008) further argued that the tropical Indian and Pacific ocean warming caused a decreasing trend in global monsoon precipitation in the second half of the 20th century. They also found the interannual monsoon variability was largely attributed to the El Nino and Southern Oscillation (ENSO). These past studies focusing on the role of tropical SST on the monsoons have shed much light on the workings of decadal and interdecadal monsoon variability, in particular for variations during the latter half of the 20th century.

In this study, we take a different tack by focusing on the monsoon climate shift that occurred during the late 1960's, focusing on the possible role of northern extratropical cooling, specifically over extratropical North Atlantic. Our motivation comes from various paleoclimate studies showing that the weakening of the Asian and African monsoons were tied to cooling over the high-latitude North Atlantic (e.g. Wang et al. 2001; Gupta et al. 2003; Shanahan et al. 2009; Stager et al. 2011). The strongest evidence comes from abrupt climate changes during the latter half of the last glacial period (~50,000 to 14,000 B.P.). Greenland ice core records (Dansgaard et al. 1993) show abrupt and large (~10K) transitions between warm 'interstadial' states and cold 'stadial' states, with the transitions occurring from a few hundred to a few thousand years. The Asian and African monsoons appear to weaken during stadial conditions: for example, a recent study by Stager et al. (2011) shows that the height of Heinrich stadial 1 (16,000-17,000 years ago) coincided with a pronounced megadrought in the Afro-Asian monsoon region. Speleothem records from Hulu cave in China (Wang et al. 2001) show impressive one-to-one correspondence between stadial events in Greenland to monsoon weakening in Asia, throughout the last glacial. The link between North Atlantic cooling and monsoon weakening also appears to have occurred during the Holocene, albeit at a weaker level: for example, Gupta et al. (2003) show Holocene weakenings in the South Asian Monsoon were tied to North Atlantic cooling; and Shanahan et al. (2009) show similar Holocene linkages but for the African monsoon.

Prevailing evidence points to the North Atlantic as the origin of these abrupt changes through changes to the Atlantic meridional overturning circulation (AMOC). This idea was first proposed by Broecker et al. (1985), and subsequently supported by many other studies (see Alley 2007). Moreover, coupled model 'hosing' simulations that simulate a slowdown of the AMOC through the artificial input of freshwater in the high-latitude North Atlantic (e.g. Vellinga and Wood 2002; Zhang and Delworth 2005; Cheng et al. 2007) show impacts similar to what is inferred from paleodata. An example 'hosing' simulation using the Community Climate System Model 3.0 (CCSM3) is shown in Figure 3.1 (the simulation is described in detail in Cheng et al. 2007). It shows intense cooling over extratropical North Atlantic that extends over Eurasia and North Africa (Figure 3.1a), and rainfall reduction over the Sahel, India and North China. A significant weakening of the monsoon winds occur over North Africa as indicated by the anomalous northeasterly wind (Figure 3.1b), co-incident with a meridional pressure gradient anomaly between the anomalous high pressure to the north, and low pressure to the south. The model results thus show a continental climate change primarily in surface temperature and sea level pressure (SLP), which may act to bridge the extratropical North Atlantic cooling to the rainfall reduction over the three monsoon systems.

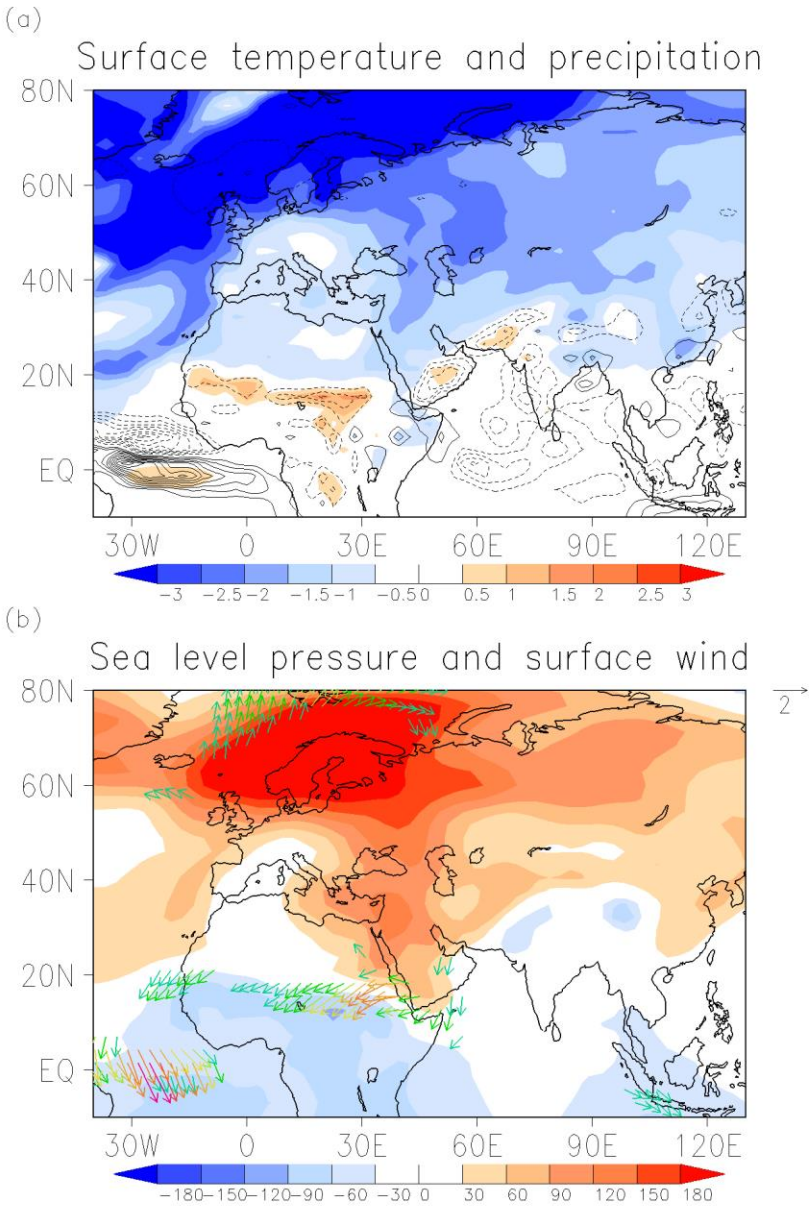

Figure 3.1 July-September climate anomalies in years 10-14 of a 'hosing' simulation with the Community Climate System Model version 3 (CCSM3), where the upper 970 m of the North Atlantic and Arctic Oceans from 55-90°N and 90°W-20°E are freshened by an average of 2 psu. Changes in (a) surface temperature (shaded, K) and rainfall (contour interval 0.5 mm day^{-1}, dashed contours are negative) and (b) sea level pressure (shaded, Pa) and surface wind (vectors, m s^{-1}, value under 1 not shown). Details of this simulation are described in Cheng et al. (2007).

Can this paleoclimate scenario – extratropical North Atlantic cooling leading to a monsoon weakening – be applicable for the 20th century? In this paper, we advance a hypothesis that this scenario may have occurred, albeit with much reduced magnitude, during the late 1960's. The seminal paper by Folland et al (1986) showed that the onset of Sahel drought was tied to an interhemispheric gradient of Atlantic SST with cooling in the Northern Hemisphere and warming in the Southern hemisphere (Figure 3.2). Apart from the interhemispheric gradient, the striking feature is the intense cooling in high-latitude North Atlantic. This pattern has been confirmed in subsequent studies, using different statistical techniques and updated global SST and rainfall data. For example, Folland et al. (1991) obtained such a pattern from cross-correlation between a Sahel rainfall time series and the Meteorological Office Historical Sea Surface Temperature data set version 3 (MONHSST3, Bottomley et al. 1990), an updated version of the SST used in Folland et al. (1986). They also captured this pattern using an empirical orthogonal functions (EOF) analysis of the SST data. Rowell et al (1995) obtained similar results using MONHSST4 and a gridded rainfall data set (Hulme 1992). Recently, Thompson et al. (2010) showed that the interhemispheric gradient suffered an abrupt shift in the late 1960's, and in particular showed sizable abrupt cooling in the high-latitude North Atlantic SST. Thus, the parallel to the abrupt climate change during the last glacial – extratropical North Atlantic cooling and weaker monsoon – appear to occur during the late 1960's shift.

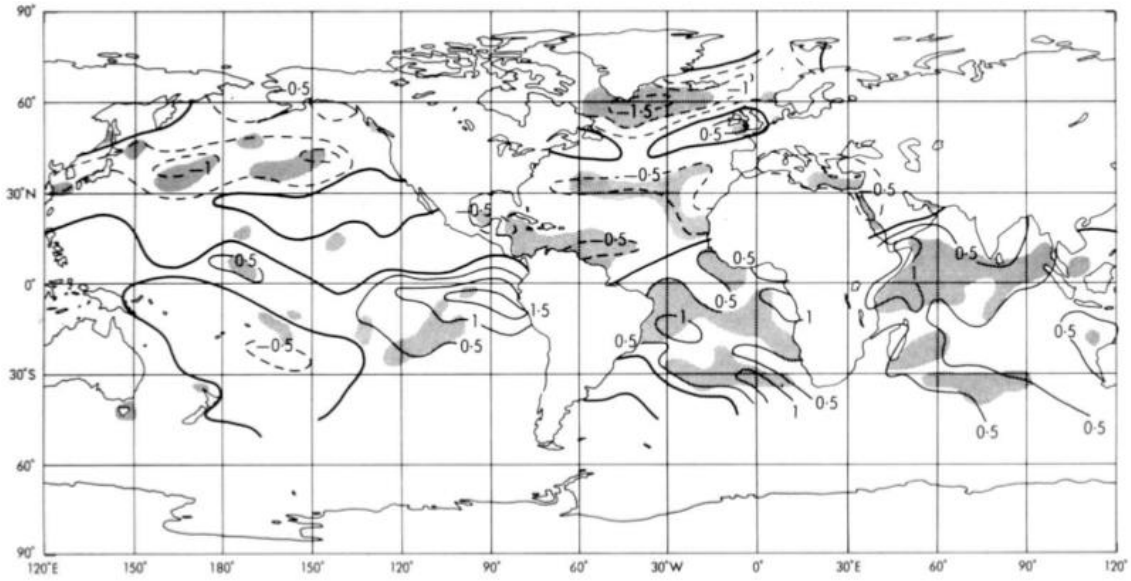

Figure 3.2 From Folland et al (1986), global boreal summer SST anomalies associated with the drought period over the Sahel. Plotted are SST, July to September, average of (1972-73, 1982- 84) (Sahel dry) minus average of (1950,1952-54, 1958) (Sahel wet). The contour interval is 0.5C, and shaded are regions where the difference is significant (at the 90% level, according to a t-test). Reproduced with permission from *Nature.*

Multidecadal changes to basinwide North Atlantic SST is commonly attributed to the Atlantic Multidecadal Oscillation (AMO), a low-frequency oscillation of the

entire (as opposed to high-latitude) North Atlantic basin; the AMO also shows a cooling trend throughout the 1960's and 1970's[1]. Paralleling the paleoclimate associations, the AMO has been postulated to be the result of variations to the Atlantic Meridional Overturning circulation (e.g. Knight et al. 2005). Furthermore, the AMO has also been linked to rainfall reduction in India and the Sahel (Zhang and Delworth 2006; Kucharski et al. 2009).

Several other studies have hinted that the pattern of climate changes occurring with the 1960's monsoonal weakening may resemble those associated with extratropical North Atlantic cooling. Haarsma et al. (2005) found that Sahel rainfall was related to mean SLP over the Sahara, north of the Sahel, which in turn was related to surface temperatures over Eurasia and North Africa. Biasutti et al. (2009) examined lead-lag correlation between the Sahara SLP and the Sahel rainfall, and argued that variation in the former caused that in latter, rather than vice versa. For the Asian monsoon, D' Arrigo et al. (2006) found from proxy data that its magnitude was correlated to Eurasia surface temperature, while Goswami et al. 2006 showed its onset and withdrawal depends on tropospheric temperature over Eurasia for modern periods. Taken together, these studies raise the possibility that the 1960s' shift in the Eurasian and North African monsoons were tied together through temperature (and hence SLP) changes over the interior Eurasia and North Africa, perhaps caused by extratropical North Atlantic cooling. We conjecture that the monsoonal rainfall weakening were the regional manifestations of this interior continental temperature and SLP shift, leading to a decreased meridional pressure gradient in the monsoon regions that ultimately weakened the monsoonal rainfall.

This study explores such possibility of a co-ordinated weakening of the Sahel and Eurasian summer monsoons in the 1960's from cooling over the Eurasian and North African continental interiors, from both observational analysis, and analysis of 20th century simulations.

3.3 Data and methods

3.3.1 Data

Our hypothesis involves changes to surface temperature and SLP over the continental interior linked to rainfall in the monsoon regions, so we use those three fields for our data analysis. We combine reanalysis and observational data into two distinct sets. The first set of data (which we call NCEP-DAI) consists of surface temperature and SLP from NCEP/NCAR reanalysis (Kalnay et al., 1996), and instrumental precipitation anomaly compiled by Dai et al. (1997) from Goddard Institute for Space Studies (GISS), NASA, both on a 2.5° x 2.5°grid. We avoid using reanalysis precipitation since rainfall is not assimilated, and therefore a

[1] We discuss the relationship between the AMO and the abrupt cooling of the high-latitude North Atlantic in section 7.

modeled quantity. The second set of data (which we call NCAR-CRU) is solely from observations, that is, 5° x 5° Northern Hemisphere SLP data from NCAR (Trenberth and Paolino 1980) and 2.5° x 3.75° precipitation and 5° x 5° surface temperature anomalies compiled by the Climatic Research Unit (CRU) of the University of East Anglia (Hulme 1992; Brohan et al. 2006). We will show that we obtain similar results from these two different sets, indicating that our results are robust.

We undertake a similar analysis using output from 20th century simulations of the Atmospheric Model Intercomparison Project (AMIP). The first set of runs (IAMIP) is forced by global observed time-varying SSTs from January 1950 through December 2000 plus volcanic, greenhouse gas, aerosol and solar forcings as used in the Intergovernmental Panel on Climate Change (IPCC) 20th century experiments (20C3M). The SST dataset used by the simulation was produced by merging the monthly mean Hadley Centre sea ice and SST dataset and the National Oceanic and Atmospheric Administration weekly optimum interpolation SST analysis (Anderson et al. 2004; Rayner et al. 2006; James W. Hurrell et al. 2010). IAMIP runs from two AGCMs are used: one is the NCAR Community Atmosphere Model 3 (CAM3 - Collins et al. 2006) and the other GFDL AM2.1 (Delworth et al. 2006). The CAM3 uses a T42 grid and 17 vertical levels and the AM2.1 a 2.0°latitude x 2.5°longitude grid and 24 vertical levels. We also analyze a second set of simulations ('VAMIP'), which has no external forcings beyond the global time-varying SST; only the CAM3 simulations were available in this format.

3.3.2 Methods

We make use of combined principal component analysis (CPCA) in our study in order to extract the leading mode of joint variability of all three fields. The PCA, also referred as EOF analysis, is commonly used to identify dominant modes (the principal components, PCs) of variability of single climate fields and separate them with different spatial structures (Wilks 2006). For the main analysis, PCA is applied to the combination of the three fields (surface temperature, SLP, and precipitation), which have been normalized prior to applying the PCA. Since the data we use have fewer time points than grid points, the CPCA extracts coupled patterns more accurately than other statistical methods like singular value decomposition or single-field-based PCA (Bretherton et al. 1992). All fields are averaged over June, July and August to obtain the summertime data. Prior to analysis, the global mean temperature is subtracted from the temperature field. This was done as we are interested not in temperature over Eurasia and North Africa per se, but rather its temperature relative to the global surroundings. Subtracting the global mean temperature brings out the spatial gradient of the temperature field in our analysis.

We choose a domain of analysis consistent with our hypothesis that the weakening monsoons over Eurasia and North Africa are tied to climate changes over the continental interior. It incorporates the Eurasian and North African landmasses: from 2.0°N to 77.0°N, and from 17°W to 132°E, and we use data only over land regions. The time period of our analysis is 1950 to 1998, and only grid points with more than 30 years of data available are used. All data are smoothed

with a seven-year running mean so that variability over decadal scales is highlighted. We normalize the data at each grid point prior to analysis, and thus use the correlation matrix for the PCA.

3.4 Observational analysis of the large-scale climate shift

3.4.1 A preview

As a first cut in showing the 1960's regime shift, we show the composite difference for the summertime (June-Aug) months between the 1970-1979 decade and 1950-1959 decade (Figure 3.3), using the NCEP-DAI dataset. We use data only up to 1979 to avoid potential artifacts within reanalysis data due to the introduction of satellite observations in the assimilation after 1979. The anomaly fields appear to capture the climate changes that we hypothesize. There is a reduction in rainfall across Sahel and North China; the Indian rainfall change shows alternative drying and wetting from northeast to southwest, but there is an overall reduction. There is cooling over the continental interiors with maxima over East Asia and eastern Central Asia; and a near-uniform SLP increase over Eurasia and North Africa, with maxima over East Asia and eastern Central Asia, and two local maxima over Europe and North Africa.

3.4.2 CPCA analysis

The leading mode from the CPCA analysis of the summertime (June-August) NCEP-DAI data is shown in left panel of Figure 3.4. This mode exhibits the 1960s' climate shift, explaining 32% of the variance, compared with the second EOF that explains 17%. The normalized PC 1 (Figure 3.4a) indicates that the three fields started changing monotonically at the beginning of the 1960's, and most of the change is achieved by the end of the decade. This new state is essentially maintained throughout the rest of the analysis period into the 1990's. The associated spatial patterns (calculated as the regression onto PC1) resemble the composites shown in Figure 3.3. The rainfall weakening is evident in all three monsoon regions (Figure 3.4c). The leading mode extracts the Sahel Drought as a band of negative values between $5°N - 20°N$ that extends across the entire latitude band within Africa. The East China "north drought, south flooding" rainfall pattern is similarly extracted, characterized by a dipole structure with negative anomaly in North China and positive anomaly in the Yangtze River Valley (Xu 2001; Li et al. 2010). The rainfall changes over India are more complex, but have drying over most of the Indian Subcontinent except for its northern extremity. The temperature structure (Figure 3.4e) shows alternative cooling and warming in mid-latitude over Eurasia and North Africa. East Asia and eastern Central Asia cools, as well as in North Africa north of the Sahel. On the other hand there is surface warming located directly over the Sahel, but this is consistent with the rainfall reduction there. The major difference from composite analysis (Figure 3.3) is the warming over Central Asia. With the cooling upstream and downstream, it appears

to form a stationary wave pattern over midlatitude Eurasia. The pressure pattern (Figure 3.4g), however, shows a uniform increase with maxima coinciding with regions of maximum cooling.

PCs derived from CPCA may be dominated by a single field with largest variance and thus may not be representative of joint variability in all the fields (Bretherton et al. 1992). To address this, we applied PCA to each individual field used in the NCEP-DAI analysis (figures not shown). The leading PCs of both surface temperature and SLP resemble those from the CPCA, so do the spatial pattern. Thus, in terms of these fields, the 1960's shift appears robust. The shift appears somewhat less robust if the individual PC analysis is applied to precipitation only. Instead of a shift in the 1960's, the leading EOF of the Dai et al.'s precipitation expresses a decreasing trend from 1960 to 1985 over the monsoon regions of interest. The somewhat ambiguous identification of the 1960's shift may be a result of mixing signals with Asian rainfall reductions in the 1970's in response to the Pacific Decadal Oscillation (PDO) (Li et al. 2010), but may also be due to the inherent nature of precipitation data. Precipitation is spatially and temporally noisy, and signals are not easily extracted; furthermore, the precipitation dataset suffers from incomplete data. As noted by Dai et al. (1997), number of northern hemisphere land stations available for their precipitation compilation decreased by over 20% since late 1970s, making them less reliable after that time. For some regions over Asia with the maximum inconsistency, station density decreased to as low as 1 station per grid (Fig. 1 in Dai et al. 1997), making the sampling error as large as 45%. For comparison, we applied PCA to the precipitation data from CRU (figures not shown). Unlike the PC using the Dai rainfall dataset, the leading PC of the CRU resembled that of the NCEP-DAI's CPCA, as did the spatial pattern of monsoon rainfall changes. We thus conclude that while the results of the PCA applied to precipitation are mixed, there are good reasons for this having to do with the uncertainty in the precipitation datasets. Overall, the individual PCA analyses support the robustness of our combined PCA analysis.

The same CPCA analysis but using the observational dataset NCAR-CRU, which consists of SLP from NCAR, and surface temperature and precipitation from CRU, also demonstrates the 1960s' shift in CPCA (Figure 3.4, right panel). The shift is captured in the leading EOF, with 23% of the variance explained. Both the PC and spatial structure are nearly identical to those of the NCEP-DAI analysis. The PC captured the jump during the 1960's to a new level after the 1970s (Figure 3.4b). The spatial patterns of temperature and SLP anomalies from NCAR-CRU, although of smaller magnitude, retain the main features in those from NCEP-DAI analysis, including cooling over Eurasia with a maximum over eastern Central Asia, slight warming over Central Asia and the Sahel, and the near-uniform increase in SLP (Figure 3.4f and h). Both the extent and magnitude of rainfall anomalies resemble those from NCEP-DAI analysis (Figure 3.4c and d), as well as its individual PCAs. This analysis, using purely observational (as opposed to reanalysis) datasets, demonstrates that the result of the previous CPCA analysis is not an artifact of using the NCEP reanalysis.

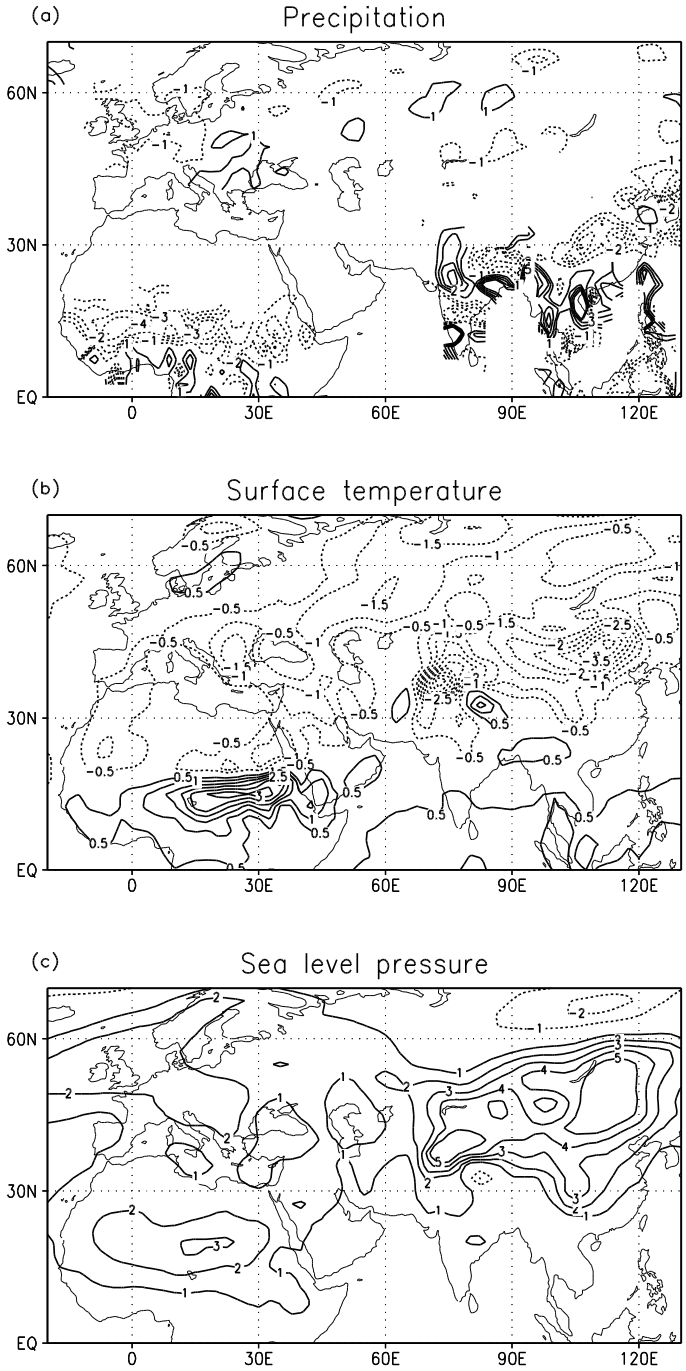

Figure 3.3 June-August composite for the period of 1970-1979 relative to the period of 1950-1959 from NCEP-DAI for (a) precipitation (cm month^{-1}) (b) surface temperature (K) (c) SLP (hPa). Dashed contours are negative.

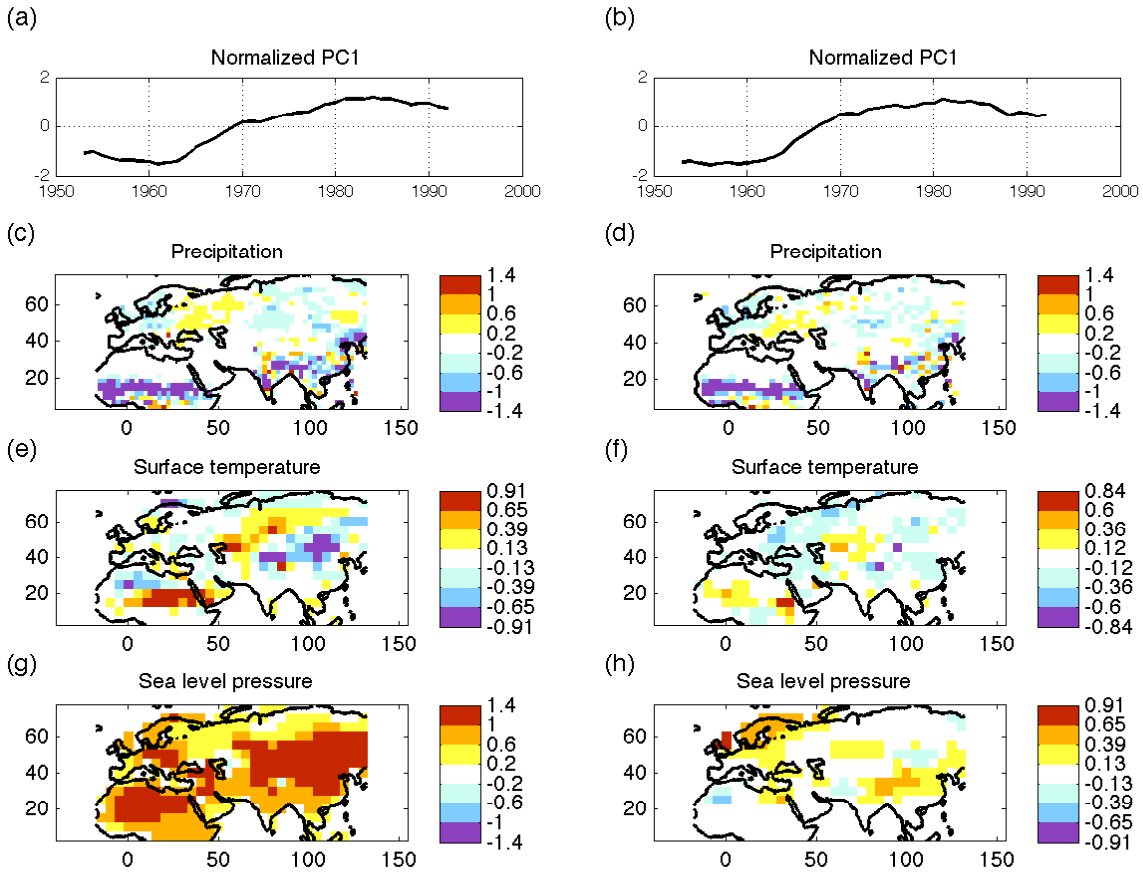

Figure 3.4 Leading EOF from CPCA for NCEP-DAI (left panels) and NCAR-CRU (right panels). (a)-(b) Normalized PC1. (c)-(h): spatial pattern shown as regressions of precipitation (c and d), surface temperature (e and f), and SLP (g and h) onto the PCs.

3.5 Response of monsoon circulation

In this section, we characterize the regional circulation changes associated with the 1960s' shift in the monsoon regions of interest.

3.5.1 Sahel

The circulation changes accompanying Sahel Drought have been extensively studied (e.g. Grist and Nicholson 2001; Nicholson 2009), and we draw connections from them to our results. Cooling over Eurasia and North Africa results in a shallower Sahara thermal low, weakening the land-sea pressure gradient and thus westerlies transporting moisture from the tropical ocean (Haarsma et al. 2005; Biasutti et al. 2009). Nicholson (2009) showed that the strength of the westerlies was strongly correlated with the surface pressure gradient, and suggested that weaker westerlies led to the Sahel rainfall reduction. Figure 3.5 shows the regional

climate over the Sahel during 1950-1959 and its response to the 1960s' climate shift. Near the surface, the SLP increase and weakening westerlies are apparent, as well as the rainfall reduction over the Sahel (Figure 3.5d and f). In low and middle troposphere, both moist static energy (MSE) and moisture convergence decrease across the Sahel latitude bands, especially in the middle and east, while moisture convergence strengthens along the southern coast. The MSE is analogous to equivalent potential temperature, and (under the assumption of a fixed upper tropospheric MSE) the lower tropospheric MSE is a measure of the moist convective instability. The decrease in lower-troposphere MSE indicates a more stable atmosphere over the Sahel. Moreover, the dipole in the moisture convergence anomaly indicates a southward displacement of land ITCZ. Cooling extends throughout the mid-troposphere, and the consequent decrease in the meridional gradient of mean tropospheric temperature weakens the upper-level tropical easterly jet (Figure 3.5b), similar to what was found in Nicholson (2009). Nicholson's analysis suggested that the change in strength of this jet influences convection by modulating upper-level divergence; a weak jet led to rainfall reduction over the Sahel.

3.5.2 East Asia

Li et al. (2010) previously examined a climate shift over the East Asian summer monsoon region associated with changes to the PDO, using the NCEP/NCAR Reanalysis and 20th century climate runs from CAM3 and GFDL AM2.1 (similar model simulations are used in our study). They identified a "southern flooding and northern drought" rainfall pattern, accompanied by a weakening of the 850hPa southwesterly winds and southward shift of the 200hPa jet stream. They attributed these changes to tropical SST forcings.

Following Li et al. (2010), we reexamined the monsoon index they employed - the EASMI, defined as the normalized zonal wind shear between 850 and 200 hPa. In our case (and different from the Li et al. analysis), we computed this quantity only over land regions, 20°N–40°N and 110°E–120°E. The index generally represents the strength of baroclinicity over the land monsoon region. The index (Figure 3.6) demonstrates a decreasing trend as stated in Li et al. (2010). We employed a regime-shift detection analysis on this timeseries using the sequential data processing technique introduced by Rodionov (2004); the result shows a shift occurring in the 1960's, indicating an abrupt weakening of the East Asian monsoon during that period, in accordance with our hypothesis.

The regional climate changes associated with this shift are shown in Figure 3.7 Same as Figure 3.5, but for the Asia sector. In the 1950s climatology, westerlies prevail in upper troposphere over East Asia (Figure 3.7 Same as Figure 3.5, but for the Asia sectora). Near the exit of the upper westerly jet, a surface low pressure region exists which acts to drive southerly winds towards eastern China from the South China Sea (Figure 3.7 Same as Figure 3.5, but for the Asia sectorc). The summer precipitation mainly falls over the central and northern parts of East China (Figure 3.7 Same as Figure 3.5, but for the Asia sectore). During the 1960s climate shift, the mean tropospheric temperature cooled by 2C over North China (Figure 3.7 Same as Figure 3.5, but for the Asia sectorb), and the upper-level

westerlies strengthened on its southern edge (Figure 3.7 Same as Figure 3.5, but for the Asia sectorc). This strengthening reduced the northward progression of the East Asian monsoon, resulting in drought in North China and excessive rain to the south (Yu and Zhou 2007). There are also SLP increases over Northeast China and a consistent low-level northerly wind anomaly indicating weakening of the East Asian monsoon (Figure 3.7 Same as Figure 3.5, but for the Asia sectord). Reduction in the lower tropospheric MSE is found over North China, similar to the Sahel. The anomalous moisture divergence (convergence) occurring over East (South) China is consistent with the rainfall changes. The moisture convergence anomaly over North China runs counter to the observed rainfall reduction; however, an examination of the surface latent heat flux suggests that the convergence is largely offset by decreased evaporation (figures not shown).

3.5.3 South Asia

The climate anomalies associated with the 1960's shift over South Asia are comparable in strength to the other monsoon regions, but spatially complex. As in East Asia, tropospheric cooling and SLP increase are present north of the summer monsoon regions (Figure 3.7 Same as Figure 3.5, but for the Asia sectorb). The rainfall decreases over Northeast India and Central India and increases at the south flanks of these two regions (Figure 3.7 Same as Figure 3.5, but for the Asia sectord and f); these rainfall changes suggest a southward displacement of the monsoon rainfall belt toward the ocean in response to the cooling in the north. Goswami et al. (2006) analyzed tropospheric temperature changes between 1950-1960 and 1970-1980 (similar to the periods chosen in our analysis) and suggested that the cooling could also lead to an earlier withdrawal of the monsoon rainy season.

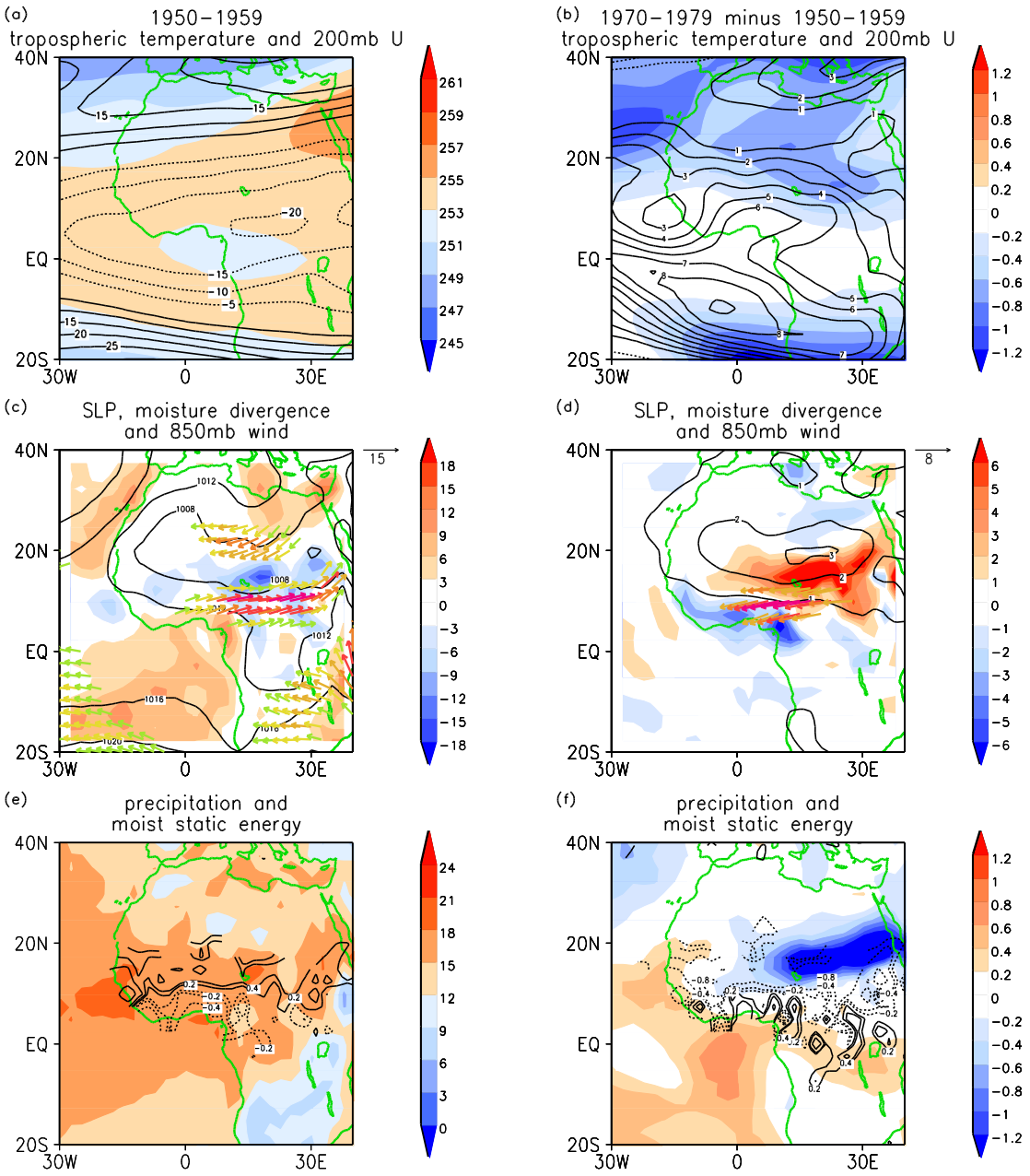

Figure 3.5 June- August climate change over the Sahel. Upper panels: mean tropospheric temperature (shaded, K) and 200mb zonal wind (contours, m s^{-1}, dashed contours are negative). Middle panels: mass-weighted integral of divergence of moisture transport from surface to 500mb (shaded, 10^{-5}kg $s^{-1}m^{-2}$), sea level pressure (contours, hPa) and 850mb wind (vectors, m s^{-1}, value under 6 not shown). Bottom panels: mass-weighted integral of moist static energy from surface to 700mb (shaded, 10^{7}J m^{-2}), precipitation anomaly (contours, mm day^{-1}, the blank spots indicate missing data). Left column is 1950-1959 mean; right column is the 1970-1979 minus 1950-1959 difference. Mean tropospheric

temperature is defined as temperature mass-weighted averaged from 600mb to 200mb. The precipitation anomaly is with respect to the 1951-1979 period. All data are from NCEP reanalysis except the precipitation is from GISS/Dai precipitation.

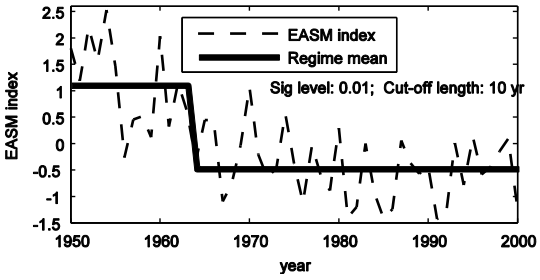

Figure 3.6 Normalized EASM index (dashed line) and its regime mean (solid line) after applying a regime-shift detection analysis. The regime mean shows two distinct states before and after 1967. The significant level is 0.01 and cut-off length is 10 year for the regime detection.

3.6 The climate shift in 20th century simulations

In this section, we present results of CPCA applied to model simulations of the 20th century to see if the climate shift is simulated, and if so to infer causes.

The ensemble means of the 20th century forced-SST IAMIP run of GFDL AM2.1 (10 members) and CAM3 (5 members) are first analyzed. Both model simulations captured the observed climate shift as the leading mode, with 45% (GFDL) and 35% (CAM3) variance explained respectively (Figure 3.8). The respective PCs resemble those derived from the observational analysis, with a similar shift occurring in the 1960's. The GFDL model was able to simulate the observed Sahel Drought and "north drought, south flooding" pattern in China. For India, a southward movement of rainbelt is suggested from the pattern of drying in the north and increased rainfall in the south, qualitatively consistent with the observations while differing in details (Figure 3.8b). The temperature changes show the correct relative strength over Eurasia, including the cooling maxima over East and eastern Central Asia, and less cooling in Central Asia where some warming is seen in observations (Figure 3.8e). Significant surface warming is seen at where rainfall decreases. SLP increases over the extratropical Eurasia and North Africa (Figure 3.8g). The models, however, appear to simulate more rainfall over south Asia's adjacent to the tropical oceans. This incorrect response may result from a lack of atmosphere-ocean interaction in the prescribed SST runs, as indicated in Zhou et al. (2008). The spatial anomalies in CAM3 CPCA analysis are basically the same, except for warming in the high latitudes of East Asia (Figure 3.8, right panels). We conclude that models forced by the observed SST are able to simulate, in a broad sense, both the temporal and spatial structure of the observed 1960s' shift. The ensemble mean substantially reduces the effects of internal variability, so

the shift must originate from the applied forcings. This is consistent with previous modeling studies of Sahel Drought (e.g. Rowell et al. 1995)

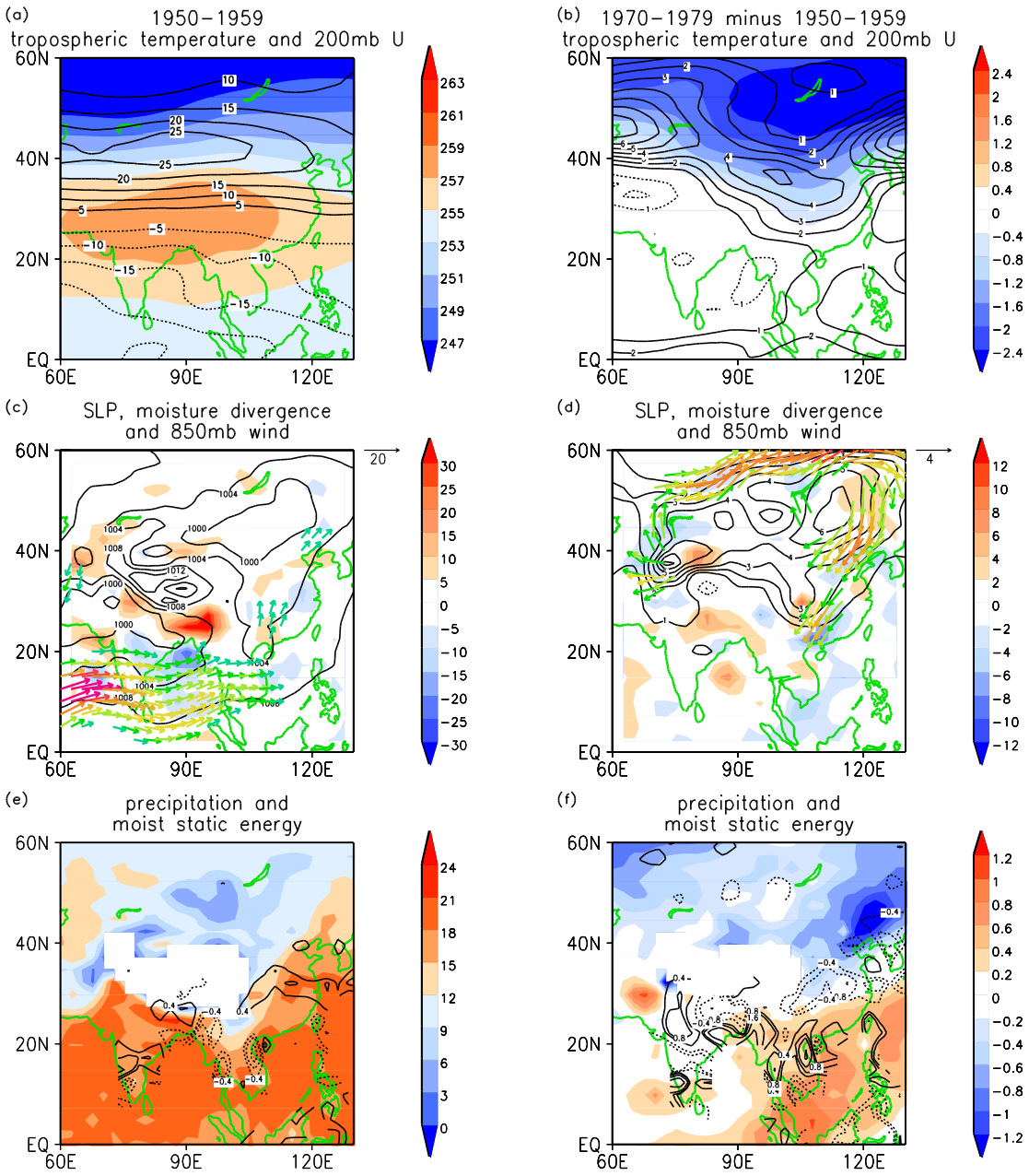

Figure 3.7 Same as Figure 3.5, but for the Asia sector

We further infer that the forcing causing the 1960's shift resides in the imposed SST. The ensemble mean of VAMIP runs from CAM3, in which SST was the only time-varying forcing imposed, was analyzed using the same CPCA procedure. The

results are basically the same as that of the CAM3 IAMIP run (figure not shown), suggesting the key role of SST over other forcing agents.

Which ocean basin's SST is responsible for the climate shift? Figure 3.9 shows regression of global SST onto PC1s from CPCA of both observation and VAMIP simulation. Consistent with previous studies, the regression picks out warming over the tropical oceans and the PDO-like pattern in Pacific as distinct influences. In addition, however, there is cooling over North Atlantic especially in the extratropics (Figure 3.9, upper panels). Indeed, the signal over North Atlantic is more pronounced in the VAMIP simulation where SST is the only forcing (Figure 3.9b). As we are interested in the abrupt shift in the 1960's, we show in the lower panels of Fig 10 the same regression but restricting the time period from 1950 to 1975, so as to avoid the accelerated warming in late 20th century and a 1976/1977 monsoon transition that originated from Pacific (Deser and Phillips 2006; Li et al. 2010). The extratropical North Atlantic becomes the region of the largest signal.

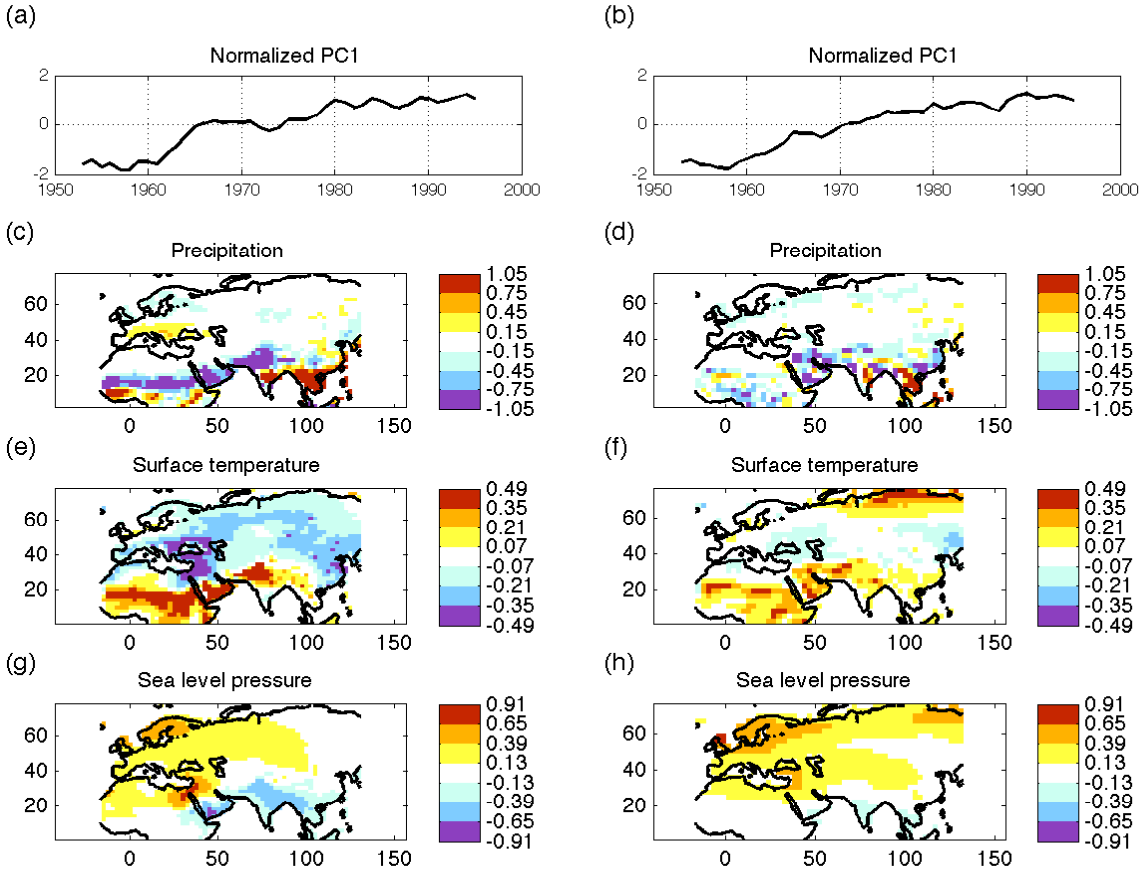

Figure 3.8 Same as Figure 3.4, but for GFDL-IAMIP (left panels) and CAM3-IAMIP (right panels)

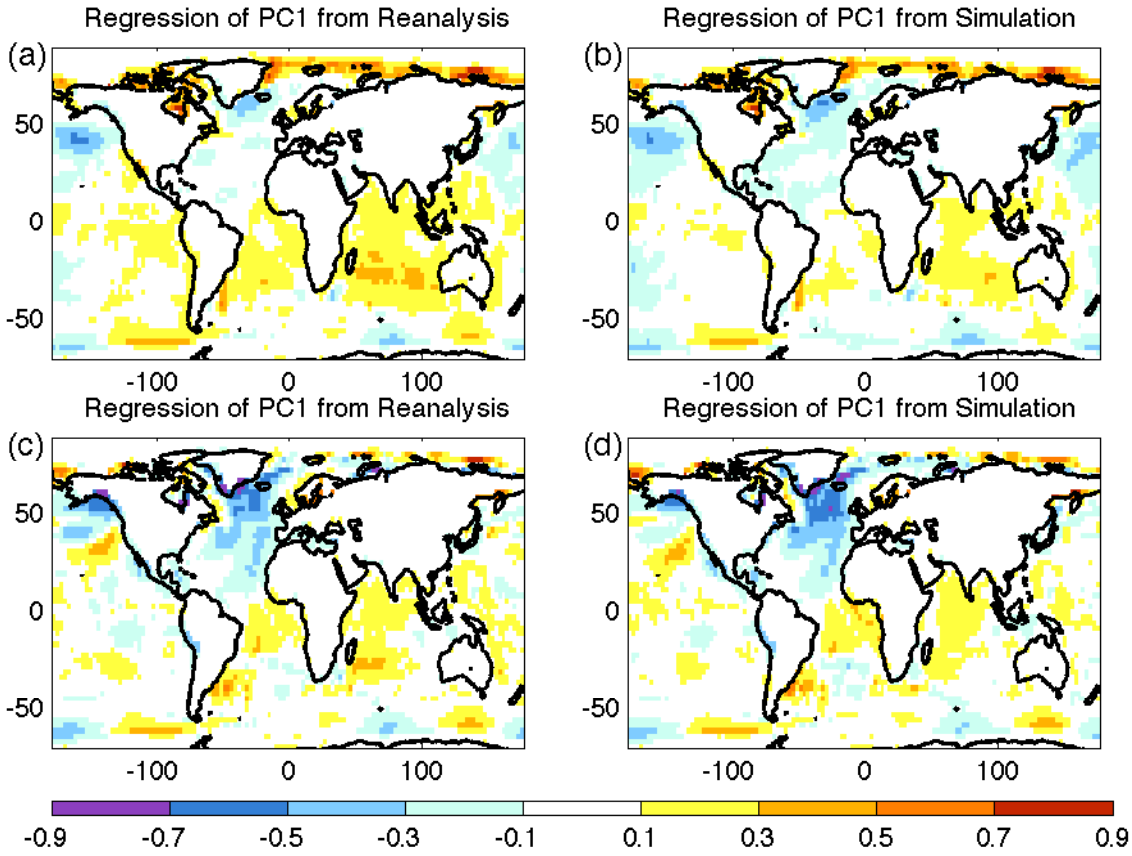

Figure 3.9 Regression of June-August global SST onto PC1 from CPCA analysis of NCEP-DAI (left column) and of CAM3-VAMIP (right column), over the period of 1950-1995 (upper panels) and 1950-1975 (lower panels).The unit is C per standard deviation of the PC. The SST is produced by merging the monthly mean Hadley Center sea ice and SST dataset and the National Oceanic and Atmospheric Administration weekly optimum interpolation SST as used in the CAM3-VAMIP simulation.

3.7 A simulation of climate impacts to extratropical North Atlantic cooling

Up to now, we have only shown diagnostic relationships between extratropical North Atlantic cooling and the monsoon weakening, with no definitive evidence for causality. In this section, we use an AGCM to demonstrate that extratropical North Atlantic cooling can drive the requisite continental climate changes and monsoon weakening, at least qualitatively.

We use the CAM3 coupled to a fixed-depth slab ocean model that interacts thermodynamically with the atmosphere, but has no representation of ocean

dynamics. A monthly-varying 'Q-flux' is applied to the model slab ocean to ensure that the simulated SST resembles the observed SST distribution; the Q-flux is derived from surface fluxes extracted from a global climatological fixed-SST simulation. The slab ocean configuration is required, as the thermodynamic ocean-atmosphere interaction is essential to bringing the extratropical influence to the tropics (Chiang and Bitz 2005). Such interaction is also crucial in correctly simulating the South Asian monsoon, as demonstrated above.

We use the above base configuration to undertake two sets of simulations. In the one set, we replace the slab ocean in the North Atlantic over the 45-60 latitude band with climatological monthly-varying fixed SSTs, and run this configuration to equilibrium. In the second set, we also apply fixed SSTs over the same North Atlantic region, but uniformly cool the applied SST by a specified amount to represent the extratropical North Atlantic cooling. All simulations are run for 20 years, and the last 10 years are taken for climatology.

The June-August anomalies, from a simulation with 4K cooling applied over the extratropical North Atlantic, are shown in Figure 3.10. The climate response is qualitatively similar to the coupled model 'hosing' simulation of Cheng et al. (Figure 3.1) and the observed 1960s' climate shift: there is cooling extending over Eurasia and North Africa; Rainfall reduces over the Sahel and South Asia; the monsoon winds over North Africa weaken with SLP increase in the north. The global SST pattern resembles the one related to AMO in Parker et al. (2007) (which will be discussed later), and the interhemispheric pattern in Folland et al. (1986). This simulation therefore suggests that extratropical North Atlantic cooling can drive the observed Eurasian and North African climate changes associated with the 1960's shift.

However, we have found in these particular simulations that a North Atlantic extratropical cooling of around 3-4K is required to get an appreciable weakening to the monsoonal rainfall. The observed abrupt shift in extratropical North Atlantic SST in the 1960s is, however, around 1K, significantly smaller than the cooling imposed here (see Figure 3.11 for example). However, we argue that the apparent mismatch in the climate response's sensitivity to extratropical North Atlantic cooling is to be expected, as the strength of the connection may depend on the magnitude of important feedbacks, of which the two most important appear to be cloud feedbacks, and moist convection.

With regards to the former, Kang et al. (2009) showed that the strength of cloud feedbacks determines the magnitude of the tropical response to extratropical cooling. They showed in their aquaplanet simulations with extratropical cooling that switching off cloud feedbacks (through prescribing clouds) effectively reduced the response of Hadley circulation and thus that of tropical rainfall. Correctly simulating cloud responses to climate changes, however, is notoriously difficult. With regards to convection, the Zhang-McFarlane (ZM) convection scheme that is used in the CAM3 model may be a weak link. Chen et al. (2010) compared ZM scheme with three other convection schemes, and showed the former is the least able in simulating the East Asian monsoon rainfall climatology. Chen et al. (2010) also argued that as convection in the tropics (subtropics) is more sensitive to surface heating (synoptic scale wave activity), a convection scheme good at simulating tropical rainfall may turn out to be less effective outside the tropics.

Furthermore, Kang et al. (2009) showed the response of tropical rainfall to extratropical forcing is sensitive to the change in the convection scheme. Taken together, these demonstrate the complexity of the various processes determining model sensitivity to extratropical thermal forcing.

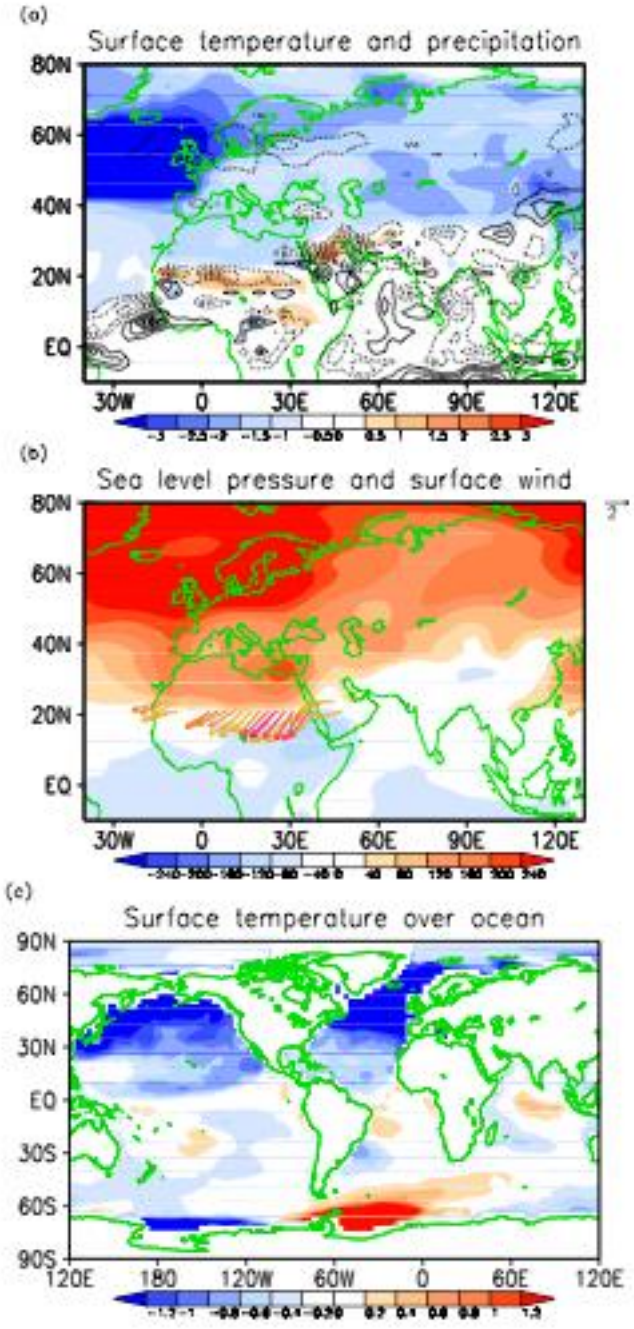

Figure 3.10 June-August climate anomalies in an AGCM simulation using CAM3 with 4-K cooling prescribed in between 45°-60° over North Atlantic. Changes in (a) surface

temperature (shaded, K) and rainfall (contour interval 0.5 mm day^{-1}, dashed contours are negative), (b) sea level pressure (shaded, Pa) and surface wind (vectors, m s^{-1}, value under 2 not shown), and (c) Surface temperature (K) over global ocean.

We take this preliminary model result using the CAM3 as encouraging, in that it is able to *qualitatively* simulate an approximately correct pattern of climate response given extratropical North Atlantic cooling. *Quantitatively*, however, we argue that it is reasonable to expect mismatches in the magnitude of the response in model simulations (as in the case with our simulations) because of known shortcomings in AGCM model physics. The resolution of this problem requires a detailed investigation of the AGCM response to extratropical North Atlantic cooling, including a focus on understanding teleconnection mechanisms, as well as exploring the role of various feedbacks such as clouds and convection in the teleconnection. This assessment, while important, is beyond the scope of this particular study, and we defer this to a later study.

3.8 Conclusion and Discussion

We objectively characterized a summertime climate shift over the monsoonal regions of North Africa and Eurasia that took place during the 1960's, following studies that documented such abrupt shifts over individual regions, especially the rainfall variability over the Sahel (Baines and Folland 2007; Folland et al. 1986). Motivated by paleoproxy studies of abrupt climate changes during the last glacial that showed co-incident changes between extratropical North Atlantic cooling and weakening monsoons (Stager et al. 2011; Gupta et al. 2003; Shanahan et al. 2009; Wang et al.2001), and modeling studies simulating the impacts of a cooler extratropical North Atlantic that suggested such coherent climate changes (Chiang and Bitz 2005; Cheng et al. 2007), we hypothesized that the abrupt monsoonal changes in the 1960's were similarly co-ordinated, and linked to the extratropical North Atlantic cooling.

Following our hypothesis, we incorporated three monsoon regions - the Sahel, South Asia and East Asia - as well as the Eurasian and North African landmasses, as part of an objective analysis of climate variations over the latter half of the 20^{th} century. Surface temperature, sea level pressure (SLP) and precipitation of the second half of 20^{th} century from both reanalysis and observation were analyzed using combined principal component analysis (CPCA). The leading mode is a large monotonic shift among all fields centered on the 1960's. The associated spatial structure of precipitation anomalies captured the Sahel Drought, the "north drought, south flooding" over East China, and a less strong drought in South Asia. The temperature pattern showed cooling over Eurasia and North Africa with warming over Central Asia and the Sahel. The SLP increased uniformly with maxima in regions corresponding to maximum cooling.

To explore the link between the large-scale climate shift and the observed rainfall reduction over the three monsoon regions, we investigated the regional atmospheric circulation changes, some of which have been characterized by

previous studies (Goswami et al. 2006; Biasutti et al. 2009; Nicholson 2009; Li et al. 2010). The results show that the cooling extends throughout the depth of the troposphere from the surface over those regions. Over the Sahel and North China, the cooling shifted or weakened the upper-level jet, which would otherwise induce low-level convergence as seen before the 1960's. In addition, the increase in SLP over land diminished the meridional pressure gradient and weakened the prevailing monsoon. For India, the weakening of monsoon is less prominent, but a southward shift of rainbelt is discernible.

20th century AGCM simulations that imposed known 20th century climate forcings as well as observed variations in global SST are able to capture the observed climate shift, as indicated by the results of a similar CPCA analysis. This result bolsters the evidence for the existence of this co-ordinated 1960's climate shift on the monsoons, and furthermore suggests that it was driven by external climate forcings or SST variations. A further analysis using simulations forced only with observed SST variations suggests that SST variations are the primary cause.

Various lines of evidence point to the extratropical North Atlantic SST cooling as the underlying driver of the climate shift. Regression of SST onto the PC of the leading mode in the CPCA analysis highlights the North Atlantic cooling, particularly in the extratropics. Moreover, a recent study by Thompson et al. (2010) shows convincing evidence of such an abrupt variation in SST in the late 1960's, especially an abrupt cooling over the high-latitude North Atlantic. An AGCM-slab ocean simulation with imposed extratropical North Atlantic cooling showed climate impacts qualitatively resembling those seen in the climate shift.

Taken together, our results are consistent with our hypothesis of a co-ordinated climate shift of the monsoons tied to extratropical North Atlantic cooling. If the results of previous studies are also considered – most significantly Thompson et al. (2010), and Baines and Folland (2007) - the implication is that North Atlantic cooling, particularly in extratropics, may have caused a near-global climate shift during that time, ranging from Northern Hemisphere cooling and subtropical monsoon rainbelt relocation, to a southward shift of ITCZ and shift in the Southern Hemisphere storm track.

We emphasize that our diagnostic study only demonstrates the plausibility this scenario. More work is needed to advance this hypothesis: in particular, a proper detection and attribution study has yet to be performed, and the mechanisms still to be elucidated. In this regard, we are currently undertaking idealized AGCM studies to investigate atmospheric teleconnection mechanisms of extratropical North Atlantic cooling to the Northern Hemisphere monsoons, and key feedbacks such as the positive cloud feedbacks that is important in determining the response of the monsoons.

What are the causes of the abrupt cooling in the high-latitude North Atlantic during the late 1960s? In their study on the 1960's climate shift, Baines and Folland (2007) argued for two potential sources: one being the multidecadal variations in North Atlantic SST known as the AMO, and the other being anthropogenic sulfate aerosol emissions over the Northern Hemisphere, particularly over Europe and North America. We first comment on the latter. It is known that sulfate aerosol emissions increased significantly in the middle of the 20th century, in

particular over Europe and North America (Smith et al. 2004), and several idealized modeling studies have shown that climate forcing resulting from such emissions cool the Northern Hemisphere and weaken the Northern Hemisphere monsoons, in particular if indirect effects are also included (e.g. Rotstayn and Lohmann 2002). While there is increasing evidence implicating anthropogenic aerosols in tropical rainfall changes, we argue that they are not the main factor in the climate shift of the 1960's. First, our own CPCA analysis of 20th century simulations suggests that SST is the main driver (though we point out two caveats: i) simulations we analyzed only included aerosol direct effects, leaving out indirect effects; and ii) anthropogenic aerosols are likely to have also affected the 20th century SST evolution, so some effects of aerosols may be folded into the SST). Second, even though the sulfur dioxide emissions ramped up since 1950's and peaked in the 1980s', black carbon emissions over South and East Asia - which have been shown to significantly perturb the monsoons (Novakov et al. 2003; Smith et al. 2004; Ramanathan and Carmichael 2008) - increased well into the 1990s. Hence, the total effects of aerosols on the monsoons, if significant, should be largest late in the 20th century rather than in the 1960's. Third, sulfur dioxide emission increased steadily within the period from 1950 to 1975, unlike the abruptness of the high-latitude North Atlantic cooling in the late 1960's as shown in Thompson et al. (2010) or the climate change demonstrated above.

We now discuss the AMO. The AMO is a coherent pattern of multidecadal variability in surface temperature centered in the North Atlantic Ocean, the leading cause of whose change is suggested to be variations in the AMOC (Knight et al. 2005). The phasing of the AMO with regards to our problem is indeed correct: the 1960s was a period when the AMO shifted from positive phase to negative phase, resulting in a cooling of the North Atlantic SST; as such, it is more likely to be relevant to the 1960's shift than sulfate aerosols. However, even the AMO may not be the most appropriate index, depending on the way that it is constructed: it is commonly defined to be the SST anomalies averaged over the entire North Atlantic basin, and then temporally low-pass filtered to extract multidecadal variations (e.g. Sutton and Hodson (2005) used annually-averaged SST from 0N-60N and 75W to 7.5W, and the resulting timeseries smoothed with a 37-point Henderson filter, and then detrended). As such, this index somewhat lacks a physical basis, but more importantly because of the temporal smoothing it obscures faster and more abrupt changes to the SST (Figure 3.11, upper timeseries). Parker et al. (2007) uses a different definition of the AMO, the third EOF of low-pass-filtered global SST. The spatial pattern mimics that associated with Sahel Drought in Folland et al. (1986). Their AMO definition therefore is the most appropriate one among others in terms of relating the 1960s' climate shift.

Overall, given that Sahel Drought occurred with equal abruptness to the high-latitude North Atlantic SST drop seen in Thompson et al. (2010) (their Fig. 3b), we argue that those findings are more relevant to the 1960's climate shift discussed here than the smoothed AMO. The middle and bottom timeseries of Figure 3.11 show a high-latitude North Atlantic SST index computed by us, together with the unsmoothed Sahel rainfall variation. The SST timeseries indeed shows a pronounced shift around the 1960's, co-inciding with the start of the Sahel Drought.

Finally, what caused the abrupt cooling in high-latitude North Atlantic? One possibility that is discussed in the literature is the Great Salinity Anomaly (GSA) in the late 1960s, when anomalously fresh water and sea ice was introduced into the North Atlantic subpolar gyre. The low-salinity water was advected into the Labrador Sea and reduced the deep-water formation there, leading to a weakening of the thermohaline circulation (Dickson et al. 1988; Zhang and Vallis 2010), thus cooling the North Atlantic SST. Sea-ice feedbacks may also have played a role in amplifying this cooling. Zhang and Vallis (2006) perturbed an ocean general circulation model with fresh water flux analogous to that in the GSA event in the second half of the 20th century. The modeled SST response compared favorably with observations, with strong cooling south of Greenland. We thus conjecture that that the GSA in the late 1960's may have cooled extratropical North Atlantic, leading to the climate shifts here discussed.

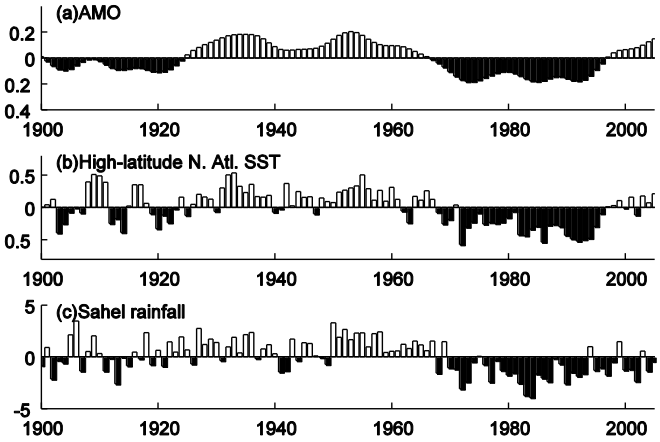

Figure 3.11 The timeseries of the AMO (°C), high-latitude North Atlantic SST (°C), and the unsmoothed June-October Sahel rainfall (cm month^{-1}). The AMO is computed by Trenberth and Shea (2006) as low filtered Atlantic SST anomaly north of the equator with global mean SST subtracted. The high-latitude North Atlantic SST timeseries is computed as SST averaged over 50N-70N and 70W-0 with global mean SST subtracted, using the HadSST2 dataset. The Sahel rainfall index is computed by Todd Mitchell at University of Washington.

Chapter 4 The Influence of the Extratropical North Atlantic on the Eurasian and North African monsoons in the twenty first century

4.1 Abstract

Extratropical North Atlantic temperature has been found to modulate the West African, South Asian and East Asian monsoons in past and present climate. We investigate if the extratropical North Atlantic is relevant for the future monsoon climate, through analyzing climate projections of the 21st century from the Coupled Model Intercomparison project phase 5 (CMIP5). We obtain common features of the spatial patterns of temperature and rainfall changes at the end of the 21st century across CMIP5 models by applying a principle component analysis (PCA) to the changes. A coherent change of extratropical North Atlantic temperature, and Eurasian and North African temperature and precipitation appears as the 2nd mode (the 1st being global warming), similar to the pattern found in past and present climate.

We then examine how the extratropical North Atlantic evolves and influences global climate throughout the 21st century by applying the PCA to the correlation of extratropical North Atlantic temperature with globally gridded temperature and precipitation. Models unanimously simulate positive correlations over Eurasia and North Africa, a pattern also found in 20th century observation.

The results suggest that the extratropical North Atlantic teleconnection to the Eurasian and North African monsoons is also relevant in future climate projections. As such, it suggests for better understanding of the processes controlling extratropical North Atlantic climate in order to constrain estimates of future monsoon activity.

4.2 Introduction

4.2.1 21st century temperature change

Global mean temperature is projected to continue increasing in the 21st century in models participating in the coupled model intercomparison project phase 5 (CMIP5). The warming exceeds 2 K under RCP4.5 and RCP6.0, and 4 K under RCP8.5 by 2100 (Collins et al. 2013). There is, however, large variability to the warming.

A key feature of the regional temperature change is the larger warming over land compared to oceans (e.g. Manabe et al. 1990). It results from land-ocean contrast in surface sensible and latent fluxes, boundary layer lapse rate changes, boundary layer relative humidity and associated low-level cloud cover changes, and soil moisture reductions under climate change, as well as the heat capacity difference of land and ocean (Collins et al. 2013). Polar amplification and minima in the subpolar North Atlantic and Southern Oceans are two other large-scale warming patterns that are consistent across climate model integrations. The former is primarily an Arctic phenomenon, and has been attributed to radiative processes characteristic for the Arctic such as the sea ice/snow feedback, and change in heat transport by both the atmosphere and ocean under climate change. The warming minima over subpolar North Atlantic has been associated with increased moisture transport to the high latitude increasing precipitation (Manabe et al. 1990), and the change in the Atlantic meridional overturning circulation (Drijfhout et al. 2012)

4.2.2 21st century precipitation change

The change in global mean precipitation is related to that of temperature, with a sensitivity of about 1 to 3% per K. From an energetic perspective of the atmosphere, radiative cooling is balanced by latent heating associated with precipitation, and sensible heating. Therefore, future precipitation changes are primarily the result of changes in the energy balance of the atmosphere and the way that they interact with circulation, moisture and temperature (Vecchi and Soden 2007; Collins et al. 2013). Increase in atmospheric temperature in response to increased greenhouse gases both enhances radiative cooling and increases water vapor, thereby increasing global precipitation (Allen and Ingram 2002; Held and Soden 2006)

Precipitation change is highly uneven in space, with its spatial variability greater than the global mean by a factor of 4 (Ma and Xie 2013). A major large-scale regional feature of the precipitation change is a wet-get-wetter and dry-get-drier type of response (Chou and Neelin 2004; Held and Soden 2006). This mainly applies for the ocean, where the lower-tropospheric water vapor increase with temperature enhances the moisture transported by the circulation. The change in water vapor leads to additional moisture convergence within the convergence zones and to additional moisture divergence in the descent zones, increasing the contrast

in precipitation minus evaporation values between moisture convergence and divergence regions (Collins et al. 2013).

4.2.3 21st century monsoon change

The strength of the monsoon depends on atmospheric humidity, land-sea thermal contrast, and other factors. As warmer air contains more water vapor, temperature increase enhances water vapor transport from the ocean into land. As a result, both the global monsoon total precipitation and the global monsoon precipitation intensity (a ratio of monsoon precipitation to monsoon area) are projected to increase by the end of the 21st century (Collins et al. 2013).

Large uncertainty, however, exists in summer precipitation over the Sahel, India and North China. Firstly, the projected rainfall change displays considerable model spread (Figure 4.1). This is partly due to their failure in simulating a credible sea surface temperature (SST) patterns relevant to the rainfall (Christensen et al. 2013).

Secondly, models are poor in reproducing important regional features of the monsoon, such as the rainband of the EASM, even they generally agree with total rainfall (Christensen et al. 2013). The rainband is key to regional precipitation in the EASM regime. Deficient rainfall was experienced in North China and excessive rainfall in South China in the late 20th century, primarily due to a shift of the rainband, even though the summer rainfall amount over East Asia shows no clear trend, as shown in Chapter 3 and previous studies (Yu and Zhou 2007; Zhang and Zhou 2011; Christensen et al. 2013). The failure in reproducing key monsoon components raises questions as to the models' credibility in projecting total monsoon rainfall.

Thirdly, the monsoon circulation that transports water vapor to the summer continent and lifts the moisture to the condensation level is slowing down as the climate warms, due to energy balance constraints in the tropical atmosphere (Allen and Ingram 2002; Held and Soden 2006; Christensen et al. 2013). As mentioned above, the increase of precipitation under global warming is less than 3% per K, constrained by the energy balance of the atmosphere. The increase of water vapor, however, is around 7% per K, following the Clausius-Clapeyron equation and given little change of relative humidity, a fairly well hypothesis under current climate. The low (high) sensitivity of precipitation (moisture) to temperature requires a decrease of vertical motion. This opposite change in circulation may add to the uncertainty in the simulated precipitation increase.

Figure 4.1 shows the fractional change of projected 21st summer rainfall over the Sahel, India and North China from the CMIP5 models. The Sahel rainfall change across models, for example, varies from a 20% decrease to a 60% increase, reflecting considerable uncertainty in the projections. A key to constraining the uncertainty and improving the predictability of future monsoon precipitation change is to understand how models simulate the spatial distribution of temperature changes, and how it is related to that of the precipitation change. This is the question we address in this Chapter.

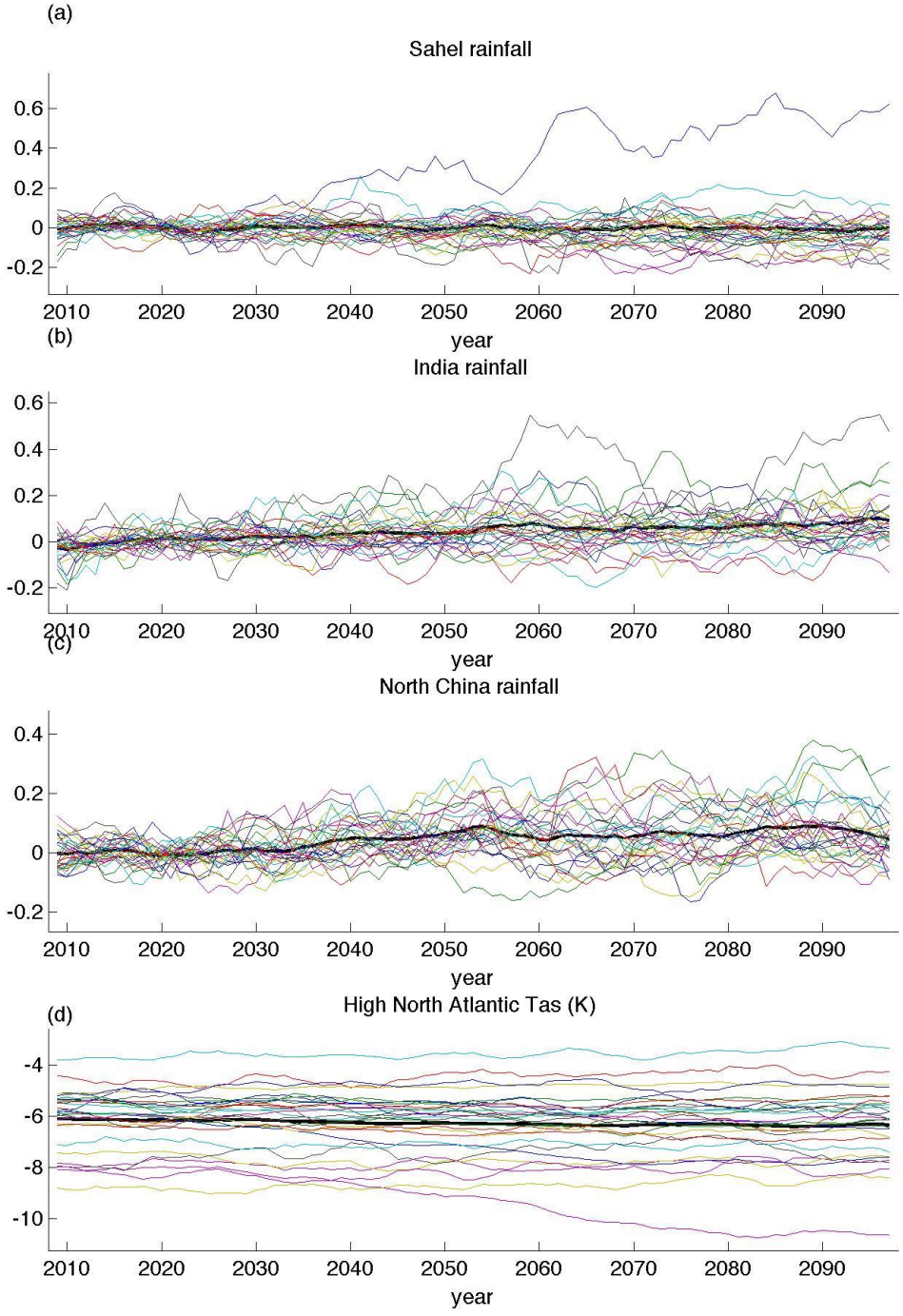

Figure 4.1 Projected summer monsoon rainfall change over (a) the Sahel (10N-20N, 20W-10E), (b) India (10N-30N, 70E-90E) and (c) North China (30N-45N, 110E-120E), and (d)

surface air temperature over high latitude North Atlantic (45N-70N, 69W-0) with global mean subtracted in CMIP5 RCP4.5 simulations for each model available. The rainfall is shown as fractional change relative to the average of the first 20 years (2006-2025). Thick Solid line is the multi-model mean. All indices are smoothed by a 7-year running mean. Models spread in simulating 21st century monsoon rainfall and North Atlantic temperature.

4.2.4 The influence of extratropical North Atlantic on Eurasian and North African monsoons

In previous chapters we have demonstrated the influence of extratropical North Atlantic climate on West African, South Asian and East Asian monsoons, in both paleoclimate and the climate of present day. All three summer monsoons weakened during Heinrich events of the last glacial period, when strong cooling occurred over extratropical North Atlantic. In Chapter 2, we showed that atmospheric temperature acts to mediate the extratropical influence to the tropics.

A similar scenario applies to the late 1960s' climate shift, as shown in Chapter 3. Summer rainfall of all three monsoons dropped, associated with cooling and sea level pressure (SLP) increase over Eurasia and West Africa. Such coordinated climate changes appear to originate from the extratropical North Atlantic.

The extratropical North Atlantic is one of a few regions where considerable model disagreement exists and internal variability makes a big difference in 21st century temperature projections (Collins et al. 2013, also see Figure 4.1). The connection of extratropical North Atlantic to monsoons indicated from studies of paleo and modern climate, if sustaining in the future, is expected to create large uncertainty in monsoon rainfall projection. In this chapter, we analyze coherent changes of rainfall and temperature to understand if the extratropical-North-Atlantic-Monsoon relationship continues to be at work in future climate; we also look at the model spread of simulated the temperature and rainfall, to understand how the former contributes to the latter.

4.3 Data and methods

Our dataset is extracted from the CMIP5 dataset, which we obtained from the Program for Climate Model Diagnosis and Intercomparison (PCMDI) Website. We analyze the 21st century integrations of 28 coupled models under the Representative Concentration Pathway (RCP) 4.5 scenario. RCP 4.5 is a scenario of long-term, global emissions of greenhouse gases, short-lived species, and land-use-land-cover which stabilizes radiative forcing at 4.5 W m-2 (approximately 650 ppm CO2-equivalent) in the year 2100 without ever exceeding that value (Moss et al. 2010; Thomson et al. 2011). We use the 21st century part of the RCP4.5 simulations, that is, from 2006 to 2100. Our choice of models was dictated exclusively by the availability of the integrations when we recovered the data. We use surface air temperature, which is strongly connected to surface temperature over the ocean. To weight each model equally, we take one ensemble from each model for the

analysis. All fields are averaged over June, July, August and September to obtain the summertime data.

Since we are interested in the major patterns of temperature and precipitation change simulated by all models, we apply a combined principal component analysis (CPCA, also referred to as combined empirical orthogonal function analysis, or combined EOF analysis) to these changes. The domain of analysis is chosen to incorporate North Atlantic, Eurasia and North Africa, from 5.0°S to 77.0°N, and from 70°W to 132°E. We first take the difference of temperature and precipitation averaged in the first and last 20 years of the period chosen, 2006-2025 and 2081-2100. We normalize the changes of both climate fields so that they both have a spatial mean of 0 and spatial standard deviation of 1, and combine the normalized change to one large map, one map per model. We then apply EOF in the way that the resulting PCs show maps of joint variability of temperature and precipitation respectively, across all models, and the EOFs represent contribution of each model to these maps. Similarly we apply EOF to the correlation of global temperature and precipitation onto extratropical North Atlantic temperature across all models, in order to understand how models simulate their relationship throughout the coming century.

4.4 RESULTS

4.4.1 Change over Atlantic and Eurasia

Figure 4.2 and Figure 4.3 present the results of the CPCA applied to the changes of temperature and precipitation through the 21st century. We project the EOF to the data prior to normalization to get the PC that incorporates the mean change of the domain. PC 1 (Figure 4.2) explains 36% of variance. The temperature change shows a general warming in the domain. The warming pattern features a land-sea temperature contrast with stronger warming over land then ocean, and a reduced warming in the subpolar North Atlantic, typical patterns associated with global warming. Precipitation generally increases in the domain, as warming increases moisture content in the atmosphere and thus increases moisture convergence in climatological convergence regions. This is in particularly true in the Atlantic intertropical convergence zone (ITCZ) and the marine part of the Asian monsoons (note that shown is summer climate). The EOF shows contribution of the change of each model to this pattern. Most models agree with such simulated warming and wetting except one with nearly zero loading.

PC 2 shows patterns related to the extratropical North Atlantic temperature and the summer monsoon rainfall, with 11% of total variance explained (Figure 4.3). The pattern over land bears remarkable resemblance with those associated with the late 1960s' climate shift (Figure 3.4). There is cooling over Eurasia and North Africa, north of the three monsoons; Surface warming appears over the Sahel, corresponding to the rainfall decrease; The lack of cooling over Central Asia observed in the late 1960s' climate shift is also present (Figure 4.3a). Precipitation drops over the Sahel, India, and North China. The Sahel dry bands within 10N –

20N spreads all across Africa, with some wetting at the Coast of Guinea. The west of coast and the northeastern part of India exhibits the largest drying. In East Asia, rainfall is reduced mainly in North China (Figure 4.3b). Related to the temperature change over land is a strong cooling over the extratropical North Atlantic, from 40N to 70N. Correspondingly, the Atlantic ITCZ shifts to the south, shown as with the dry (wet) band north (south) of 10N.

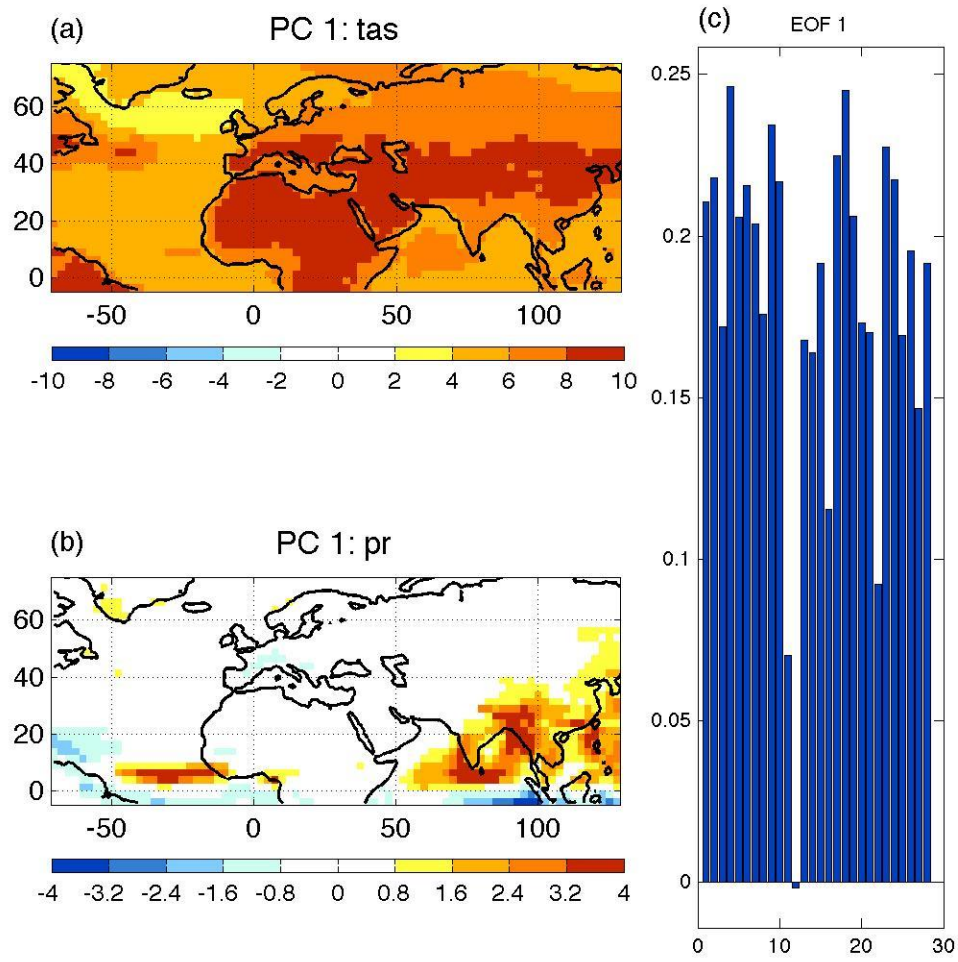

Figure 4.2 The leading mode from the CPCA of the 21st century change of June-September temperature and precipitation over North Atlantic and Eurasia. PC 1 for (a) temperature and (b) precipitation show a general warming and wetting. EOF 1 (c) shows that models agree on the change pattern shown in PC 1.

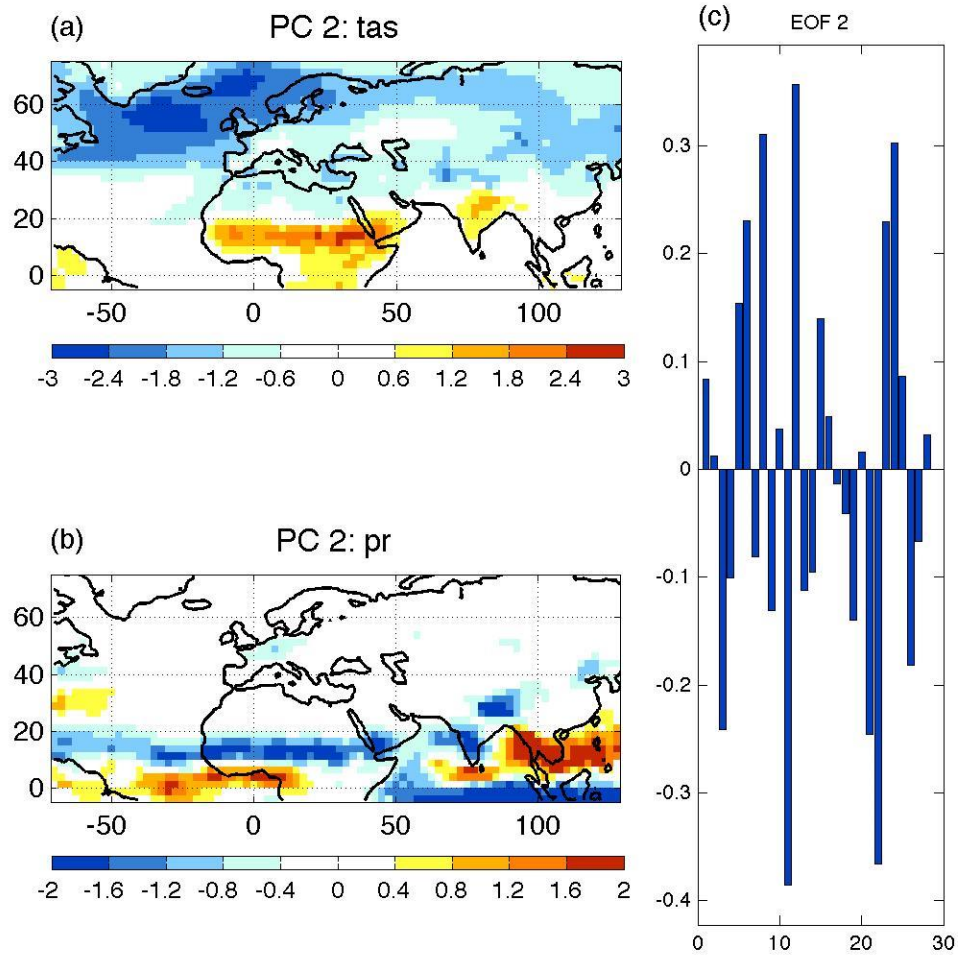

Figure 4.3 Same as Figure 4.2 but for the 2nd mode

Models disagree with the sign of future change of temperature and precipitation related to this pattern (Figure 4.3c). Some simulate a cooling over extratropical North Atlantic, Eurasia and North Africa, and precipitation decrease over the Sahel, India and North China as shown in Figure 4.3a and b; some simulate the opposite. Nevertheless, they all capture a consistent relationship between temperature over extratropical North Atlantic, and a climate shift over Eurasia and North Africa.

How does the spread of this North-Atlantic-Eurasia pattern across models contributed to the model spread in simulating the monsoon rainfall change? We take JJAS precipitation averaged over the Sahel, India and China respectively from all models, and correlate each precipitation index to this EOF. To show the total effect on all three monsoon regions, we also take the average of the three

precipitation indices to create a total monsoon rainfall index, and apply the correlation. Figure 4.4 shows a scatter plot of the EOF and all four indices. The EOF correlates with the India, Sahel and average rainfall significantly at the 5% level, the significance level of the latter two exceeding 0.1%. The correlation over North China is less significant. The model spread in simulating the effect of extratropical-North-Atlantic-temperature can explain over half the spread of the average rainfall over all three monsoon regions.

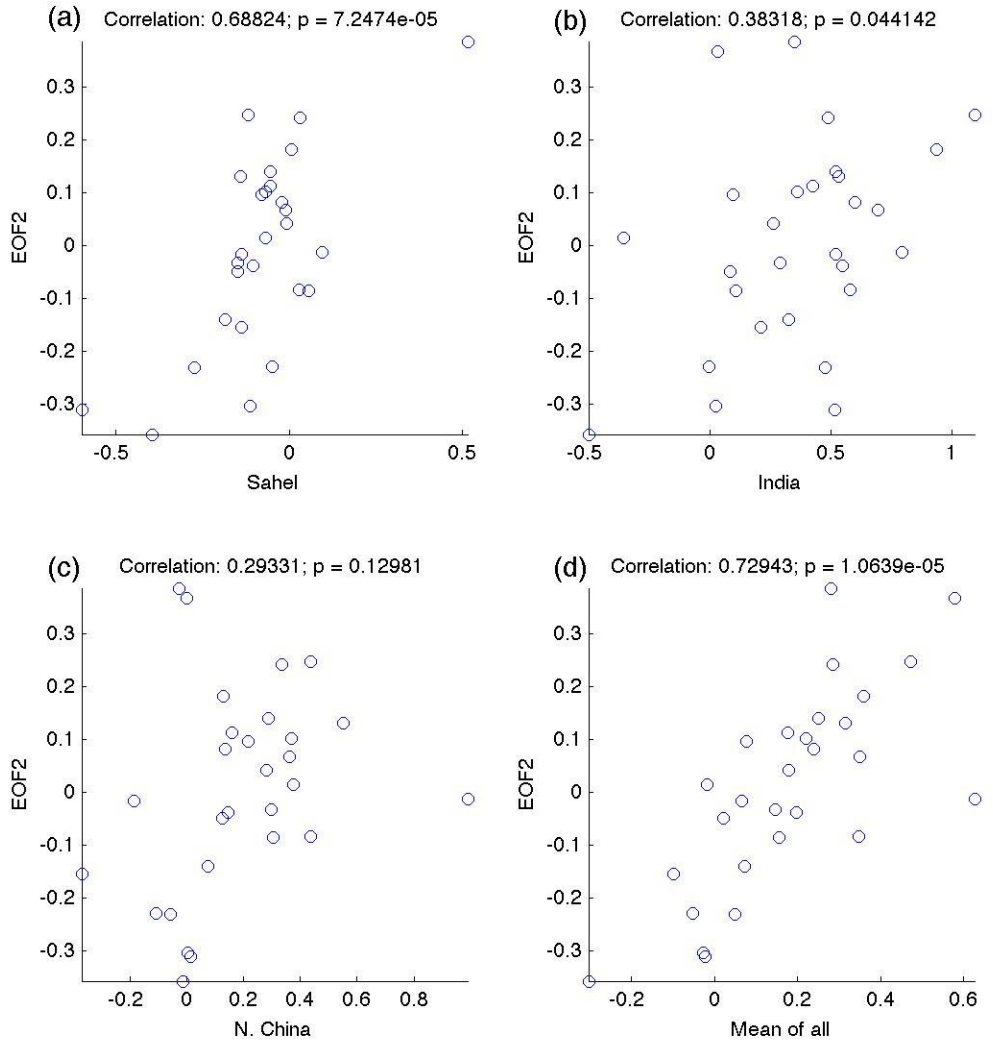

Figure 4.4 Scatter plots of the EOF 2 from Figure 4.3 vs. the rainfall change over (a) Sahel, (b) India, (c) North China, and (d) their average. One outlier is removed in (a)

4.4.2 Global changes and their interpretation

We show a global picture of the changes by projecting the EOF from JJAS Atlantic sector to annual mean global fields. The global pattern of temperature of PC 1 shows all three key features related to the global warming: land-sea contrast, polar amplification, and reduced warming over subpolar North Atlantic and the Southern Ocean (Figure 4.5). Precipitation generally increases in the tropics, with maximum increase over the ocean (Figure 4.5a).

Putting PC 2 in a global context reveals a hemispheric pattern of temperature change and a precipitation response centered on the tropics (Figure 4.6). The temperature change peaks in the extratropical North Atlantic (Figure 4.6a). Changes in precipitation of the same sign are present over the Sahel, India and East Asia (Figure 4.6b), although the signal is weaker as precipitation of those regions mainly comes the summer monsoon, and shown here is annual mean. The overall pattern resembles remarkably model simulations with prescribed thermal forcing over the extratropical North Atlantic (e.g. Figure 2.1). Together with the location of temperature change maximum, this suggests the extratropical North Atlantic being the source of change.

4.4.3 Correlation in both 20th and 21st century

The above results suggest that extratropical North Atlantic continues to play a crucial role in changing monsoon rainfall at the end of the 21st century, as it did for the late 1960s' climate shift. It begs the question of how the extratropical North Atlantic evolved throughout the 21st century (and not just the end of the century), and how the global climate responded to it. To answer this question, we look at the correlation of extratropical North Atlantic changes across the models onto various climate fields.

As shown in Figure 4.1d, there is a wide range in the model simulated extratropical North Atlantic temperature relative to the global mean temperature of the 21st century. While there is a decreasing trend in the multi-model mean, some individual models do simulate relative warming over this period. If the association between extratropical North Atlantic temperature and monsoon rainfall hold, it means that these models that simulate a relative warming trend would tend to project increased monsoonal rainfall, whereas those that simulate cooling would tend to project the opposite.

To test this hypothesis, we calculate the correlation of the detrended, area-averaged extratropical North Atlantic temperature with temperature and precipitation respectively in the North-Atlantic-Eurasia sector in each model. Then, similar to the earlier calculation using composite changes, we normalize and combine the correlation of temperature and precipitation of each model, then apply a CPCA to the combined map across all models. The PCs highlight the joint spatial variability of the correlation across all models for temperature and precipitation respectively, and the EOFs represent the contribution of each model.

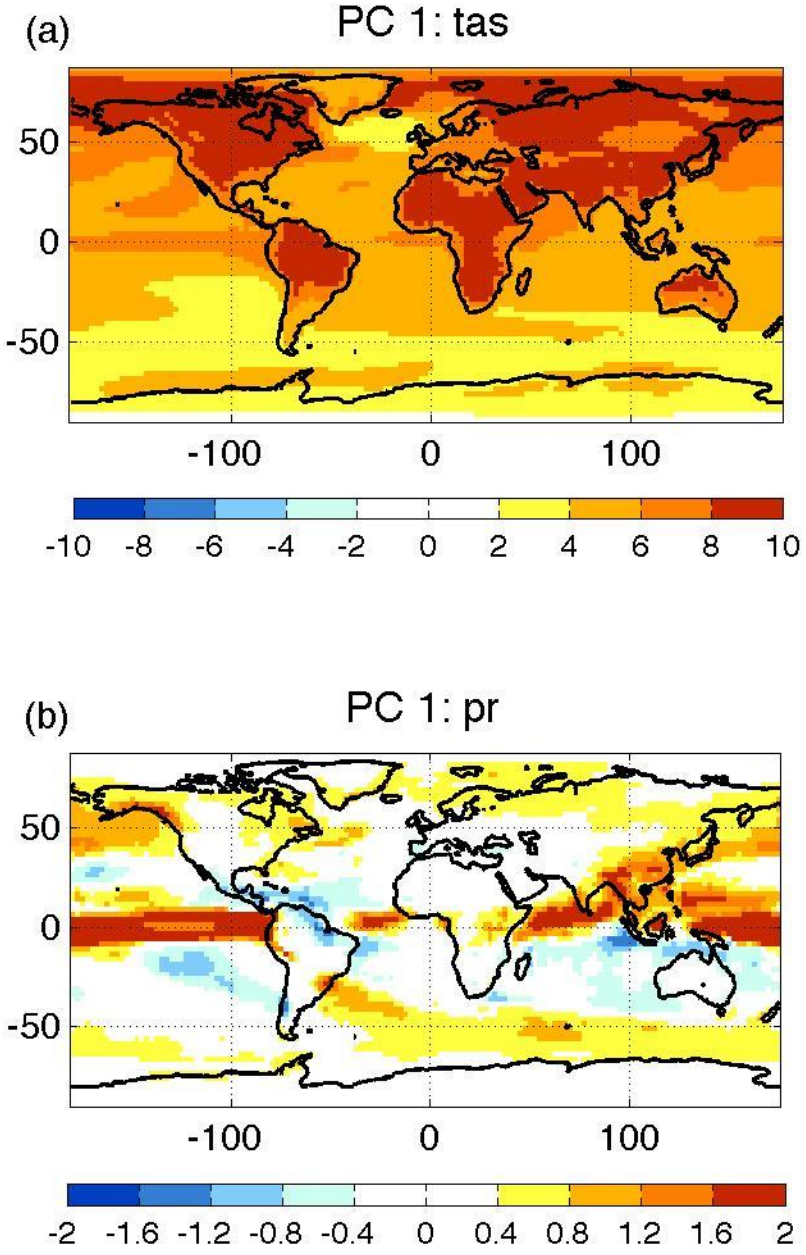

Figure 4.5 Projection of the leading EOF as in Figure 4.2 onto annual mean global composite changes.

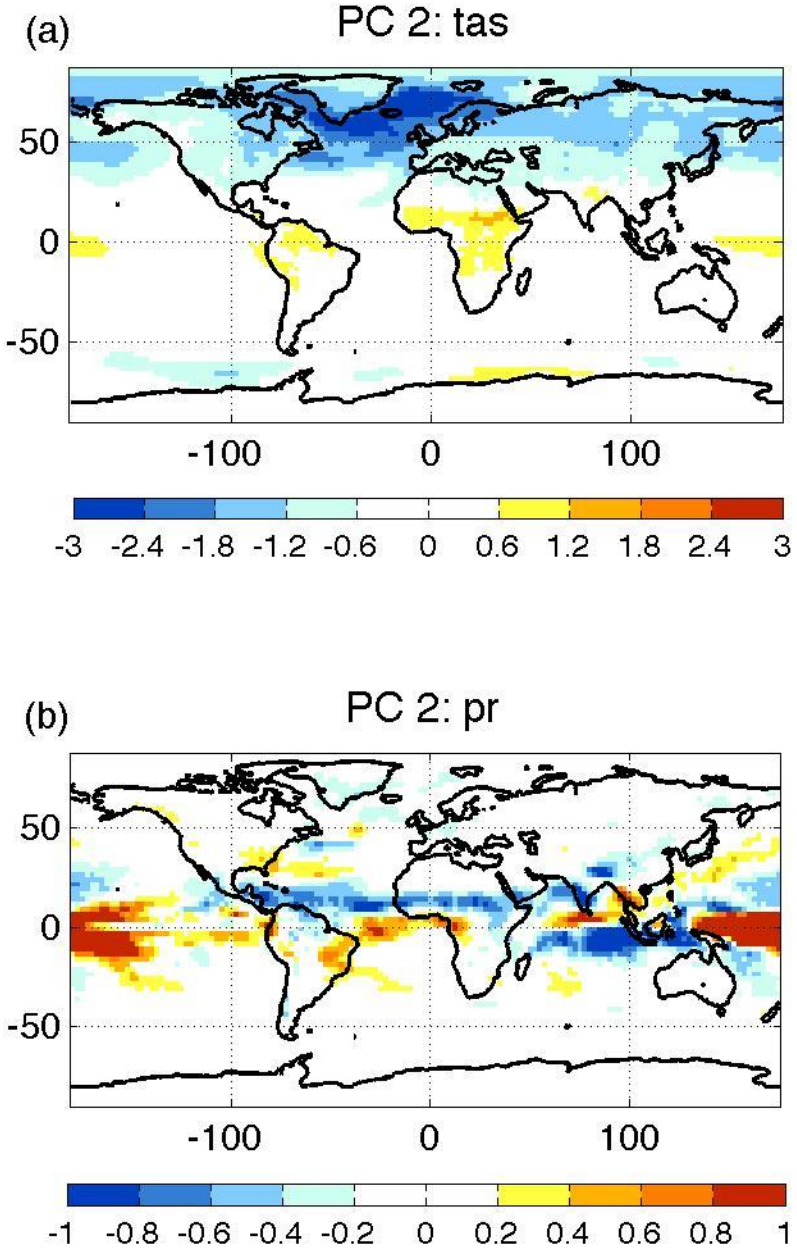

Figure 4.6 Same as Figure 4.5 but for the projection of the 2nd EOF

The leading mode, which explains 21% of total variance (vs. 10% for the 2nd mode), is shown in Figure 4.7. The leading PC of temperature (Figure 4.7a)

exhibits a tripole over North Atlantic, with high positive correlation over subpolar and subtropical region, and a narrow band of low positive correlation in between. The tripole is a typical interannual variability pattern over the North Atlantic, and is thought to arise from the interaction of the SST and the atmospheric circulation above (Kwon et al. 2010). The positive correlation extends downstream in the midlatitude and subtropics, to Eurasia and North Africa, suggesting changes in extratropical North Atlantic temperature induces with temperature changes of the same sign over Eurasia and North Africa.

The leading PC of the correlation of global precipitation onto extratropical North Atlantic temperature across all models is shown in Figure 4.7b. Rainfall over the Sahel, India and East Asia all positively correlates with the extratropical North Atlantic temperature. The Sahel, right beside the Atlantic, exhibits the strongest signal.

The EOF, standing for the contribution of each model in simulating this relationship, is presented in Figure 4.7c. The loadings are positive across all models but one. The results indicate that the relationship of extratropical North Atlantic temperature, with global temperature and precipitation in the 21st century, is a consistent feature across almost all models.

How does the signature of simulated 21st century extratropical North Atlantic temperature on global climate compare with the 20th century observation? We present the latter figure in Figure 4.8. As in the model, the observed temperature correlation shows high positive value over North Atlantic, extending over Eurasia and North Africa. The Sahara, where models simulate high positive correlation, shows no substantial signal due to the lack of data. The observed correlation of precipitation, as with the modeled, shows positive value over the Sahel and Asia, with some exceptions over northeast India. Overall, models simulate a 21st century relationship between extratropical North Atlantic temperature, and global temperature and precipitation that is consistent with that over the 20th century.

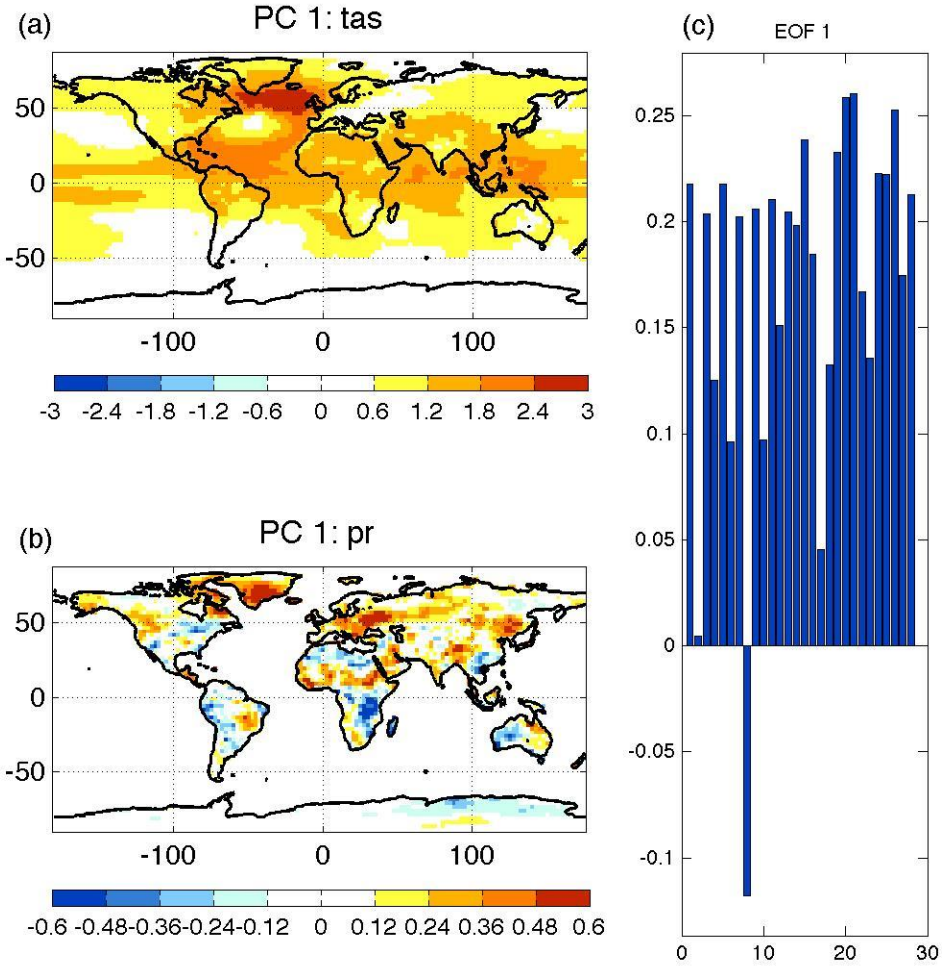

Figure 4.7 EOF of the correlation of JJAS global temperature and precipitation onto extratropical North Atlantic surface air temperature, in CMIP5 21st century model simulations. Precipitation over ocean is masked out for better comparison with 20th century observation

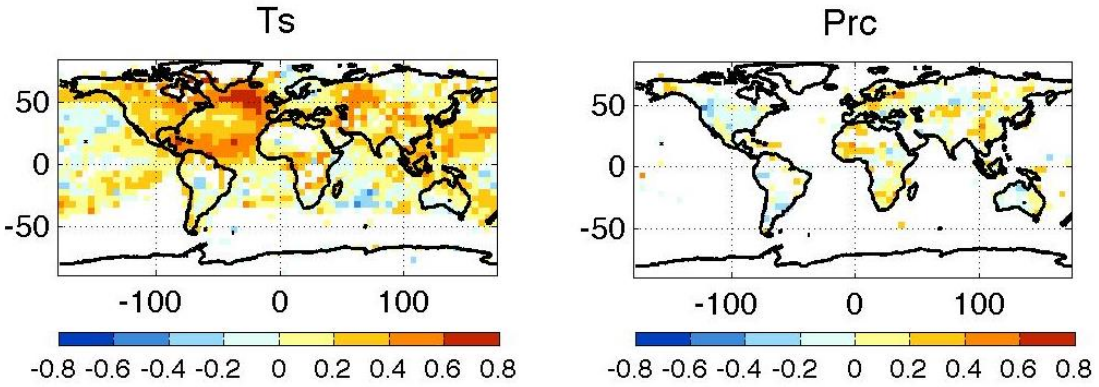

Figure 4.8 correlation of global surface temperature and precipitation onto average extratropical North Atlantic SST in 20th century observation

4.5 Concluding remarks

Global mean temperature is projected to increase through the 21st century, in response to accelerating greenhouse gas emissions. Global mean precipitation increases accordingly, as a result of increased radiative cooling and moisture content in the troposphere. The spatial patterns of the temperature and precipitation responses in the 21st century are, however, highly variable (Collins et al. 2013).

Future monsoon precipitation change is of crucial importance to the society in West Africa and Asia, where half of the world population reside. Models, however, cannot offer a consistent projection of the precipitation change with high confidence. At first order, tropical and monsoon precipitation increases with global warming. Despite the precipitation increase, a weakening of monsoon circulation is predicted, as the precipitation increase does not follow closely to that of water vapor (Collins et al. 2013). Nevertheless, the monsoon is influenced by not only the mean temperature, but the spatial distribution of temperature change at both local and remote areas. We have found in previous chapters that extratropical North Atlantic temperature is able to modulate the West African, South Asian and East Asian monsoons in the last glacial period and in present day. In this chapter, we investigate if this is the fact in the future.

First, we investigated to what extent extratropical North Atlantic SST variations and associated changes to monsoonal rainfall featured in future climate projections. In order to do this, we obtained the spatial patterns of temperature and rainfall changes for each CMIP5 model at the end of the 21st century, and applied a CPCA method to extract the common features across the model projections. While the first mode is (not surprisingly) tied to global warming, the second mode resembles the climate features we have seen before in the previous chapters, including changes in temperature over Eurasia and North Africa and summer rainfall over the Sahel, India, and North China. Those changes follow that of extratropical North Atlantic temperature, even though models disagree with the sign of the latter.

We then examined how the extratropical North Atlantic evolved throughout the 21st century, and how it influenced global climate. Similar to our previous analysis, we obtained the correlation of extratropical North Atlantic temperature with global temperature and precipitation respectively, for each CMIP5 model at the end of the 21st century, and applied a CPCA method to extract the common features across the model projections. A unanimous pattern of positive correlation over Eurasia and North Africa appears across models, which resembles that from 20th century observation. The results suggest that the 20th century North-Atlantic-temperature-and-Eurasia-and-North-Africa-climate relationship works through future climate.

Although we do not know with confidence the sign of expected changes in summer monsoon rainfall over the coming century, our identification of the remote source of influence points a way forward. The model spread in extratropical North Atlantic climate simulation limits our ability to confidently project monsoon changes. Therefore, better characterization and reduction of this spread should be a focus of efforts to estimate possible evolution of monsoon activity.

What is the origin of the different extratropical North Atlantic temperature projections? Greenhouse gases, aerosols, and the internal variability of the Atlantic Meridional Overturning Circulation, AMOC have all been considered to modulate 20th century North Atlantic temperature include (Knight et al. 2005; Mann and Emanuel 2006; Booth et al. 2012; Chiang et al. 2013). In the 21st century projection, a common forcing of greenhouse gases and aerosols are applied to each model as designed for the CMIP5 framework. Therefore, external forcings are not likely the source of model spread. Although the response to the common forcing may vary in each models, the radiative forced pattern of the North Atlantic SST demonstrates a warming in response to both the increase of greenhouse gas and decline of aerosol prescribed in the RCP4.5, as shown in (Drijfhout et al. 2012). Drijfhout et al. (2012) also found in the projected North Atlantic SST a fingerprint of AMOC centered over extratropical North Atlantic that remarkably resembles the 2nd mode we obtained in future temperature changes. It is possible that the change of AMOC dominates that of North Atlantic SST.

There is large uncertainty in AMOC projection, as a result of uncertainty in the simulations of both its internal variability and response to forcing. The internal variability of AMOC has been considered a primary driver of the North Atlantic SST in decadal timescale; The latter, in the form as the Atlantic multidecadal oscillation (AMO), is of a magnitude comparable to that of externally forced trend in the 20th century (Knight et al. 2005; Zhang and Wang 2013). The chaotic nature of the climate system makes precise simulation of the phasing of AMOC internal variability impossible and thus contributes to the uncertainty in both AMOC and AMO projections. Even in the forced part, a study of the ensemble mean simulation from CMIP5 models by (Cheng et al. 2013) found a change of AMOC ranging from 5% to 40% across models, under the common forcing of RCP4.5. We thus posit that the dominant source of uncertainty in the projected extratropical North Atlantic climate comes from the simulation of AMOC.

Bibliography

Adler RF, Huffman GJ, Chang A, et al. (2003) The version-2 global precipitation climatology project (GPCP) monthly precipitation analysis (1979-present). J Hydrometeorol 4:1147– 1167. doi: 10.1175/1525-7541(2003)004¡1147:TVGPCP¿2.0.CO;2

Allen MR, Ingram WJ (2002) Constraints on future changes in climate and the hydrologic cycle. Nature 419:224– 232. doi: 10.1038/nature01092

Alley RB (2007) Wally was right: Predictive ability of the North Atlantic " conveyor belt" hypothesis for abrupt climate change. Annu Rev Earth Planet Sci 35:241– 272.

Anderson J, Balaji V, Broccoli A, et al. (2004) The new GFDL global atmosphere and land model AM2-LM2: Evaluation with prescribed SST simulations. J Clim 17:4641– 4673.

Bader J, Latif M (2003) The impact of decadal-scale Indian Ocean sea surface temperature anomalies on Sahelian rainfall and the North Atlantic Oscillation. Geophys Res Lett 30:2169.

Baines P, Folland C (2007) Evidence for a rapid global climate shift across the late 1960s. J Clim 20:2721– 2744. doi: 10.1175/JCLI4177.1

Biasutti M, Giannini A (2006) Robust Sahel drying in response to late 20th century forcings. Geophys Res Lett. doi: 10.1029/2006GL026067

Biasutti M, Sobel A, Camargo S (2009) The Role of the Sahara Low in Summertime Sahel Rainfall Variability and Change in the CMIP3 Models. J Clim 22:5755– 5771. doi: 10.1175/2009JCLI2969.1

Booth BBB, Dunstone NJ, Halloran PR, et al. (2012) Aerosols implicated as a prime driver of twentieth-century North Atlantic climate variability. Nature 484:228– 232. doi: 10.1038/nature10946

Bottomley M, Massachusetts Institute of Technology (Cambridge, Estados Unidos). Department of Earth A, Sciences P (1990) Global Ocean Surface Temperature Atlas:" GOSTA." Meteorological Office

Bretherton C, Smith C, Wallace J (1992) An intercomparison of methods for finding coupled patterns in climate data. J Clim 5:541– 560.

Broecker WS, Peteet DM, Rind D (1985) Does the ocean-atmosphere system have more than one stable mode of operation? Nature 315:21– 26. doi: 10.1038/315021a0

Brohan P, Kennedy JJ, Harris I, et al. (2006) Uncertainty estimates in regional and global observed temperature changes: a new dataset from 1850. J Geophys Res 111:

Chen H, Zhou T, Neale RB, et al. (2010) Performance of the New NCAR CAM3.5

in East Asian Summer Monsoon Simulations: Sensitivity to Modifications of the Convection Scheme. J Clim 23:3657– 3675. doi: 10.1175/2010JCLI3022.1

Cheng W, Bitz CM, Chiang JCH (2007) Adjustment of the global climate to an abrupt slowdown of the Atlantic meridional overturning circulation. Geophys Monogr-Am Geophys Union 173:295.

Cheng W, Chiang JCH, Zhang D (2013) Atlantic Meridional Overturning Circulation (AMOC) in CMIP5 Models: RCP and Historical Simulations. J Clim 26:7187– 7197. doi: 10.1175/JCLI-D-12-00496.1

Chiang JC, Chang C-Y, Wehner MF (2013) Long-Term Behavior of the Atlantic Interhemispheric SST Gradient in the CMIP5 Historical Simulations. J. Clim. 26:

Chiang JCH, Bitz CM (2005) Influence of high latitude ice cover on the marine Intertropical Convergence Zone. Clim Dyn 25:477– 496.

Chiang JCH, Friedman AR (2012) Extratropical Cooling, Interhemispheric Thermal Gradients, and Tropical Climate Change. Annu Rev Earth Planet Sci Vol 40 40:383– 412.

Chou C, Neelin J (2004) Mechanisms of global warming impacts on regional tropical precipitation. J Clim 17:2688– 2701. doi: 10.1175/1520-0442(2004)017¡2688:MOGWIO¿2.0.CO;2

Chou C, Neelin J, Su H (2001) Ocean-atmosphere-land feedbacks in an idealized monsoon. Q J R Meteorol Soc 127:1869– 1891. doi: 10.1002/qj.49712757602

Chou C, Neelin JD, Chen C-A, Tu J-Y (2009) Evaluating the "Rich-Get-Richer' ' Mechanism in Tropical Precipitation Change under Global Warming RID H-4337-2011. J Clim 22:1982– 2005. doi: 10.1175/2008JCLI2471.1

Christensen JH, Krishna Kumar K, Aldrian E, et al. (2013) Climate Phenomena and their Relevance for Future Regional Climate Change. Clim. Change 2013 Phys. Sci. Basis

Collins M, Knutti R, Arblaster J, et al. (2013) Long-term Climate Change: Projections, Commitments and Irreversibility. Clim. Change 2013 Phys. Sci. Basis

Collins W, Rasch P, Boville B, et al. (2006) The formulation and atmospheric simulation of the Community Atmosphere Model version 3 (CAM3). J Clim 19:2144– 2161.

Cook K (1999) Generation of the African easterly jet and its role in determining West African precipitation RID B-4998-2011. J Clim 12:1165– 1184. doi: 10.1175/1520-0442(1999)012¡1165:GOTAEJ¿2.0.CO;2

Cronin TM (2013) Paleoclimates: Understanding Climate Change Past and Present. Columbia University Press

D' Arrigo R, Wilson R, Li J (2006) Increased Eurasian-tropical temperature amplitude difference in recent centuries: Implications for the Asian monsoon. Geophys Res Lett. doi: 10.1029/2006GL027507

Dai A, Fung I, DelGenio A (1997) Surface observed global land precipitation variations during 1900-88. J Clim 10:2943– 2962.

Dansgaard W, Johnsen SJ, Clausen HB, et al. (1993) Evidence for general instability of past climate from a 250-kyr ice-core record. Nature 364:218– 220.

Delworth T, Broccoli A, Rosati A, et al. (2006) GFDL' s CM2 global coupled climate models. Part I: Formulation and simulation characteristics. J Clim 19:643– 674.

Deser C, Phillips AS (2006) Simulation of the 1976/77 climate transition over the North Pacific: Sensitivity to tropical forcing. J Clim 19:6170– 6180.

Dickson R, Meincke J, Malmberg S, Lee A (1988) The great salinity anomaly in the northern north-atlantic 1968-1982. Prog Ocean 20:103– 151.

Drijfhout S, van Oldenborgh GJ, Cimatoribus A (2012) Is a Decline of AMOC Causing the Warming Hole above the North Atlantic in Observed and Modeled Warming Patterns? J Clim 25:8373–8379. doi: 10.1175/JCLI-D-12-00490.1

Folland CK, Owen J, Ward MN, Colman A (1991) Prediction of seasonal rainfall in the sahel region using empirical and dynamic methods. J Forecast 10:21–56. doi: 10.1002/for.3980100104

Folland CK, Palmer TN, Parker DE (1986) Sahel Rainfall and Worldwide Sea Temperatures, 1901-85. Nature 320:602–607.

Fontaine B, Trzaska S, Janicot S (1998) Evolution of the relationship between near global and Atlantic SST modes and the rainy season in west Africa: statistical analyses and sensitivity experiments. Clim Dyn 14:353–368. doi: 10.1007/s003820050228

Gadgil S (2003) The Indian monsoon and its variability. Annu Rev Earth Planet Sci 31:429–467.

Giannini A, Saravanan R, Chang P (2003) Oceanic forcing of Sahel rainfall on interannual to interdecadal time scales. Science 302:1027–1030.

Goswami BN, Madhusoodanan MS, Neema CP, Sengupta D (2006) A physical mechanism for North Atlantic SST influence on the Indian summer monsoon. Geophys Res Lett 33:L02706.

Grist J, Nicholson S (2001) A study of the dynamic factors influencing the rainfall variability in the West African Sahel. J Clim 14:1337–1359.

Gupta AK, Anderson DM, Overpeck JT (2003) Abrupt changes in the Asian southwest monsoon during the Holocene and their links to the North Atlantic Ocean. Nature 421:354–357. doi: 10.1038/nature01340

Haarsma RJ, Selten FM, Weber SL, Kliphuis M (2005) Sahel rainfall variability and response to greenhouse warming. Geophys Res Lett 32:L17702.

Heinrich H (1988) Origin and consequences of cyclic ice rafting in the Northeast Atlantic Ocean during the past 130,000 years. Quat Res 29:142–152. doi: 10.1016/0033-5894(88)90057-9

Held I, Delworth T, Lu J, et al. (2006) Simulation of Sahel drought in the 20th and 21st centuries. Proc Natl Acad Sci United States 103:1152–1153. doi: 10.1073/pnas.0510844103

Held IM, Soden BJ (2006) Robust responses of the hydrological cycle to global warming. J Clim 19:5686–5699. doi: 10.1175/JCLI3990.1

Hoerling M, Hurrell J, Eischeid J, Phillips A (2006) Detection and attribution of twentieth-century northern and southern African rainfall change. J Clim 19:3989–4008.

Hulme M (1992) A 1951-80 GLOBAL LAND PRECIPITATION CLIMATOLOGY FOR THE EVALUATION OF GENERAL-CIRCULATION MODELS. Clim Dyn 7:57–72.

James W. Hurrell, James J. Hack, Dennis Shea, et al. (2010) A New Sea Surface Temperature and Sea Ice Boundary Dataset for the Community Atmosphere Model. http://journals.ametsoc.org/doi/abs/10.1175/2008JCLI2292.1. Accessed 5 Aug 2010

Janjic Z (1994) The Step-Mountain Eta Coordinate Model - Further Developments of the Convection, Viscous Sublayer, and Turbulence Closure Schemes. Mon Weather Rev 122:927–945. doi: 10.1175/1520-0493(1994)122¡0927:TSMECM¿2.0.CO;2

Janjic Z (1996) The surface layer in the NCEP Eta Model. Elev Conf Numer Weather Predict Norfolk Va 19-23 August Amer Meteor Soc Boston Ma 354–355.

Janjic ZI (2002) Nonsingular implementation of the Mellor–Yamada level 2.5 scheme in the NCEP Meso model. Ncep Off Note 437:61.

Kalnay E, Kanamitsu M, Kistler R, et al. (1996) The NCEP/NCAR 40-year reanalysis project. Bull Am Meteorol Soc 77:437–471.

Kanamitsu M, Ebisuzaki W, Woollen J, et al. (2002) NCEP-DOE AMIP-II Reanalysis (R-2). Bull Am Meteorol Soc 83:1631–1644.

Kang SM, Frierson DMW, Held IM (2009) The Tropical Response to Extratropical Thermal Forcing in an Idealized GCM: The Importance of Radiative Feedbacks and Convective Parameterization RID F-1763-2010. J Atmospheric Sci 66:2812–2827. doi: 10.1175/2009JAS2924.1

Kang SM, Held IM, Frierson DMW, Zhao M (2008) The Response of the ITCZ to Extratropical Thermal Forcing: Idealized Slab-Ocean Experiments with a GCM. J Clim 21:3521–3532. doi: 10.1175/2007JCLI2146.1

Kawase H, Abe M, Yamada Y, et al. (2010) Physical mechanism of long-term drying trend over tropical North Africa. Geophys Res Lett. doi: 10.1029/2010GL043038

Knight JR, Allan RJ, Folland CK, et al. (2005) A signature of persistent natural thermohaline circulation cycles in observed climate. Geophys Res Lett 32:L20708.

Koutavas A, Lynch-Stieglitz J (2004) Variability of the marine ITCZ over the eastern Pacific during the past 30,000 years: Regional perspective and global context. Hadley Circ Present Future 347–369.

Van Kreveld S, Sarnthein M, Erlenkeuser H, et al. (2000) Potential links between surging ice sheets, circulation changes, and the Dansgaard-Oeschger cycles in the Irminger Sea, 60-18 kyr. Paleoceanography 15:425–442. doi: 10.1029/1999PA000464

Kucharski F, Scaife AA, Yoo JH, et al. (2009) The CLIVAR C20C project: skill of simulating Indian monsoon rainfall on interannual to decadal timescales. Does GHG forcing play a role? Clim Dyn 33:615–627.

Kwon Y-O, Alexander MA, Bond NA, et al. (2010) Role of the Gulf Stream and Kuroshio–Oyashio Systems in Large-Scale Atmosphere–Ocean Interaction: A Review. J Clim 23:3249–3281. doi: 10.1175/2010JCLI3343.1

Lee M-Y, Hsu H-H (2013) Identification of the Eurasian-North Pacific Multidecadal Oscillation and Its Relationship to the AMO. J Clim 26:8139–8153.

Li H, Dai A, Zhou T, Lu J (2010) Responses of East Asian summer monsoon to historical SST and atmospheric forcing during 1950–2000. Clim Dyn 34:501–514. doi: 10.1007/s00382-008-0482-7

Lin Y, Farley R, Orville H (1983) Bulk Parameterization of the Snow Field in a Cloud Model. J Clim Appl Meteorol 22:1065–1092. doi: 10.1175/1520-0450(1983)022¡1065:BPOTSF¿2.0.CO;2

Liu Y, Chiang JCH (2012) Coordinated Abrupt Weakening of the Eurasian and North African Monsoons in the 1960s and Links to Extratropical North Atlantic Cooling. J Clim 25:3532–3548. doi: 10.1175/JCLI-D-11-00219.1

Liu Y, Chiang JCH, Chou C, Patricola CM (2014) Atmospheric teleconnection mechanisms of extratropical North Atlantic SST influence on Sahel rainfall. Clim Dyn 1–15. doi: 10.1007/s00382-014-2094-8

Luo F, Li S, Furevik T (2011) The connection between the Atlantic Multidecadal Oscillation and the Indian Summer Monsoon in Bergen Climate Model Version 2.0. J Geophys Res 116:9 PP. doi: 201110.1029/2011JD015848

Ma J, Xie S-P (2013) Regional Patterns of Sea Surface Temperature Change: A Source of Uncertainty in Future Projections of Precipitation and Atmospheric Circulation. J Clim 26:2482–2501. doi: 10.1175/JCLI-D-12-00283.1

Manabe S, Bryan K, Spelman M (1990) Transient-Response of a Global Ocean Atmosphere Model to a Doubling of Atmospheric Carbon-Dioxide. J Phys Ocean 20:722–749. doi: 10.1175/1520-0485(1990)020¡0722:TROAGO¿2.0.CO;2

Mann ME, Emanuel KA (2006) Atlantic hurricane trends linked to climate change. Eos Trans Am Geophys Union 87:233–241.

Martin ER, Thorncroft C, Booth BBB (2013) The Multidecadal Atlantic SST - Sahel Rainfall Teleconnection in CMIP5 Simulations. J Clim 130924140137007. doi: 10.1175/JCLI-D-13-00242.1

Mlawer EJ, Taubman SJ, Brown PD, et al. (1997) Radiative transfer for inhomogeneous atmospheres: RRTM, a validated correlated-k model for the longwave. J Geophys Res-Atmospheres 102:16663–16682. doi:

10.1029/97JD00237

Monin AS, Obukhov Am (1954) Basic laws of turbulent mixing in the surface layer of the atmosphere. Contrib Geophys Inst Acad Sci Ussr 151:163–187.

Moss RH, Edmonds JA, Hibbard KA, et al. (2010) The next generation of scenarios for climate change research and assessment. Nature 463:747–756.

Mulitza S, Prange M, Stuut JB, et al. (2008) Sahel megadroughts triggered by glacial slowdowns of Atlantic meridional overturning. Paleoceanography. doi: 10.1029/2008PA001637

Nicholson S (1979) Revised Rainfall Series for the West-African Subtropics. Mon Weather Rev 107:620–623. doi: 10.1175/1520-0493(1979)107¡0620:RRSFTW¿2.0.CO;2

Nicholson S (2009) On the factors modulating the intensity of the tropical rainbelt over West Africa. Int J Clim 29:673–689. doi: 10.1002/joc.1702

Nicholson S, Tucker C, Ba M (1998) Desertification, drought, and surface vegetation: An example from the West African Sahel. Bull Am Meteorol Soc 79:815–829.

Niedermeyer EM, Prange M, Mulitza S, et al. (2009) Extratropical forcing of Sahel aridity during Heinrich stadials. Geophys Res Lett. doi: 10.1029/2009GL039687

Novakov T, Ramanathan V, Hansen J, et al. (2003) Large historical changes of fossil-fuel black carbon aerosols. Geophys Res Lett. doi: 10.1029/2002GL016345

Parker D, Folland C, Scaife A, et al. (2007) Decadal to multidecadal variability and the climate change background. J Geophys Res 112:D18115.

Parthasarathy B, Munot A, Kothawale D (1994) All-India monthly and seasonal rainfall series: 1871–1993. Theor Appl Clim 49:217–224.

Patricola CM, Cook KH (2008) Atmosphere/vegetation feedbacks: A mechanism for abrupt climate change over northern Africa. J Geophys Res-Atmospheres. doi: 10.1029/2007JD009608

Patricola CM, Cook KH (2010) Northern African climate at the end of the twenty-first century: an integrated application of regional and global climate models. Clim Dyn 35:193–212. doi: 10.1007/s00382-009-0623-7

Peterson LC, Haug GH, Hughen KA, Röhl U (2000) Rapid Changes in the Hydrologic Cycle of the Tropical Atlantic During the Last Glacial. Science 290:1947–1951. doi: 10.1126/science.290.5498.1947

Ramanathan V, Carmichael G (2008) Global and regional climate changes due to black carbon. Nat Geosci 1:221–227.

Rayner NA, Brohan P, Parker DE, et al. (2006) Improved analyses of changes and uncertainties in sea surface temperature measured in situ since the mid-nineteenth century: the HadSST2 dataset. J Clim 19:446–469.

Ren B, Lu R, Xiao Z (2004) A possible linkage in the interdecadal variability of rainfall over North China and the Sahel. Adv Atmospheric Sci 21:699–707.

Rodionov S (2004) A sequential algorithm for testing climate regime shifts. Geophys Res Lett. doi: 10.1029/2004GL019448

Rotstayn LD, Lohmann U (2002) Tropical rainfall trends and the indirect aerosol effect. J Clim 15:2103–2116.

Rowell DP, Folland CK, Maskell K, Ward MN (1995) Variability of summer rainfall over tropical north-africa (1906-92) - observations and modeling. Q J R Meteorol Soc 121:669–704. doi: 10.1256/smsqj.52310

Shanahan T, Overpeck J, Anchukaitis K, et al. (2009) Atlantic Forcing of Persistent Drought in West Africa. SCIENCE 324:377–380. doi: 10.1126/science.1166352

Shell K, Kiehl J, Shields C (2008) Using the radiative kernel technique to calculate climate feedbacks in NCAR's Community Atmospheric Model. J Clim 21:2269–2282. doi: 10.1175/2007JCLI2044.1

Skamarock WC, Klemp JB, Dudhia J, et al. (2008) A description of the Advanced Research WRF Version 3. NCAR/TN-475+ STR

Smirnova TG, Brown JM, Benjamin SG (1997) Performance of different soil model configurations in simulating ground surface temperature and surface fluxes. Mon Weather Rev 125:1870–1884. doi: 10.1175/1520-0493(1997)125¡1870:PODSMC¿2.0.CO;2

Smith SJ, Andes R, Conception E, et al. (2004) Historical sulfur dioxide emissions, 1850-2000: methods and results. Pacific Northwest National Laboratory

Soden B, Held I, Colman R, et al. (2008) Quantifying climate feedbacks using radiative kernels. J Clim 21:3504–3520. doi: 10.1175/2007JCLI2110.1

Stager J, Ryves D, Chase B, Pausata F (2011) Catastrophic Drought in the Afro-Asian Monsoon Region During Heinrich Event 1. SCIENCE 331:1299–1302. doi: 10.1126/science.1198322

Sutton RT, Hodson DLR (2005) Atlantic Ocean Forcing of North American and European Summer Climate. Science 309:115 –118. doi: 10.1126/science.1109496

Thompson D, Wallace J, Kennedy J, Jones P (2010) An abrupt drop in Northern Hemisphere sea surface temperature around 1970. NATURE 467:444–447. doi: 10.1038/nature09394

Thomson AM, Calvin KV, Smith SJ, et al. (2011) RCP4. 5: a pathway for stabilization of radiative forcing by 2100. Clim Change 109:77–94.

Trenberth K, Paolino D (1980) The northern hemisphere sea-level pressure data set - trends, errors and discontinuities. Mon Weather Rev 108:855–872.

Trenberth KE, Shea DJ (2006) Atlantic hurricanes and natural variability in 2005. Geophys Res Lett 33:L12704.

Vecchi GA, Soden BJ (2007) Global Warming and the Weakening of the Tropical Circulation. J Clim 20:4316–4340. doi: 10.1175/JCLI4258.1

Vellinga M, Wood R (2002) Global climatic impacts of a collapse of the Atlantic

thermohaline circulation. Clim Change 54:251–267. doi: 10.1023/A:1016168827653

Wang S–., Gong D–., Ye J–. (2000) Seasonal precipitation series of eastern China since 1880 and the variability. Acta Geogr Sin-Chin Ed- 55:292–300.

Wang Y, Cheng H, Edwards R, et al. (2001) A high-resolution absolute-dated Late Pleistocene monsoon record from Hulu Cave, China. SCIENCE 294:2345–2348.

Wang Y, Li S, Luo D (2009) Seasonal response of Asian monsoonal climate to the Atlantic Multidecadal Oscillation. J Geophys Res Atmospheres 114:n/a–n/a. doi: 10.1029/2008JD010929

Wilks DS (2006) Statistical Methods in the Atmospheric Sciences, vol. 91. Int. Geophys. Ser. 630:

Woodruff SD, Worley SJ, Lubker SJ, et al. (2011) ICOADS Release 2.5: extensions and enhancements to the surface marine meteorological archive. Int J Clim 31:951–967. doi: 10.1002/joc.2103

Xu Q (2001) Abrupt change of the mid-summer climate in central east China by the influence of atmospheric pollution. Atmos Environ 35:5029–5040. doi: 10.1016/S1352-2310(01)00315-6

Xue Y, Jagadish S (1993) The influence of land surface properties on Sahel climate. Part 1: desertification. J Clim 6:2232–2245.

Yu R, Zhou T (2007) Seasonality and three-dimensional structure of interdecadal change in the East Asian monsoon. J Clim 20:5344–5355. doi: 10.1175/2007JCLI1559.1

Zhang G, Mcfarlane N (1995) Sensitivity of Climate Simulations to the Parameterization of Cumulus Convection in the Canadian Climate Center General-Circulation Model. Atmos-Ocean 33:407–446.

Zhang L, Wang C (2013) Multidecadal North Atlantic sea surface temperature and Atlantic meridional overturning circulation variability in CMIP5 historical simulations. J Geophys Res Oceans 118:5772–5791. doi: 10.1002/jgrc.20390

Zhang L, Zhou T (2011) An assessment of monsoon precipitation changes during 1901–2001. Clim Dyn 37:279–296.

Zhang R, Delworth T (2006) Impact of Atlantic multidecadal oscillations on India/Sahel rainfall and Atlantic hurricanes. Geophys Res Lett. doi: 10.1029/2006GL026267

Zhang R, Delworth TL (2005) Simulated tropical response to a substantial weakening of the Atlantic thermohaline circulation. J Clim 18:1853–1860.

Zhang R, Vallis GK (2010) Impact of great salinity anomalies on the low-frequency variability of the North Atlantic climate.

Zhou T, Yu R, Li H, Wang B (2008) Ocean forcing to changes in global monsoon precipitation over the recent half-century. J Clim 21:3833–3852.